Spacetime in the brain: Deep Learning Analysis of Rapid Brain Network Neuromodulation in Visual Function and Vision Restoration

Dissertation zur Erlangung des akademischen Grades
Doktoringenieurin
(Dr.-Ing.)

Angenommen durch die Fakultät für Informatik der
Otto-von-Guericke-Universität Magdeburg

von M.Sc. **Zheng Wu**
geb. am 01.09.1989 in Shanxi China

Gutachter:
Prof. Dr. Andreas Nürnberger
Prof. Dr. Bernhard A. Sabel
Prof. Dr. Paolo Maria Rossini

Magdeburg, 05. März 2024

Zheng Wu:
Spacetime in the brain: Deep Learning Analysis of Rapid Brain Network Neuromodulation in Visual Function and Vision Restoration. Dissertation, Otto-von-Guericke- Universität Magdeburg, 2023.

Abstract

The optic nerve is an essential bridge between the eye and the brain, holding a crucial position in the entire visual pathway. Damage to the optic nerve, such as that caused by glaucoma and anterior ischaemic optic neuropathy, not only causes visual field deficits and perceptual abnormalities, but also visual cognitive processing. Repetitive transorbital alternating current stimulation (rtACS) shows promise in enhancing visual field function and improving vision-related quality of life in patients with optic neuropathy. However, it remains unclear how localized visual impairment and rtACS-induced neuromodulation affects upstream cognitive processing mechanisms in the brain.

Neuronal synchronization, the underlying mechanism of overall behaviour and thought, must be well orchestrated in time and space to ascertain flawless interactions of different functional domains such as sensorimotor and multisensory integration, attention or cognition. Functional connectivity networks (FCN) are the physiological basis of brain synchronization to integrating neural activity. They are not rigid but can reorganize under pathological conditions or during mental or behavioral states, which provides an avenue to better understand the mechanisms of visual cognition and to analyze visual impairment and vision restoration. Tightly connected clusters of nodes, called communities, interact in a time-dependent manner in brain FCN to support complex cognitive functions. However, little is known if and how different nodes synchronize their neural interactions to form functional communities ("modules") during visual processing and if and how this modularity is affected post-lesion (progression or recovery) by neuromodulation.

Using the damaged optic nerve as a paradigm, I now studied brain FCN dynamics to better understand dynamic reconfigurations and interactions before and after neuromodulation with non-invasive rtACS. EEG-recordings were time-locked to visual stimulus presentation and graph analysis of neurophysiological oscillations was used to characterize millisecond FCN dynamics in healthy subjects and in patients with optic nerve damage before and after treatment and were correlated with visual performance.

I found that rapid and transient FCN synchronization patterns in humans can evolve and dissolve in millisecond speed during visual processing. This rapid reorganization is functionally relevant because disruption and recovery after microcurrent treatment in optic nerve patients correlated with impaired and recovered visual performance, respectively. Because FCN hub and node interactions can evolve and dissolve in millisecond speed to manage spatial and temporal neural synchronization during visual processing and recovery, I propose "Brain Spacetime" as a fundamental principle of the human mind not only in visual cognition but also in vision restoration.

In both patients and controls, local inter-module interactions correlated with visual performance. However, patients' recovery of vision after treatment with rtACS was associated with improved interaction strength of pathways linked to the attention module, and it improved global modularity and increased stability of FCN. Temporal coordination of multiple cortical modules and inter-module interaction are functionally relevant for visual processing. This modularity can be neuromodulated with rtACS which induces a more optimal balanced and stable multilayer modular structure for visual processing by enhancing the interaction of neural pathways with the attention network module.

However, treatment efficacy varies considerably between subjects and treatment outcome

remains unpredictable. In order to identify individual vision recovery predictor (VRP), existing trial data from optic nerve patients were analysed and trained using deep learning algorithms. In this way, I developed a vision recovery prediction model for post-rtACS effects by training the node centralities of the functional brain networks during visual cognition from optic nerve damage patients.

In addition, I analyzed the potential of a deep learning-based early warning model to identify potential visual field damage in "intact" visual fields. However, the generalization ability of the model remains to be further investigated.

In conclusion, this study reveals that rapid and transient synchronization patterns in functional brain networks play a crucial role in visual processing and recovery, proposing "Spacetime of the Brain" as a fundamental principle. Treatment with rtACS in optic nerve patients enhances inter-module interactions, particularly with the attention network module, improving global modularity and stability of functional brain networks. Additionally, a deep learning-based vision recovery prediction model and an early warning system for identifying visual field damage were developed, offering insights into individualized treatment outcomes and timely interventions.

Keywords: Optic nerve damage; brain network; graph theory, cognition; alternating current stimulation; brain stimulation; Multilayer modularity; Brain stimulation; EEG; Deep Learning.

Zusammenfassung

Der Sehnerv ist eine essentielle Verbindung zwischen dem Auge und dem Gehirn und nimmt eine entscheidende Stellung im gesamten visuellen System ein. Schäden am Sehnerv, wie zum Beispiel bei Glaukom und anteriore ischämische Optikusneuropathie, führen nicht nur zu Gesichtsfeldausfällen und Wahrnehmungsstörungen, sondern auch zu einer Vielzahl kognitiver Beeinträchtigungen. Wiederholte transorbitale Wechselstromstimulation (rtACS) zeigt vielversprechende Ergebnisse bei der Verbesserung des Gesichtsfelds und der Steigerung der lebensbezogenen Sehqualität bei Patienten mit Optikusneuropathie. Es ist jedoch noch unklar, wie die lokalisierte Sehbeeinträchtigung und die durch rtACS ausgelöste Neuromodulation die höheren kognitiven Verarbeitungsmechanismen im Gehirn beeinflusst.

Die neuronale Synchronisation, der zugrunde liegende Mechanismus von Verhalten und Denken, muss zeitlich und räumlich gut orchestriert sein, um fehlerfreie Interaktionen zwischen verschiedenen funktionellen Bereichen wie sensorimotorischer und multisensorischer Integration, Aufmerksamkeit oder Kognition zu gewährleisten. Funktionelle Konnektivitätsnetzwerke (FCN) bilden die physiologische Grundlage der Gehirnsynchronisation zur Integration neuronaler Aktivität. Sie sind nicht starr, sondern können sich unter pathologischen Bedingungen oder während mentaler oder Verhaltenszustände neu organisieren, Dies bietet einen Ansatz, um die Mechanismen der visuellen Kognition und die Analyse von Sehbeeinträchtigung und Sehwiederherstellung besser zu verstehen. Eng miteinander verbundene Knotencluster, sogenannte “Gemeinschaften“, interagieren in zeitabhängiger Weise im Gehirns des FCN, um komplexe kognitive Funktionen zu unterstützen. Es ist jedoch wenig bekannt, ob und wie verschiedene Knoten ihre neuronalen Interaktionen synchronisieren, um funktionale Gemeinschaften (”Module”) während der visuellen Verarbeitung zu bilden, und ob und wie diese Modularität nach einer Läsion (Fortschreiten oder Wiederherstellung) durch Neuromodulation beeinflusst wird.

Unter Verwendung des geschädigten Sehnervs als Paradigma haben wir nun die Dynamik des Gehirn-FCN untersucht, um dynamische Neukonfigurationen und Interaktionen vor und nach der nicht-invasiven rtACS-Neuromodulation besser zu verstehen. EEG-Aufzeichnungen wurden zeitlich auf die Präsentation visueller Reize abgestimmt, und die graphische Analyse neurophysiologischer Schwingungen wurde verwendet, um Millisekunden-FCN-Dynamik bei gesunden Probanden und bei Patienten mit Sehnervschäden vor und nach der Behandlung zu charakterisieren und mit der visuellen Leistung zu korrelieren.

Wir fanden heraus, dass schnelle und vorübergehende Synchronisationsmuster in den FCN des Gehirns beim Menschen in Millisekundenschnelle während der visuellen Verarbeitung entstehen und wieder verschwinden können. Diese rasche Reorganisation ist funktional relevant, da Störungen und Erholung nach der Behandlung mit Mikroströmen bei Patienten mit Sehnervschäden mit beeinträchtigter bzw. wiederhergestellter visueller Leistung korrelierten. Da die Wechselwirkungen von FCN-Hubs und Knoten in Millisekundenschnelle räumliche und zeitliche neuronale Synchronisation während der visuellen Verarbeitung und Wiederherstellung verwalten können, schlagen wir die ”Raumzeit im Gehirn” als ein grundlegendes Prinzip des menschlichen Geistes vor, nicht nur in der visuellen Kognition, sondern auch in der Sehwiederherstellung.

In beiden Patienten und Kontrollgruppen korrelierten lokale Intermodul-Interaktionen

mit der visuellen Leistung. Allerdings war die Wiederherstellung der Sehkraft bei Patienten nach der Behandlung mit rtACS mit einer verbesserten Interaktionsstärke der Pfade, die mit dem Aufmerksamkeitsmodul verbunden sind, assoziiert, und sie verbesserte die globale Modularität und erhöhte die Stabilität der FCN. Die zeitliche Koordination mehrerer kortikaler Module und die Intermodul-Interaktion sind funktional relevant für die visuelle Verarbeitung. Diese Modularität kann mit rtACS neuromoduliert werden, was eine ausgewogenere und stabilere multischichtige modulare Struktur für die visuelle Verarbeitung durch die Verbesserung der Interaktion neuronaler Pfade mit dem Aufmerksamkeitsnetzwerkmodul ermöglicht.

Die Behandlungseffizienz variiert jedoch erheblich zwischen den Probanden, und die Behandlungsergebnisse bleiben unvorhersehbar. Um individuelle Vorhersagen zur Wiederherstellung der Sehkraft zu identifizieren, wurden vorhandene Versuchsdaten von Patienten mit Sehnervschäden analysiert und mithilfe von Deep-Learning-Algorithmen trainiert. Auf diese Weise haben wir ein Vorhersagemodell zur Wiederherstellung der Sehkraft nach rtACS-Effekten entwickelt, indem wir die Knotenzentralitäten der funktionellen Gehirnnetzwerke während der visuellen Kognition von Patienten mit Sehnervschäden trainiert haben.

Darüber hinaus habe ich das Potenzial eines auf Deep Learning basierenden Frühwarnmodells analysiert, um potenzielle Sehfeldschäden in 'intakten' Sehfeldern zu identifizieren. Die Generalisierungsfähigkeit des Modells muss jedoch weiter untersucht werden.

Zusammenfassend zeigt diese Studie, dass schnelle und transiente Synchronisationsmuster in funktionellen Gehirnnetzwerken eine entscheidende Rolle bei der visuellen Verarbeitung und Genesung spielen, und schlägt "Brain Spacetime" als grundlegendes Prinzip vor. Die Behandlung mit rtACS bei Patienten mit Sehnervenschäden verbessert die Interaktionen zwischen den Modulen, insbesondere mit dem Aufmerksamkeitsnetzwerkmodul, und steigert die globale Modularität und Stabilität der funktionellen Gehirnnetzwerke. Darüber hinaus wurde ein auf Deep Learning basierendes Modell zur Vorhersage der Erholung der Sehleistung. Dies liefert nicht nur bessere Einblicke in individualisierte Behandlungsergebnisse sondern könnte potentiell von Vorteil sein frühzeitigere Interventionen zu Therapie von Sehschädigungen anbieten zu können.

Schlüsselwörter: Sehnervschaden; Gehirnnetzwerk; Graphentheorie; Kognition; Wechselstromstimulation; Gehirnstimulation; Mehrschichtige Modularität; EEG; Deep Learning.

Contents

List of Figures viii

List of Tables x

1 Introduction 1

1.1 Damage and Plasticity of the Visual System . . . 2

1.1.1 The Visual System . . . 2

1.1.2 Damage to the Visual System . . . 4

1.1.3 Vision Restoration Therapy . . . 5

1.1.4 Brain Stimulation for the Treatment of Neurological Disorders . . . 6

1.2 Brain Networks and Cognition . . . 9

1.2.1 Neuroimaging of Brain Activity . . . 9

1.2.2 Brain Connectome and Cognition . . . 11

1.2.3 Graph Theory in Brain Networks . . . 12

1.3 Artificial Intelligence (AI) in Medical Research . . . 13

1.3.1 Artificial Intelligence in Medicine . . . 13

1.3.2 Artificial Intelligence in Ophthalmology . . . 14

1.4 Research Objectives . . . 15

1.5 Thesis Outline . . . 15

2 Methods to Explore Spacetime of the Brain and Plasticity 19

2.1 Data Collection and Pre-processing . . . 19

2.1.1 Participants . . . 19

2.1.2 Visual Field Assessment . . . 19

2.1.3 EEG Recording of Visual Evoked pPotentials . . . 20

2.1.4 Repetitive Transorbital Alternating Current Stimulation (rtACS) . . . 21

2.1.5 EEG Pre-processing and Source Reconstruction of Brain Activities . . . 21

2.2 Network Metrics of Graph Models . . . 22

2.2.1 Defining of Brain Networks . . . 22

2.2.2 Global Network Measures . . . 22

2.2.3 Hubs and Node Centralities . . . 23

2.2.4 Multilayer Module Detection and Qualification . . . 23

2.3 Machine Learning and Deep Learning . . . 25

2.3.1 Artificial Neural Networks (ANN) . . . 26

2.3.2 Feedforward Neural Network (FFNN) . . . 26
2.3.3 Convolutional Neural Networks (CNN) . . . 27
2.3.4 Recurrent Neural Network (RNNs) . . . 28

3 Global Alteration and Adjustment in Visual Evoked Brain Network 31
3.1 Introduction . . . 31
3.2 rFCN Response to Visual Stimulus in Intact Vision Area (IVA) . . . 32
3.3 rFCN Response to Visual Stimulus in Areas of Residual Vision (ARV) . . . 32
3.4 Intact Area vs. Areas of Residual Vision . . . 34
3.5 Probing Global Network Adjustments using rtACS Neuromodulation in Patients . . . 37
3.6 Discussion . . . 37

4 Modulate Local Core Hubs and Nodes After Optic Nerve Damage 39
4.1 Introduction . . . 39
4.2 Brain Spacetime in Normal Subjects . . . 40
4.3 Brain Spacetime in Patients - Realignment of Node Centralities . . . 40
4.4 Probing Spacetime Causality of rtACS Neuromodulation in Patients . . . 43
4.5 Correlation between FCN Parameters and Visual Performance . . . 43
4.6 Discussion . . . 44

5 Modularity Dynamics of Brain Networks Following Local Damage 49
5.1 Introduction . . . 49
5.2 Multilayer Modularity Diagnostics . . . 50
5.3 Multilayer Modular Organization . . . 51
5.4 Representative Partitions in Dynamic Multilayer Networks . . . 54
5.5 The Architecture of Multilayer Networks in Optic Nerve Patients . . . 54
5.6 Interaction Strength Correlates with Performance . . . 54
5.7 Discussion . . . 57

6 Deep Learning of Brain Spacetime: Predicting Outcome of Vision Restoration following Non-invasive Brain Stimulation 63
6.1 Introduction . . . 63
6.2 Datasets and Preprocessing . . . 65
6.3 Deep Learning Algorithms and Models . . . 66
6.4 Training and Evaluation Metrics . . . 66
6.5 Results . . . 68

6.6 Discussion 70
6.7 Conclusions 74

7 Towards an Early Warning Model for Vision Loss Based on Deep Learning 75

7.1 Introduction 75
7.2 Dataset Preparation 76
7.3 Deep Learning Algorithms and Models 77
7.4 Training and Evaluation Metrics 78
7.5 Results 79
7.6 Discussion 83
7.7 Conclusion 85

8 Summary and Outlook 87

8.1 Network Science in Understanding Spacetime of the Brain 87
8.2 Non-invasive Brain Stimulation for Vision Restoration 88
8.3 Deep Learning Models for Vision Restoration and Early Warning 89
8.4 Outlook 89

References 91

A Appendix 119

B Ehrenerklärung 121

List of Figures

1.1 Schematic illustration of visual pathway and visual field deficits 3
1.2 Diagrammatic representation of brain stimulation techniques 7
1.3 Research Framework of the study 16
2.1 Typical perimetric visual field chart of a patient 20
2.2 Schematic representation of network parameters 23
2.3 Schematic representation of a multilayer network 25
2.4 General schematic of Feedforward Neural Network (FFNN) 27
2.5 Architecture of a conventional convolutional neural network (CNN) 27
2.6 Overview of the bidirectional long short-term memory (LSTM) model . . . 28
3.1 Group average values for global and node strength distribution between healthy and optic neuropathy patients 33
3.2 Transient dynamics of global rFCN parameters 33
3.3 Global and node PLV strength changes during visual related task in ARV . 35
3.4 Global network parameters comparison between valid hit and miss response to stimulation in ARV 35
3.5 Global and node strength difference between IVA and ARV in the high alpha band 36
3.6 The functional network measures difference between IVA and ARV during visual cognition 37
4.1 Hub score distribution and changes across time in high alpha FCN – Part 1 41
4.1 Hub score distribution and changes across time in high alpha FCN – Part 2 42
4.2 Imaging “Brain Spacetime” in visual processing 42
4.3 Significant node centralities as a function of the network state 42
4.4 Visual detection performance in patients correlate with network metrics . . 45
5.1 Comparison of real networks versus null networks 51
5.2 The presence of modular structure in real network compared to null networks 52
5.3 Modularity of multilayer networks for visually evoked brain networks 53
5.4 Comparison of FCN modularity and flexibility during visual processing in rtACS and sham patients group 53
5.5 Representative partitions of multilayer networks during visual processing . . 55
5.6 Modular allegiance between groups during visual processing 56
5.7 Schematic diagram of visual field distribution and correlations of interaction strength of modules with behavioral performance 58
6.1 Structure of the proposed feedforward neural network 67

6.2 Structure of the proposed bidirectional LSTM 67
6.3 Performance of Bi-LSTM model constructed using ARV and IVA data, respectively. 69
6.4 Performance of both FFNN and Bi-LSTM using PLV data from ARV in high alpha band. 70
6.5 Individual performance of LOSO cross-validation on Bi-LSTM 71
6.6 Individual performance of LOSO cross-validation on FFNN 72
6.7 Boxplot of MSE for FFNN and Bi-LSTM using LOSO cross-validation . . . 73
7.1 Schematic of the structure of the CNN model used in the study 78
7.2 Schematic of the structure of the FFNN model using networks as input data 79
7.3 Performance of CNN and FFNN models in beta band using COH networks data after 3-Fold cross validation 80
7.4 Performance of CNN and FFNN models using PLV networks data of beta band after 3-Fold cross validation 81
7.5 Performance comparison of the CNN and FFNN models using LOSO cross-validation in the beta frequency band 82
7.6 Boxplot of accuracy for FFNN and CNN models after using LOSO cross-validation in the beta band 82

List of Tables

6.1 MSE of the models for rtACS induced vision recovery prediction model using COH data after 3-fold cross-validation 68

6.2 MSE of the models for rtACS-induced vision recovery prediction model using PLV after 3-fold cross-validation 68

6.3 MSE of FFNN and Bi-LSTM models using COH data after LOSO cross-validation 70

6.4 MSE of FFNN and Bi-LSTM models using PLV data after LOSO cross-validation 71

7.1 Comparison of classification accuracy results across frequency bands using CNN and FFNN models 81

A.1 Subjects information 119

1 Introduction

There are different diseases affecting the optic nerve such as glaucoma, traumatic injury or Anterior ischemic optic neuropathy (AION), and the clinical manifestations include visual field defects, slowed reaction times, lower contrast, dyschromatopsia, foggy vision and abnormal papillary response (Martínez-Lapiscina et al., 2014; Medeiros et al., 2005). Optic nerve damage is generally viewed as a purely sensory and not a cognitive problem.

However, some "optic nerve diseases" are also associated with damage to different brain structures. For example, glaucomatous optic nerve damage is associated with degeneration of retinafugal brain regions such as the lateral geniculate nucleus of the thalamus, visual cortex and even non-visual structures like the amygdala (Frezzotti et al., 2014; Nuzzi et al., 2018; Wang et al., 2016; Williams et al., 2013). Also Dominant Optic Atrophy (DOA) has not only a significant atrophy of the optic nerves but also significantly lower mean diffusivity, axial and radial diffusivity in the white matter of the cerebellum, brainstem, thalamus, fronto-occipital-temporal lobes, including the cingulum, corpus callosum, corticospinal tract and optic radiation bilaterally (Rocca et al., 2015).

Given the wide spread central changes in a disease which is peripheral, the question arises, how a local "sensory" problem impacts the upstream cognitive processing mechanisms in the brain. In my search to better understand response fluctuations and to find means to improve or restore vision, I wish to further explore the physiology of global FCN changes in optic nerve patients. Here, areas of residual vision (ARV, also known as "relative defects") are of particular interest because these regions are not fully blind but partially impaired, with some degree of residual vision. ARV are rather variable and therefore of particular clinical interest because activating them leads to vision recovery (Sabel et al., 2011b) and this vision restoration can be achieved by behavioural vision training (Kasten et al., 1998; Poggel et al., 2004; Veraart et al., 2003) or non-invasive brain current stimulation. Because our recent findings that rtACS alters resting state FCN in patients with vision loss, optic nerve damage is a preferred lesion paradigm to explore the role of FCN in normal and abnormal vision.

Functional connectivity networks, the physiological basis of behaviour, and their alterations have been studied recently in normal and diseased subjects (Bullmore and Sporns, 2012). In patients with optic nerve damage, for example, FCN changes are observed in the resting state in the alpha and theta band (Bola et al., 2014). FCN during a cognitive decision-making task show transient FCN alteration such as stronger clustering and lower modularity (Bola and Sabel, 2015). Yet, it is not yet known, if the rapid and transient network reorganization observed during cognitive processing in normal brains is altered by optic nerve damage.

Graph modelling of the brain, as proposed by the graph theory (Bullmore and Sporns, 2009), is a valuable measure of topological properties of complex brain networks such as clustering coefficient, small-world attributes, and heterogeneous degree distributions (Bassett and Bullmore, 2006; Bullmore and Sporns, 2009). Complex networks have been studied in many cognitive emotional disorders which indicate abnormal connectivity syndromes between brain regions (Catani and Ffytche, 2005) like Alzheimer's disease (Pievani et al., 2011), schizophrenia (Lynall et al., 2010; Yu et al., 2015), early blindness (Shu et al., 2009) or optic nerve damage (Bola et al., 2014). Thus, the value of graph theory in cog-

nitive and clinical neuroscience is now well recognized.

The EEG can measure neuronal oscillatory activity with a high temporal resolution and it can effectively estimate temporal processing of the highly dynamic functional brain network with modern techniques (Mantini et al., 2007; Stam et al., 2006). There are different imaging methods that can chart the complexity of the human brain networks including the functional MRI (fMRI) (Fox et al., 2005) and EEG (van den Heuvel et al., 2008). In contrast to MRI connectivity studies, the excellent time resolution of electroencephalography (EEG) can reveal time-locked FCN changes in the msec.-range as revealed by the evoked-response network (Bola and Sabel, 2015).

Transcranial alternating current stimulation (rtACS) has been proposed to modulate the ongoing brain activity rhythm using oscillatory current stimulation on the human scalp. rtACS can influence cortical excitability, motor function and higher order cognition. It has been suggested that rtACS can influence motor function (Brignani et al., 2013; Feurra et al., 2011), enhance individual EEG alpha activity (Zaehle et al., 2010), and have a long lasting effect on endogenous EEG power (Kasten et al., 2016; Neuling et al., 2013). But the specific mechanism underlying these effects is still unknown. Two main suggestions are entrainment of brain oscillations by rtACS (Antal et al.; Herrmann et al., 2013) and spike-timing dependent plasticity via synaptic changes (Vossen et al., 2015; Zaehle et al., 2010). In the present study, rtACS was used as non-invasive brain stimulation to explore its mechanism from a functional network reorganization perspective.

Therefore, using the method of "event related network analysis" (ERNA), I characterized how brain functional connectivity networks react to visual stimuli presented either inside the intact visual field regions or in areas of residual vision in damaged visual fields. My hypothesis is that optic nerve damage not only leads to local anatomical damage but also to global and local alterations in the brain functional connectivity network during the cognitive state. I then analysed the possibility of vision restoration by FCN comparison in pre and post rtACS. Specifically, I tried to describe the brain modularity and their community interaction structure, and to explore rtACS influences on local communities. Finally, I wish to build a vision recovery prediction model to support the progress towards improved clinical treatment of visual system disorders.

1.1 Damage and Plasticity of the Visual System

1.1.1 The Visual System

Vision has been studied extensively as the most important and basic sense. The visual system, a prominent part of the central nervous system, has also been the focus of intense research. It acts as a receiver of information and a processor of visual sensory input, helping us to understand our environment and contributing to our successful navigation in physical space and interaction with surroundings objects.

The human visual system is responsible for a series of visual information processing, from the knowledge acquisition of the surroundings by the sensory organ to the extraction and interpretation of information by the brain cortex. It comprises several major components including the retina, optic nerve, optic chiasm, lateral geniculate nucleus (LGN) and visual cortex of the occipital lobe.

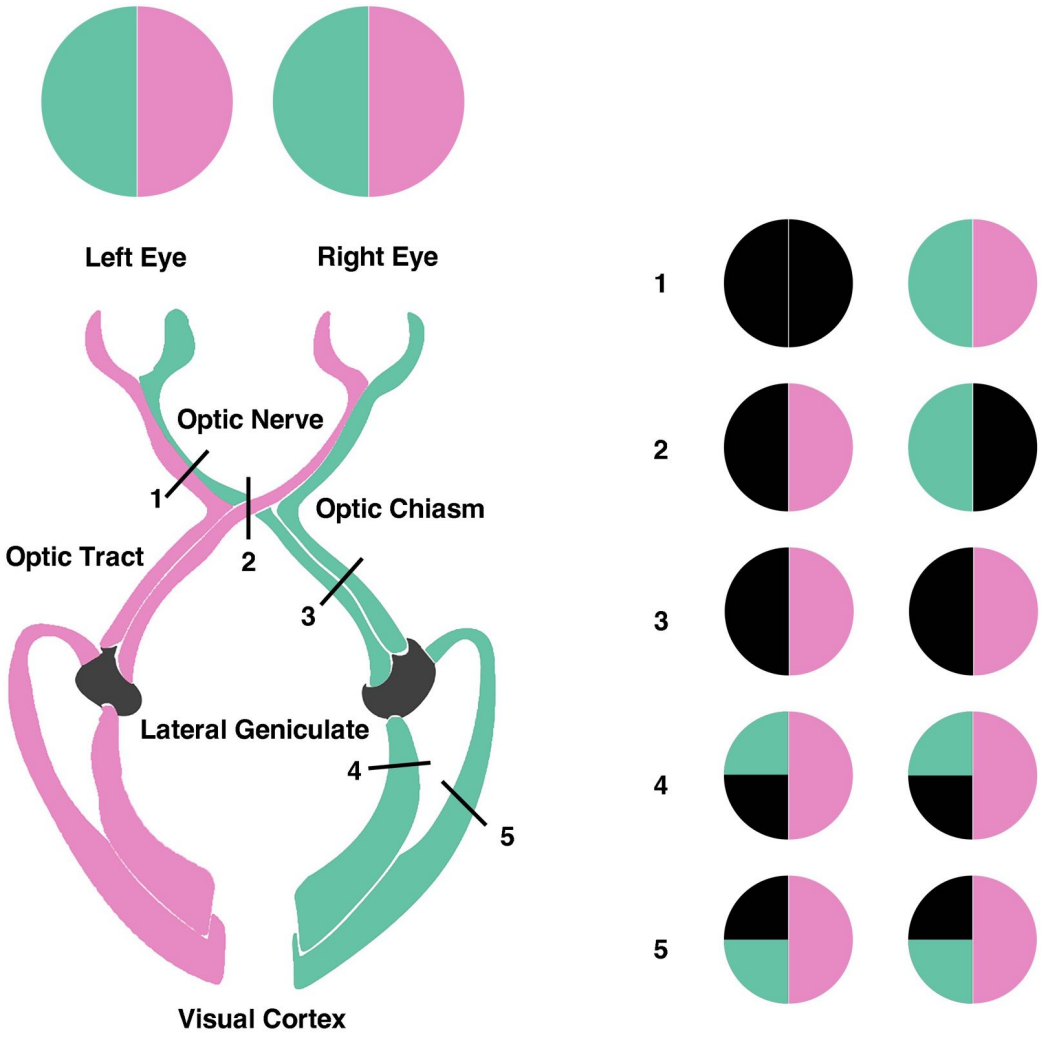

Figure 1.1: Schematic illustration of visual pathway and visual field deficits caused by lesions in the visual pathway.

There are two types of photoreceptors in the retina, rods and cons, for the detection of light. The optic nerve is responsible for sending the detected input from the retina to the brain, which consists of more than a million nerve fibers. The optic nerves cross the optic chiasm, allowing the visual cortex to receive information from both eyes. The LGN organized all sensory information from the retina. Once inside the brain, the input received from the retina begins to be processed within the brain by visual cortex, including V1 as the primary visual cortex or striate cortex, as well as secondary visual areas such as V2, V3, V4 and V5/MT, for further interpretation. Fig. 1.1 shows a schematic structure of the human visual system.

During visual perception, light enters the eye and then hits photosensitive cells in the retina, triggering electrical signals that are subsequently transmitted through the optic nerve to the lateral geniculate nucleus and finally reach the visual cortex within the brain for further processing. The brain can then build a representation of the surrounding environmental stimuli based on these electrical impulses and take action to accomplish complex tasks. The various types of visual processing include color vision, adaption,

depth perception, form perception, illusions, motion perception and more.

The brain plays a crucial role in this visual process. There are more than 30 visual areas in the brain that interact with each other tremendously. Studies of how the brain is organized during visual processing can produce fundamental insights into higher-order brain functions like cognition, behavior or learning. Generally, the visual information passing through the cortex hierarchy may be processed into two streams, one going to the ventral pathway to the temporal lobe and another to the dorsal pathway to the parietal lobe (Mishkin and Ungerleider, 1982). The ventral pathway, also called the "what" pathway, is usually involved in object discrimination, such as object identification and recognition. While the dorsal pathway, on the other hand, is referred to as "where" pathway and deals with spatial localization and how to interact with specific visual stimuli. However, there is still much debate about the independence of these two streams, since dorsal-ventral stream integration occurs (Budisavljevic et al., 2018; Farivar, 2009).

Although a great deal is known about the visual system in general, much remains to be understood about how activity in different areas of the visual cortex – and visual related attention areas – are efficiently reorganized not only spatially but also at high temporal resolution to accomplish higher-order cognition.

1.1.2 Damage to the Visual System

Ideally, the visual pathway is efficient and smooth in its transmission of information, from the optic nerve to the visual cortex in the brain. However, this visual processing can be interrupted if damage appears along this pathway, such as damage to the eye, within the visual pathways or in the visual cortex. These disruptions could cause multiple visual impairments, including reduced visual acuity, diminished contrast and light brightness sensitivity and visual field defect among others.

There are numerous abnormalities that can damage or compress the visual pathways, resulting in vision loss or other symptoms. For example, eye diseases that affect the retina include age-related macular degeneration (AMD), a degenerative disease that affects the macula of the retina; diabetic retinopathy, defined as a complication of diabetes that affects the blood vessels of the retina; and retinitis pigmentosa, a genetic disorder that can damage the retina and the LGN leading to progressive vision loss. Glaucoma is an eye illness involving damage of the optic nerve and the LGN, including primary open-angle glaucoma, angle-closure glaucoma, congenital glaucoma and secondary glaucoma, which may lead to progressive loss of peripheral vision. Optic neuritis, an inflammation of the optic nerve, can impair color vision and result in an abrupt loss of central or peripheral vision. Additionally, gliomas, a type of brain tumor, can develop in the region of the optic chiasm and cause blindness. Another significant contributor to blindness is impairment to the visual cortex, such as cortical blindness, which is commonly brought on by stroke or traumatic brain injury.

Different defects of the visual pathway may evoke various vision problems. But almost all kinds of vision related diseases lead to impaired visual field. The visual field refers to the entire area of space that can be perceived by the eye when looking straight ahead in stationary state. It can be measured through perimetry testing. Additionally, the pattern of visual field defects also varies with the type of disease. Visual field defects in AMD often appear in central vision, leaving intact peripheral vision. Glaucoma typically

causes an initial loss of peripheral vision, while central vision will also be involved as the glaucoma progresses. However, diabetic retinopathy can result in blind patches, also known as scotomas, that are often present in the peripheral visual field. And hemianopsia is characterized by a loss of vision in half of the visual field. Fig. 1.1 is an illustration of visual field scenarios of different eye and brain diseases.

1.1.3 Vision Restoration Therapy

Visual impairment, which can range from limited vision to blindness, describes a broad loss of visual function. These complete or partial vision losses can significantly affect a person's ability to maintain independence and quality of life. It also has substantial impact to the economic and society. Therefore, it is crucial to develop a technology and vision restoration therapies in order to advance our comprehension of the underlying causes of visual impairment and ways to help patients. In addition, it offers patients with visual impairments the opportunity to accomplish some visual performance goals, enhancing their quality of life.

Vision loss is usually considered irreversible, despite the availability of different medications and surgery treatment that aim to slow down or prevent further vision loss. However, a variety of considerable vision restoration therapies, such as vision training, gene therapy, brain stimulation and others have been proposed to improve or restore visual function that has been lost.

Vision training refers to a type of therapy that aims to improve visual abilities and performance through a series of exercises and activities. One of the approaches most commonly used in vision training is perceptual learning. There is increasing evidence showing improvement of perceptive capacity in amblyopia (Rodán et al., 2022) and presbyopia (Deveau and Seitz, 2014) through repetitive training of a visual task. And training is also effective in other diseases such as visual cortex stroke (Kasten et al., 1998) and glaucoma (Sabel and Gudlin, 2014).

Depending on the underlying pathophysiology, the electrode-based visual prosthesis can be implanted in the retina, optic nerve, LGN or cortex to restore visual perception by targeting the most efficient area along the visual pathway. It can interface directly with the neural tissue. Although, the concerns of tissue and cell damage caused by invasive implantation, the limited spatial resolution and data transmission still need further study; Stem cell therapy attempts to transplant healthy stem cells into the eye to replace damaged or diseased cells and restore vision. It allows the derivation of new photoreceptor cells, which are subsequently integrated into existing retinal circuits; And finally, using viral vectors, optogenetic approaches can precisely transfer genes encoding optic proteins into targeted tissues and cell populations, allowing for excellent temporal and spatial resolution. The cells are then stimulated and controlled by light through expressed proteins to restore vision. However, the limitation is its restriction of depth through tissue and clinical trials with patients are still underway.

Moreover, visual perception is not only a local activity of the brain, but also a coordination of distributed brain regions that requires synchronization of different visual and non-visual brain sub-networks. De-synchronization among different regions in brain network may result in impaired visual function. Therefore, brain network modulation may be a potential mechanism to activate any residual vision.

Residual vision activation theory (Sabel et al., 2011b) focuses on areas of partial visual functions to achieve vision reactivation. In general, patients' responses to visual stimuli in the residual visual field are uncertain and vary greatly on repeated testing due to impairment. However, most patients retain residual structure and function after damage and have hidden recovery potential, especially in these gray areas of the visual field that are not completely blinded. The recovery potentials of residual visual field areas after therapy can be easily quantified through perimetric vision testing. Beyond residual visual amplification, whether and how neuronal networks change and how functional brain connections are reorganized locally and globally to vision restoration therapies remains unclear, which will be further explored in my study. In these vision restoration therapies that reactivate residual vision, brain stimulation appears to offer a promising rehabilitation potential (Sabel et al., 2018).

1.1.4 Brain Stimulation for the Treatment of Neurological Disorders

Brain stimulation techniques have become one of the most acceptable neuromodulation tools for the treatment of various neurological or psychiatric disorders in recent years. By modulating cognitive functions, brain stimulation methods have shown promising effects on Alzheimer's disease (AD), obsessive-compulsive disorder, post-traumatic stress disorder, pain, epilepsy and movement disorders. Brain stimulation includes invasive brain stimulation (IBS) and non-invasive brain stimulation (NIBS) (Fig. 1.2).

IBS involves deep brain stimulation (DBS) and invasive vagus nerve stimulation (iVNS). Electrical stimulators are implanted directly over specific brain structures during DBS in order to modulate dysregulated neural circuits. In addition to the continuous stimulation applied to the target structure by conventional DBS, adaptive DBS allows real-time adjustment of stimulation parameters according to the patients' functional status to achieve symptom relief especially in common DBS indications for movement disorders, such as Parkinson's disease and essential tremor (Guidetti et al., 2021). However, continuous and uninterrupted stimulators remain the dominant option of treatment, apart from technical drawbacks, the unrobust of adaptive DBS as an established treatment for movement disorders needs to be overcome.

The vagus nerve as the longest cranial nerve, consists of a complex neuro-endocrine-immune network that establishes a vital bridge between the brain and surrounding organs, to maintain homeostasis. With a subcutaneously implanted device, iVNS can send electrical impulses through the left vagus nerve to modulate the autonomic nerve. It has been commonly used as an adjunctive treatment for seizures and chronic or recurrent depression in adults. There are also ongoing clinical trials using iVNS for the treatment of heart failure. Yet iVNS may cause bradycardia and/or rarely contractions due to implantation.

The most prominent of currently used NIBS methods includes electroconvulsive therapy (ECT), transcranial magnetic stimulation (TMS), and transcranial electrical stimulation (tES). ECT is a controversial therapy that induces seizures through strong electrical stimulation of the brain and can be used to treat psychotic disorders. It is effective and currently available for the treatment of patients with severe depression (Rhee et al., 2022), or mania (Elias et al., 2021). TMS is a technology that can use magnetic pulses to produce neurological effects in the brain (Hallett, 2007). The stimulation of nerve cells is achieved by the electric currents induced from the electromagnetic device (magnetic coil).

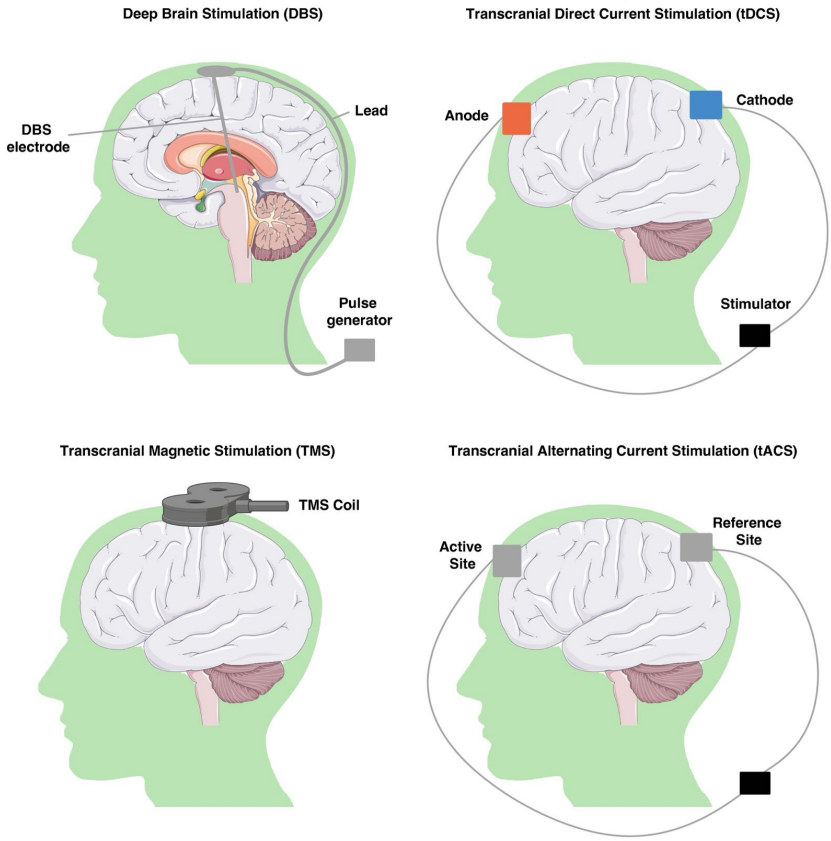

Figure 1.2: Diagrammatic representation of brain stimulation techniques.

Most TMS studies have been conducted on motor cortex. TMS that can generate rapid succession of pulses, called repetitive TMS (rTMS), has been studied as a treatment for interrupting migraine headaches or for rehabilitating of addicted brain (Diana et al., 2017) and psychiatric disorders such as depression (Cappon et al., 2022; Ferrucci et al., 2021). rTMS also contributes to brain plasticity in motor recovery after stroke (Agarwal et al., 2019).

tES is considered to be well tolerated as a non-invasive method of neurostimulation. It allows the use of low intensity direct or alternating currents to modulate spontaneous central activity, producing reorganizations in neural networks. Several major methods of delivering current to the brain have been intensively studied in recent years that differ according to the pattern of the current, including transcranial direct current stimulation (tDCS), transcranial alternating current stimulation (rtACS), and transcranial random noise stimulation (tRNS). These methods use electrical currents that can pass through the skull and reach the underlying brain tissue transcranially. Although the neurophysiological mechanisms underlying the operation of tES are still not fully understood, studies have identified stimulation effects of tES that are related to the initial state and stimulation location.

The administration of tDCS is quite simple. A low intensity constant direct current (usually 0.5-2mA) is typically used to enter the brain from the anode, travel through the tissue, and exit from the cathode. The current of tDCS activates not only the area of interest under the electrodes, but also spans other cortical and subcortical areas. Combined

with the poor electrical conductivity of the brain, the stimulation efficiency of tDCS is low, with at least 50% of the current lost to other surrounding tissues. In most studies, anodal stimulation increased tissue excitability, whereas cathodal stimulation diminished tissue excitability through depolarization and hyperpolarization of membrane potentials (Nitsche and Paulus, 2000; Radman et al., 2009; Summers et al., 2016). For example, motor skill learning can be enhanced by anodal stimulation on motor cortex (Fritsch et al., 2010). However, there are also some exceptions with no effect or opposite pattern (Accornero et al., 2007; Dockery et al., 2009; Terhune et al., 2011). The effectiveness of tDCS has been tested in the reduction of pain (Luedtke et al., 2015), improvement in dyskinesias and verbal fluency of parkinsonian patients (Ferrucci et al., 2016; Pereira et al., 2013), facilitation of post-stroke motor learning (Kang et al., 2016), improvement of speech and language performance (Campana et al., 2015; Marangolo et al., 2014) and alleviation of negative symptoms in various neuropsychiatric disorders (Brunelin et al., 2012; Brunoni et al., 2013; Hill et al., 2016), and also enhancement of working memory in healthy populations.

Unlike tDCS, which regulates the excitability threshold of neuronal membrane potentials through constant current, rtACS interacts directly with neural activity by a specific frequency range of non-constant alternating current, such as sinusoidal or rectangular waves, leading to intrinsic cortical oscillations (Antal and Paulus, 2013). Brain network oscillates differently in various ongoing cognitive processes (Herrmann et al., 2013). Therefore, the application of frequency-specific stimulation may affect the synchronization patterns of those neural network oscillations, causing changes in behavior or cognition (Fröhlich et al., 2015; Herrmann et al., 2016). The potential neuromodulation effects of rtACS have been studied in healthy subjects, including improvements in working memory capacity (Jaušovec et al., 2014; Meiron and Lavidor, 2014), retrieval accuracy (Fresnoza et al., 2018) and contrast detection (Laczó et al., 2012). Furthermore, rtACS facilitates in several psychiatric disorders, such as reduction in the delusions (Sreeraj et al., 2020) and improvement of auditory hallucinations (Ahn et al., 2019) in schizophrenia. In addition, rtACS appears to be feasible in vision restoration after optic neuropathy with increased defected visual field and vision related quality of life (Gall et al., 2011, 2016). To better understand the exact mechanisms of rtACS, especially the potential roles of rtACS in neural network oscillations, here I investigated the pattern of visually evoked brain networks before and after rtACS treatment.

tRNS applied alternate current with randomly assigned amplitude and frequency to the scalp. Studies in healthy subjects have shown excitability on motor cortex (Chaieb et al., 2011; Terney et al., 2008) and better accuracy on the perceptual task (Fertonani et al., 2011) in high frequency tRNS. In addition, tRNS induces short and long-term enhancement of learning and high level brain function with an efficient neurovascular coupling (Snowball et al., 2013). In addition to these traditional stimulation methods, the potential of other technological applications, such as transcranial focused ultrasound (Gorick et al., 2022; Krishna et al., 2018; Sarica et al., 2022) and photobiomodulation (Caldieraro and Cassano, 2019; Mosilhy et al., 2022; Salehpour et al., 2018), have been reported to modulate the inhibition or excitation of cellular activity.

Brain stimulation provides a distinctive opportunity to directly manipulate neural processes, enabling us to gain a deeper understanding of the mechanisms underlying various brain disorders from a cognitive and neurobiological basis. Moreover, with advances in

high density localization and depth systems, it offers novel techniques to intervene neural networks in the neurogenesis and achieve neuromodulation to further unfold the plasticity of the human brain.

1.2 Brain Networks and Cognition

It is generally known that vision, like other mental functions, are supported by brain networks which have functional connectivity interacting in complex neuronal networks. The functional brain network can be studied with different techniques that record the brain´s hemodynamic, magnetic or electric signals using techniques such as like electroencephalography (EEG), magnetoencephalography (MEG) and functional magnetic resonance imaging (fMRI) which can uncover neuronal oscillatory activity of the normal or diseased brain. For example, functional connectivity analysis research was carried out with chronic tinnitus patients using resting state MEG to estimated directed functional connectivity of the resting brain to identify the structure of intrinsic cortical networks which revealed a decrease in efficiency and small-worldness of tinnitus patients (Paraskevopoulos et al., 2019). Research on schizophrenia patients used fMRI to identify alterations in schizophrenia genetic risk on dynamic functional brain networks during working memory (Braun et al., 2016). The functional connectivity analysis characterized by EEG–functional magnetic resonance imaging (fMRI) datasets in patients with idiopathic generalized epilepsy found BOLD activation in the thalamus, the frontomesial cortex, and the cerebellum and BOLD deactivation in default mode areas (Moeller et al., 2011).

To analyze brain networks, graph theory has been developed and is now widely used in cognitive and clinical neuroscience. It is an accepted and useful method to investigate multiple fields of application in neuroscience to characterize network topological properties.

1.2.1 Neuroimaging of Brain Activity

Neuroimaging is able to image nervous system for live human by using radiological, magnetic resonance and other technologies, such as computed tomography (CT), magnetic resonance imaging (MRI), positron emission tomography (PET), magnetoencephalography (MEG), and electroencephalography (EEG). There is a growing body of research demonstrating that neuroimaging plays an important role not only in the diagnosis of disease, but also in the assessment of brain activation. They have been commonly used to measure structural morphometry and functional brain activities, especially in pathophysiological conditions.

Computed tomography (CT) allows for structural and anatomical evaluation of tissues from cross-sectional images. With its ease of acquisition and diagnostic capabilities, CT remains the recommended imaging method for various surgical conditions, particularly in skull (Stiell et al., 2001), bone (Pickhardt et al., 2013) and spinal evaluation (Dunham et al., 2008). In addition, it is the modality of choice for the evaluation of acute intracranial hemorrhage (Yuh et al., 2021).

Magnetic resonance imaging (MRI) is an alternative cross-sectional imaging modality that has been widely utilized to evaluate tissues and their biomedical properties, including volumetric and morphological MRI to assess anatomical structures, diffusion MRI (dMRI)

to assess white matter, MR spectroscopic imaging to assess metabolite concentrations, and functional MRI to assess neuronal activation.

Volumetric and morphological MRI can quantify shape or structural changes within the brain by evaluating relative regional volume changes using atlas-based segmentation method, or by assessing changes in the alignment of the nuclei and sub-nuclei of a region, providing fine-grained information on cortical patterns. For example, visualization of the hippocampus by high resolution structural MRI not only identified changes in the morphological features of the hippocampal dentition and demonstrated its association with memory, but also allowed for clear visualization of its internal architecture (Beattie et al., 2017; Ver Hoef et al., 2021). dMRI reveals detailed architecture of tissue by measurement of the molecular diffusion of water, particularly in the white matter and structural connectivity. dMRI has been widely used in stroke recovery to understand the location and severity of strokes (DiBella et al., 2022; Lampinen et al., 2021). It is also a promising method for exploring connectomics as well as pathological changes in neurological studies of the brain (Jeurissen et al., 2019; Harrison et al., 2020). In addition, MR spectroscopic imaging has generally been used to quantify the metabolic alterations of human brain glucose and neurotransmitter metabolism, providing metabolic impairment information which was linked to several neurological disorders (Bednarik et al., 2023; Lipka et al., 2023; Niess et al., 2023). fMRI depicts cortical activation by measuring the changes of blood oxygen level dependent in the brain. It has become a powerful tool in neuroscience research, especially in the functional connectivity of cognitive networks. fMRI offers several advantages in brain analysis, being non-invasive, well tolerated, and providing millimeter-level spatial resolution. The application of fMRI in mapping cognitive functions, such as attention, language processing, memory (Shurtleff et al., 2022; Mekki et al., 2022; Itthipuripat et al., 2019), and detecting brain alterations in neurological disorders (Johansson et al., 2022; Yan et al., 2020) has been well established over the past decades. However, the temporal resolution of fMRI is several seconds which has a significant limitation.

Compared to fMRI, MEG provides a more direct measure of neural activity by evaluating the oscillating magnetic field resulting from the electrical activity of neurons. It has been commonly exploited to analyze large scale brain activities with a high temporal resolution as EEG and good spatial resolution combined with fMRI. More recently, MEG has been used to identify complex dynamics of task and object processing to better understand cognition in humans (Cichy et al., 2016; Hebart et al., 2018). MEG is also appealing to track spatiotemporal brain activity of word recognition during spoken language interpretation (Klimovich-Gray et al., 2019). In addition, MEG can also provide reliable localization for seizures (Alkawadri et al., 2018).

However, MEG has relatively high acquisition and maintenance costs compared to EEG, which measures direct and real-time millisecond brain electric fields (postsynaptic potentials) generated by current flow of neuron populations. The EEG could be measured if neurons were activated simultaneously. With its long history and wide range of applications, EEG can not only provide solutions to find promising features for clinical diagnosis (Slater et al., 2022)(Slater et al., 2022), but it can also be used as a neuroimaging method to map brain activity to better understand the neural mechanisms underlying complex brain functions (Fernandez and Lüthi, 2020; Vecchio et al., 2019).

With its excellent temporal resolution and in combination with underlying source ac-

tivity estimation, the EEG becomes feasible to characterize various aspects of brain activities, including brain states, the spatial-temporal dynamics of brain connectivity, as well as the extent to parallel or serial information processing of brain networks under cognition. EEG is also a vital instrument for analyzing neurological disorders, such as Attention Deficit/Hyperactivity Disorder (ADHD) (Slater et al., 2022), chronic neuropathic pain (Mussigmann et al., 2022) or depression (de Aguiar Neto and Rosa, 2019).

In this project, I therefore use EEG signals and aim to provide a comprehensive and complete connectome analysis by studying the spatial-temporal dynamic organization of visually related brain networks.

1.2.2 Brain Connectome and Cognition

These sets of advances in neuroimaging methods enabled insights into the complete connectivity mapping of the nervous system, from micrographs of synaptic or cells, and axons connections, to the mesoscopic connectome at cellular level between neuronal types, to macroscopic graphing of anatomical connections among cortical parcellations. These diverse hierarchy of connections were described as connectome (Elam et al., 2021; Swanson and Lichtman, 2016).

The microscale connectome provides a clear view of the connectivity between individual neurons at the synaptic level and typically relies on electron microscopy (EM). Whole-brain microscale connectivity mapping has been realized in some simple species such as C. elegans (Varshney et al., 2011), Drosophila (Takemura et al., 2013), zebrafish (Hildebrand et al., 2017), etc., but studies of the mammalian brain are still limited to circuits activity in the cerebral cortex to analyze neuronal connections (Lee et al., 2016; Schmidt et al., 2017). The mesoscopic connectome has also been widely used in neuronal circuit related studies, through utilization of various tracing methods (Callaway and Luo, 2015; Schwarz et al., 2015; Zeng, 2018). Imaging connectomes at macroscopic scale not only characterize the interactions between anatomically distinct brain regions, but also reflect functional connectivity. It is also widely employed in human brain due to its non-invasive approaches such as DTI, dMRI, fMRI and M/EEG et al (Craddock et al., 2013; Glasser et al., 2016; Herbet and Duffau, 2020). In particular, connectome related studies using diffusion MRI have not only introduces the possibility of reconstruction of white matter fiber connections and estimation of fiber orientation in the living human brain (Fan et al., 2014; Jones et al., 2018; McNab et al., 2013), but also of assessment of tissue microstructure properties such as axon diameter (Dyrby et al., 2013; Sepehrband et al., 2016).

These studies of multiscale connectomes have set the stage for understanding the organization principles of brain regions during cognition and emotions. Studies in the field of developmental neuroscience have demonstrated the relationships between white matter microstructure development and high level cognitive processes, especially in executive functions (Wang et al., 2018; Fiske and Holmboe, 2019; Goddings et al., 2021). And in the analysis of human language connectome, scientists have explored direct, functional and effective connections between cortical regions, providing new insights into the brain regions involved in language (Friederici et al., 2017; Milton et al., 2021; Rolls et al., 2022). In addition, advances in the brain connectome are crucial to the study of cognitive disorders. Impaired cognition, for example, has been found to be associated with increased axon diameter and decreased axon density in the corpus callosum in patients with multiple

sclerosis (Huang et al., 2019). Moreover, a range of brain connectome studies have been conducted in disorders affecting the brain such as epilepsy, Alzheimer's Disease and low vision (Chu et al., 2023; Kammen et al., 2016; Sun et al., 2020).

1.2.3 Graph Theory in Brain Networks

Based on the key concept of "connectome", how brain networks are constructed and estimated across multiple spatial and temporal scales is critical for comprehensively mapping brain structure, function, and exploring brain-behavior relationships. Graph theory provides an effective solution for modeling and evaluating the brain network dynamics from the perspective of complex network science, in which the entire brain network was modeled as a graph with nodes and the links constituted between them (Bullmore and Sporns, 2009).

Graph theory is a primary and generalized method in the analysis of complex networks. Complex networks often contain complex and elaborate interactions with each other, making it difficult to assess each individual connection. The core principle of graph theory is focusing on the topology of graph, that is, how the links were organized. This facilitates the extraction of key information from complex networks, while ignoring the detailed connections among nodes. In graph theory, the key topological principles have been shown to be universal for superficially different complex networks. They share common topological properties across systems such as hubs, communities and small-worlds. These network topologies have been observed in several neuronal networks (Newman, 2003; Bullmore and Sporns, 2009; Fornito et al., 2013). By analyzing these properties, graph theory contributes to the exploration of cognitive processes and establishes links between morphological structures and brain functions (Sporns et al., 2005; Griffa et al., 2013).

Advances of graph theory have made it a powerful tool for studying the structural and functional organization of brain networks in depression, showing weakened functional intra-modular connections in default and limbic networks, as well as altered structural local centralities (Yun and Kim, 2021). The importance of graph theory in Alzheimer's disease has also been highlighted in tracking disease progression and making early diagnoses. In fact, investigation on the topology of gray matter networks revealed that path lengths decrease 13 years before the onset of Alzheimer's symptoms (Stam et al., 2009; Vermunt et al., 2020). More recently, the distinctive features of network in neurological disorders such as epilepsy were explored applying graph theory to characterize network dynamics including hub mapping (Royer et al., 2022) and predict epileptic seizure (Christiaen et al., 2020; Vecchio et al., 2017). Furthermore, application of graph theory has also provided new insights into the practice of neurosurgery with the goal to improve patient safety and preserve functional brain regions (Tanglay et al., 2023).

In addition to measuring macroscopic connectivity between brain regions, graph theory has also been used to characterize functional or structural networks at the microscopic neuronal level, from functional calcium imaging or structural electron microscopy. Combining graph theory with calcium imaging provides a better understanding of the spontaneous activity of single cell or neural assemblies, such as the biological network of neurons in mouse auditory cortex (Betzel et al., 2019), the developmental process in zebrafish (Avitan et al., 2017), or the process of looming detection in Xenopus tadpoles (Khakhalin, 2019).

Overall, using graph theory to study structural or functional brain network opens up

greater understanding of the topological organization of brain networks and their dynamics during cognitive processes, as shown by common complex network features including small-world topology, modularity and hub distributions. This knowledge can be useful not only for developing, validating, and comparing computational models of specific neural networks at multiple resolutions, but also for understanding the vulnerability of brain networks to lesions. This could be applied, for example, in labeling or predicting the risk of disease onset, or in measuring the therapeutic effect of interventional treatments on functional networks.

Therefore, this study also incorporates graph theoretic methods to systematically model brain network lesions during visual processing in visually impaired patients and to measure functional network recovery following non-invasive electrical stimulation treatment (Bola et al., 2014, 2015). A variety of graph-theoretic properties were also utilized to predict the treatment effect of visual improvement in patients.

1.3 Artificial Intelligence (AI) in Medical Research

Artificial intelligence (AI), as a disruptive technology, has been widely used to solve high level pattern recognition such as data mining, language processing and image/speech recognition. The principle of AI aims to develop algorithms that mimic human intelligence so that computers could be made to think and reason like humans. To achieve this goal, various approaches have been developed, such as machine learning and deep learning. As one of the most promising application areas of AI, biomedical applications have displayed promising potentials from automated medical imaging analysis to clinical diagnosis and prognosis (Rajkomar et al., 2019).

1.3.1 Artificial Intelligence in Medicine

In recent years, Artificial Intelligence has received increasing attention in the field of medicine, especially in medical imaging analysis. Recent studies have demonstrated the potential of AI in developing automated diagnostic and predictive tools for various diseases. Significantly, convolutional neural networks (CNNs) (Krizhevsky et al., 2012)as a subset technology of deep learning neural networks, have shown to be powerful in image recognition, and segmentation, leading it to be an essential part of AI in medical applications.

CNN is a promising tool in the area of radiology (Pianykh et al., 2020). Combined with CT or MRI data, CNN models were also capable of detecting emergent neurological disorders such as hemorrhage, mass effect (Prevedello et al., 2017), or predicting isocitrate dehydrogenase mutation status in gliomas which is the malignant primary brain tumor in adults (Choi et al., 2021). CNN based lesion detection models, especially those that utilize chest radiographs to classify tuberculosis or frontal chest abnormalities, were able to achieve remarkably high levels of accuracy for clinical applications. In addition, CNN models have also been trained in applications for pulmonology like lung cancer treatment (Xu et al., 2019) or lung nodule detection and classification (Nasrullah et al., 2019), as well as for liver diseases (Cheng et al., 2021) or colorectal cancer (Rompianesi et al., 2022).

There has also been a growing trend of AI neural networks being used in dermatology for skin cancer detection and diagnosis. A prominent study using a clinical and dermo-

scopic images demonstrated that the performance of CNN models was comparable or even superior to that of all dermatologists when it came to classifying the most common and deadliest skin cancer lesions (Esteva et al., 2017). Other recently published studies, particularly those utilizing CNNs for melanoma diagnosis, have also confirmed the practical performance of AI algorithms for automated diagnosis of skin lesions (Tschandl et al., 2018, 2019).

AI has as well played an significant role in the field of cardiology, with major achievements in almost all areas (Johnson et al., 2018; Lopez-Jimenez et al., 2020). For example, AI platforms recently investigated in echocardiography appear to play an increasingly important role in recognizing pathological features such as cardiomyopathy (Zhang et al., 2018), and regional wall motion abnormalities (Kusunose et al., 2020). In addition, the popularity for AI techniques has especially risen in other disciplines of cardiology like ECG analysis (Tison et al., 2018), nuclear cardiology (Betancur et al., 2018), coronary angiography and interventional Cardiology (Cho et al., 2019).

In addition to the applications of AI in medicine described above, AI based various models have also been developed during the diagnosis and evaluation of a wide range of diseases and fields, such as oncology (Lu et al., 2021), and psychiatry (Fiske et al., 2019; Monteith et al., 2022) and dentistry (Ahmed et al., 2021).

1.3.2 Artificial Intelligence in Ophthalmology

In the field of ophthalmology, the application of AI methods has begun to receive a lot of attention given the widespread use of various images. In particular, the implementation of teleophthalmology has already started to play a significant role in the field of digital health, that rely and lend on AI and imaging big data (Ting et al., 2020; Li et al., 2021; Han et al., 2022).

Research has been done to build novel deep learning architecture using optical coherence tomography (OCT) images of patients with retinal diseases. It can be used to successfully detect more than 50 common diseases, with even better performance in partial clinical diagnosis and referral (de Fauw et al., 2018).

Specifically, recent studies have demonstrated the potential of AI in developing diagnostic tools for diabetic retinopathy and diabetic macular edema diseases (Gulshan et al., 2016; Abràmoff et al., 2018; Ruamviboonsuk et al., 2019; Grzybowski et al., 2020). The autonomous AI diagnostic system for diabetic retinopathy detection has been authorized by FDA for its exceedingly high sensitivity and specificity (Abràmoff et al., 2018).

In addition to diabetic retinopathy, automatic screening and diagnose system have also been well established for other common vision-threatening diseases. For example, a deep learning system was trained using fundus photographs for the diagnosis of glaucoma, showing a sensitivity and specificity of greater than 90% (Liu et al., 2019; Li et al., 2022). The use of OCT alone also demonstrated the potential of glaucoma detection in developing AI tools (Hood et al., 2022). In age-related macular degeneration (AMD), deep learning-based predictive model has been largely reported to be capable of classifying eye disease severity scale (Grassmann et al., 2018; Venhuizen et al., 2017). Neural networks are also promising tools for vision estimation of AMD (Aslam et al., 2018; Rohm et al., 2018).

Several studies have implemented AI for the diagnosis of plus disease that is dilation

and tortuosity of retinal vessels with expert-level performance in retinopathy of prematurity (ROP) (Brown et al., 2018). And CNNs have been implemented to automatically assess the quality of fundus images to make accurate ophthalmic diagnoses (Coyner et al., 2018). AI models are also being expanded to the field of strabismus (Chen et al., 2018), cataracts (Dong et al., 2017; Wu et al., 2019) and Keratoconus (Lavric and Valentin, 2019).

Thus, given the potential of AI advances in the field of ophthalmology, AI may not only be able to substitute for specialized ophthalmologists in classifying and referring ophthalmic images, but it has already proven to be a valuable and feasible diagnostic tool in early recognition and proper management of eye diseases.

1.4 Research Objectives

Brain organization is an economic trade-off between wiring cost and adaptively topological value. My project tried to explore brain reorganization pattern by characterizing global and local FCN metrics. The aims of my study are to learn the following:

Q1: Whether and how a local (peripheral) lesion of the optic nerve affects global FCN dynamics?

H1: My hypothesis is optic nerve damage may affect global FCN dynamical organization on patients with reduced efficiency of information transfer or weaken of network specialization.

Q2: How does the lesion affect hub brain areas and modularity distribution during visual processing?

H2: My hypothesis is that hub regions and module distribution are disrupted on FCN after optic nerve damage, and their dynamic reorganization patterns are different from those of normal subjects.

Q3: Does network metrics can be modified by rtACS, and how does this impact vision restoration?

H3: My hypothesis is that after receiving rtACS treatment, patients' FCN capabilities of balancing wiring cost and functional specialization are enhanced.

Q4: How to develop a vision recovery prediction model using the analysis of baseline EEG recordings and baseline visual field charts to predict post-rtACS EEG effects and vision recovery?

H4: My hypothesis is that vision recovery can be predicted at baseline using EEG biomarkers, and visual field charts.

Q5: Is it possible to develop an early warning model based on deep learning for visual field impairment?

H5: My hypothesis is that an EEG-based early warning system can recognize individuals at risk for visual field disorders through deep learning models.

1.5 Thesis Outline

To facilitate the understanding of the goal of my thesis, a brief explanation of how optic nerve deficits affect brain networks and cognition is provided, and a focus is placed

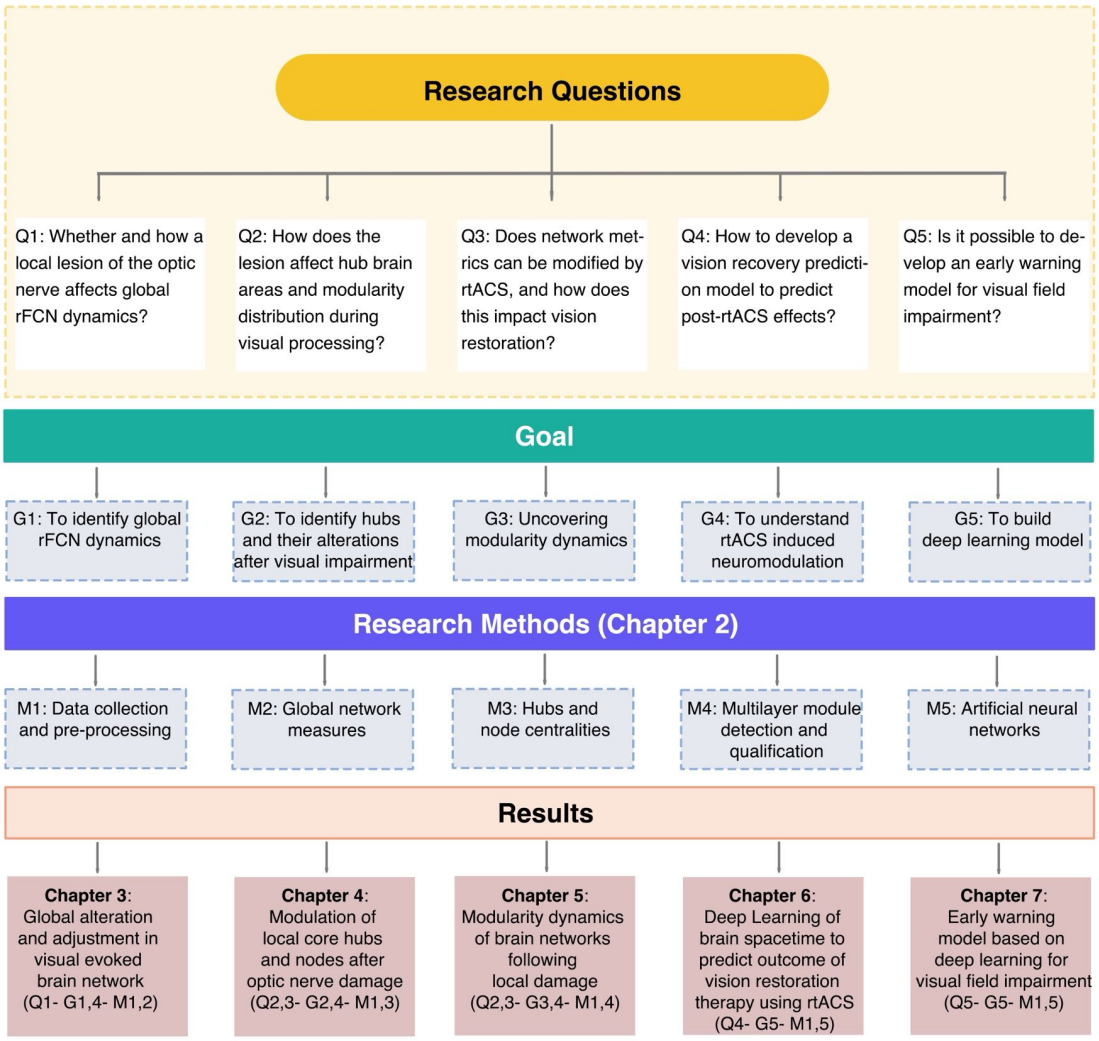

Figure 1.3: Research Framework of the study.

on how the brain connectome achieves vision recovery after receiving non-invasive brain stimulation. I related different topological brain features to the visual performances and then developed a predictive model for vision recovery using network topological metrics based on deep learning algorithms (Fig. 1.3). The thesis is structured as follows: Chapter 1 already outlined the basic background required for visual system deficits, vision restoration therapies, and technologies applied to brain connectome analysis and cognition. In addition, I described the use of AI in various medical studies, particularly in the field of ophthalmology.

Chapter 2 summarises the fundamental methods needed to understand and use throughout my whole project, including data collection, and graph theory characteristics for quantifying topological structures such as hubs and community modularity as well as also describing various artificial neural network algorithms.

Chapter 3 focuses on the global alterations and adjustments in visually evoked brain networks after optic nerve damage and demonstrates the spacetime causal effects of rtACS neuromodulation on global network properties. It demonstrates how localized lesions of the optic nerve affect global rapid and transient functional connectivity network (rFCN) dynamics and presents how rtACS neuromodulation provokes visual recovery by affecting

the rFCN. The results of this section have been published in the Scientific Report.

Chapter 4 addresses the regulation of local core hubs and nodes of rFCN after optic nerve damage and their changes and adjustments after receiving rtACS. It proved how the lesion affects the centrality of brain regions and how the local nodes are realigned during visual processing as a result of the disruption of the hubs. I also presented how the centrality of the hubs and nodes changed after patients received rtACS. The findings of this segment have been published in the Scientific Report.

Chapter 5 illustrates the differences in the architecture of the rFCN multilayer network between normal subjects and patients with optic nerve damage before and after rtACS treatment. I identified representative partitions of the dynamic multilayer networks and explored the multilayer modular organization during visual processing and recovery. I also assessed the interactions among modules and related them to visual performance. The results presented in this section have been published in the Cerebral Cortex.

Chapter 6 describes a visual recovery prediction model for the post-treatment effects of rtACS. Several artificial neural networks were constructed to predict the treatment effects of noninvasive brain stimulation using baseline functional brain network responses from EEG during visual cognition. The findings in this section are under review.

Chapter 7 explores the potential of deep learning models to serve as an early warning system for visual field impairment by analyzing EEG-based functional brain networks. The conclusions in this section are under review.

Finally, Chapter 8 summarizes all the results and contributions of this study and informs future directions for possible research.

2 Methods to Explore Spacetime of the Brain and Plasticity

The fundamentals of this study are rooted in the exploration of brain network dynamics in patients with optic neuropathy and healthy controls, and to explore the functional reorganization of brain networks induced by non-invasive brain stimulation. In this chapter, I provided an overview of the data collection methods, including participant recruitment and visual field assessment, as well as the recording of visual evoked potentials using EEG. I also involved the repetitive transorbital alternating current stimulation (rtACS) to modulate visual functions and functional connectivity.

Specifically, brain activity during visual processing was analyzed employing EEG preprocessing and source reconstruction techniques. Network metrics were studied with graph theory to assess the functional connectivity and topology of the brain. Insights into the role of specific brain regions in visual function were gained through the study of hub and node centrality and multilayer modules.

Machine learning and deep learning techniques are also an important part of this study, focusing on artificial neural networks (ANN), including convolutional neural networks (CNN) and recurrent neural networks (RNN). These methods are used to uncover patterns and relationships in complex neural data, offering a deeper understanding of brain network dynamics in the context of optic neuropathy.

In summary, this study encompasses a variety of methodologies, from data collection to advanced neural network modeling, aiming to reveal the complex dynamics of the brain in patients with optic nerve damage, thereby elucidating fundamental issues in visual processing and vision restoration.

2.1 Data Collection and Pre-processing

2.1.1 Participants

Following local ethics committee approval, 22 patients with optic neuropathy (8 females, 52.1 ± 15.7 years old) and 15 healthy controls (7 females, 42.8 ± 16.9 years old) were recruited for this clinical trial. Patients were randomized, double-blinded, placebo-controlled trial which were treated either with rtACS ($n = 12$, 52.3 ± 14.3 years old) or placebo ($n = 10$, 51.9 ± 17.3 years old). Causes of optic nerve damage were anterior ischaemic optic neuropathy/AION (N=6), post-inflammatory (N=4), and various other causes. Inclusion criteria were residual (patients) or normal vision (controls). Exclusion criteria were instable intraocular pressure (> 27mmHg) or history of epilepsy, heart pacemakers, photosensitive epilepsy, psychiatric diseases (schizophrenia etc.), high blood pressure or diabetes.

2.1.2 Visual Field Assessment

The visual field of patients was obtained using computer-based high-resolution perimetry (HRP) (Gall et al., 2011). Subjects sat 42 cm in front of the monitor and responded to 475 consecutive white target stimuli appearing at random locations with a central fixation point. Fixation was monitored using an infrared-based eye tracker (Tobii ET1750, Tobii

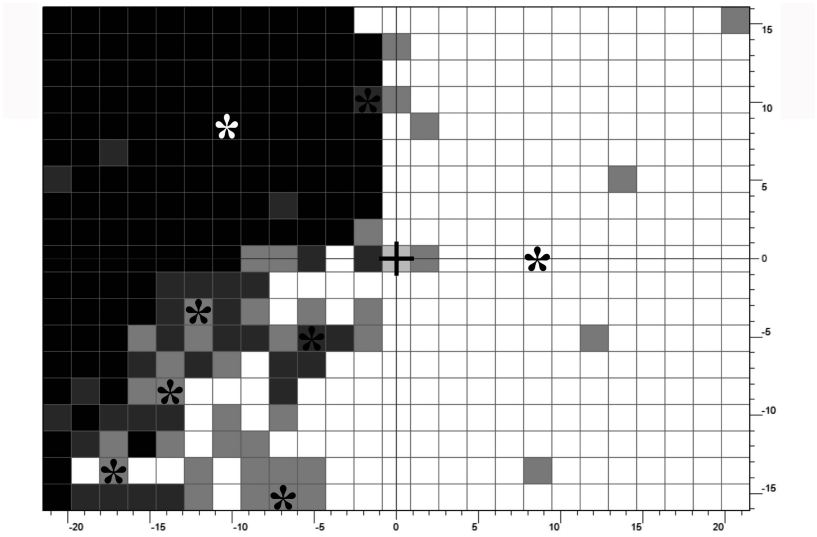

Figure 2.1: Typical perimetric visual field chart of a patient with optic nerve damage, with the central fixation (black cross) obtained, showing individual placement of the stimulus positions (*stars). Visual field areas were categorized into intact (white spots), partially defect (grey spots), and blind regions (black spots). Eight stimulus locations were then selected for visual evoked potentials (VEPs) testing. One was located in the intact area, six in the gray area of the "partial" visual field, and one in the black area.

Technology AB, Sweden), capturing the subject's focal point on the computer screen. As Fig. 2.1 shows, the visual field was divided into three functional areas as defined by detection rate: the intact vision area (IVA), shown in white, where subjects detect correctly 3/3 stimuli at the same location; the partly defective regions ("areas of residual vision"), where 1-2 of 3 stimuli were detected, and the blind visual field that showed no response. Eight positions were then individually selected per patient for additional visual evoked potential (VEPs) testing: one in IVA, six in the ARV, and one in the blind area.

2.1.3 EEG Recording of Visual Evoked pPotentials

Visual evoked potentials (VEPs) were collected with an EEG amplifier (Brain Products, Munich, Germany) with 32 sintered Ag/AgCl electrodes mounted in an Easycap (Falk Minow Services, Munich, Germany) according to the 10-10 system, referenced to nose-tip with ground electrode at Fz and Cz. The signal was sampled with 500 Hz frequency. VEPs were recorded monocularly on patients' damaged eye and the same eye for matched normal subjects. The VEP stimulus (400ms) was either a circle (1° diameter) or a square ($1 * 1°$) which had to be acknowledged by corresponding bar press. The stimuli were presented at eight different locations on the basis of HRP for 400ms, and at each location, 180 trials were performed for each subject (random inter-stimulus-interval of $1,300 - 1,700$ms). Two patients in the rtACS group dropped out without EEG after HRP. One patient in rtACS group and one patient in placebo group had to be excluded because of the limited number of detected trials (< 50), leaving 9 patients in rtACS group and 9 patients in placebo group (Table A.1). On average 140 ± 2 (s.e.m.) trials were analyzed for each subject/condition.

2.1.4 Repetitive Transorbital Alternating Current Stimulation (rtACS)

Non-invasive brain current stimulation is now a well-established method to alter functional connectivity networks (Rossini et al., 2019). rtACS is the preferred method to modulate both normal and abnormal visual functions and functional connectivity (Sabel et al., 2020a). The patients were treated with established protocols (Gall et al., 2016) using four stimulation electrodes (sintered Ag/AgCl ring electrodes, Easycap, Germany) placed near the eyeball. The current pulses were generated by a multichannel device (EBS Technologies, Kleinmachnow, Germany).

The amplitude of the current pulses was $< 2,000$ µA (peak-to-peak) and set at 125% below the individual phosphene threshold, with individually set frequencies between alpha and the flicker fusion frequency of phosphenes. The rtACS treatment was given daily for 10 days of for both eyes irrespective of which eye was damaged and the daily sessions lasted from $30 - 40$ minutes per day. The placebo group used the same electrode montage setup but with click sound instead of rtACS. rtACS is both effective, safe, and well tolerated (Sabel et al., 2020a).

The study was approved by the ethical standards committee for human subjects (institutional). All participates were treated in accordance with the Declaration of Helsinki and written informed research consent was obtained for the study.

2.1.5 EEG Pre-processing and Source Reconstruction of Brain Activities

EEG epochs were filtered to 1-100Hz, notch 50Hz FIR filter, down sampled to 250Hz and average re-referenced and time-locked -0.8s to 1.7s. Epochs with artifacts and noisy channels were removed with independent component analysis (ICA). For each subject, 15 ± 3 components were selected and projected back into sensor space.

Following EEG pre-processing, source-localized activities were obtained by applying geometry and electrical conductivity of the tissues in the head using a forward model to estimate how neuronal currents propagate from source regions within the brain to the EEG sensors (electrodes). Here, the anatomical Colin27 head template was used as a common geometric model. The forward model was calculated using the boundary element method (BEM) (Gramfort et al., 2010) to describe electrical current properties of the head, and source current distributions were applied to estimate the weighted minimum norm estimate (wMNE) (Iwaki and Ueno, 1998). wMNE is a classical EEG inverse transformation to overcome the limitations of preference in superficial sources, but it can also induce deep generator activities with high accuracy. The dipole orientation was constrained perpendicular to the cortex. The average of all dipoles belonging to the same region was calculated representing the activity of each area. In this way, sensor signals were projected onto an anatomical framework so that source-reconstructed neuronal activities could be obtained for 68 cortical regions of interest (ROIs; 34 per hemisphere) and the mean voxel time series for each ROI could be computed as defined by Desikan–Killiany (Desikan et al., 2006).

2.2 Network Metrics of Graph Models

2.2.1 Defining of Brain Networks

Source data were then digitally filtered (band pass filter 3.9-30 Hz) using Morlet wavelets. A sliding window fixed at 211 samples (844ms) irrespective of the frequency was used to analyse the signal. The time-frequency representation of the data was thus estimated from a minimum frequency of 3.9Hz with 3 cycles to a maximum frequency of 30Hz with 11.4 cycles. The data with 8ms and 0.7Hz resolution were then generated. In this way, instantaneous measurements of EEG data were decomposed into temporal and spectral bands. Frequency bands were identified as theta (3-7Hz), low alpha (7-10Hz), high alpha (10-12Hz), and beta (13-30Hz).

Phase locking value (PLV) (Lachaux et al., 1999) were used to estimate the functional connectivity between all pairwise ROI combinations. PLV represents synchronies, commonly describing long-range synchronization patterns between widely separated brain regions which was computed as:

$$PLV_{(f,t)} = \frac{1}{N}\left|\sum_{n=1}^{N} \exp\left(i\left(\triangle\varphi_n\left(f,t\right)\right)\right)\right| \tag{1}$$

Here, $\triangle\varphi_n\left(f,t\right)$ denotes the phase difference between ROIs for frequency f and time point t. N is the number of trials, and || the absolute value. The PLV measures the inter-trial variability of the phase difference at t. It ranges between 0 and 1, where PLV close to 1 shows that the phase difference varies little across the trials ("phase locking"). A threshold of 0.29 was applied to convert full PLV values into edges of weighted network.

2.2.2 Global Network Measures

To describe Brain Spacetime, I used graph theory to mathematically characterize brain FCN (Stam et al., 2009). Variations of global strength of connections between pairs of brain regions were firstly evaluated. This captures the sum of weights of connectivity attached to all nodes. Furthermore, the global network parameters were extracted for the comparison of network topology. Integration of global measures in the brain that evaluates the ability of rapid combinations between distributed brain regions were calculated, like characteristic path length (CPL). CPL, as one of the most commonly used integration measures, shows efficiency of information transfer between nodes in the network. The functional segregation of the network, clustering coefficient (CC) (Watts and Strogatz, 1998) were also investigated, capturing the presence of clusters within the network. This was primarily used to quantify the local information processing capacity in topological networks. In addition, the small-worldness (SW) index of the networks was measured which characterize the simultaneous balance of specialization and segregation (Bullmore and Sporns, 2009; Rubinov and Sporns, 2009; Power et al., 2011). It was identified by assessing the clustering of networks and the topological distance between nodes, with high clustering and short path length (Fig. 2.2A, B).

Both study groups were statistically comparable in age and gender. Statistical analyses of network metrics were calculated with cluster mass permutation tests. Because the EEG signal was sampled and analyzed multi-dimensionally (time and frequency bands), I

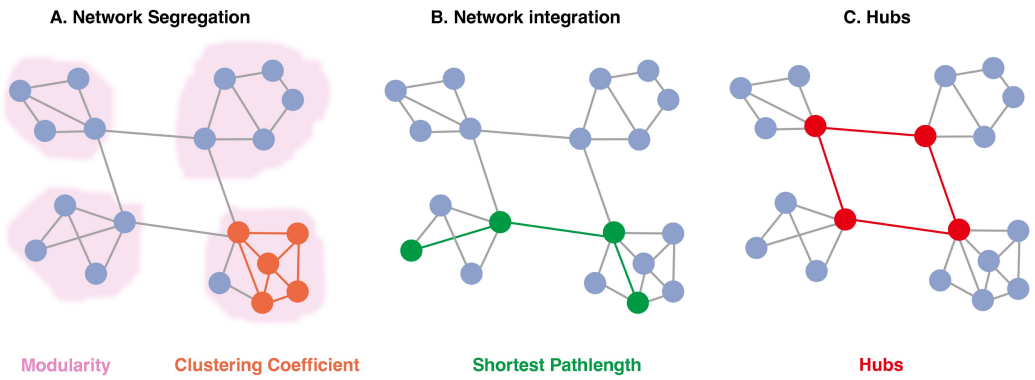

Figure 2.2: Schematic representation of network parameters. A: Graphical properties of network segregation, including modularity degree and local clustering coefficients. There are four modules in the graph, where the interaction within modules is more than the interaction between modules. The clustering coefficient describes the tendency of nodes to form triangles in the network. B: The shortest path length shows the integration of the network and evaluates the minimum number of steps between nodes. C: Hubs with dense connectivity play a key role in the network by being densely connected to local nodes.

considered the multiple comparisons problem (MCP) (Maris and Oostenveld, 2007) with appropriate alpha-adjustments. The cluster mass permutation test (Pernet et al., 2015) was used to control family-wise error rate (FWER) at some critical alpha level which solves the MCP. Here, a false alarm rate of $p = 0.05$ was chosen and the cluster inclusion threshold was set at $p = 0.025$.

2.2.3 Hubs and Node Centralities

Hubs can be viewed as local topological "centers" of synchronization, and the "Hub scores" represents their relevance for a given function (here: vision). The hub score varies from 0-4, where the top score of 4 is reached when the following criteria of centrality are fulfilled: high weighted node degree, node betweenness, and node closeness, but low node clustering coefficient (Sporns et al., 2007). This means that the higher the hub score, the higher up is the node in the FCN hierarchy(van den Heuvel and Sporns, 2013). A node receives a score of 1, if it ranks in the top 20% of nodes with highest degree in one of the four node criteria. In my study, a node was identified as a "hub" only if the hub score was 2 or higher and lasting $>$ 50ms (Pöppel, 1997). Otherwise, the node was termed "non-hub" (Fig. 2.2C).

2.2.4 Multilayer Module Detection and Qualification

To investigate the modularity structure of topological networks, I firstly decomposed networks into modules with high intrinsic connections and weaker extrinsic connectivity. The basic technique is to group individual data points into clusters to make sure the similarity within clusters is high and the similarity between clusters is low, or find divisions for a large set of observations into small subsets (Newman and Girvan, 2004). I quantified the quality of modularity to determine the reliability of communities' partition and calculated the modularity index Q. The Louvain algorithm (Blondel et al., 2008) was then applied, a fast and powerful method to agglomerate nodes into community with maximal Q. It is applicable in large networks and multiple scale hierarchical analysis, and it was shown to be more accurate than other community detection methods (Lancichinetti and Fortunato,

2009).

Because the network of functional connectivities can fluctuate, dissolving and/or evolving rapidly, I expected the brain community structure also to change dynamically. A straightforward approach to assess how modules evolve over time was single-level modularity analysis, where static modularity analysis was performed at each time point. However, the limitation of this approach was that the dependencies between time points, which were important for the temporal evolution of brain network modules were ignored. Therefore, to adequately explore these dynamics of modularity, I examined the multilayer modularity of FCN as previously described by Mucha (Mucha et al., 2010) to find the optimal partitioning across layers, where time points were considered as layers (Fig. 2.3). In this way, both connection topology within each network layer/time point and the coupling between layers/times were optimized. The multilayer modularity index Qml of weighted networks was defined as follows:

$$Q_{ml} = \frac{1}{2\mu}\sum_{ijsr}\left[\left(A_{ijs} - \gamma_s e_{ijs}\right)\delta_{sr} + \delta_{ij}C_{jsr}\right]\delta\left(g_{is}, g_{jr}\right) \tag{2}$$

, where A_{ijs} specifies the weight of edges between node i and node j in layer s, and γ_s is defined as the spatial resolution parameter that can be used to tune the influence of the null model, to adjust the size or number of partitions. e_{ijs} is the weight of the edge between nodes i and j in layer s in the null model. δ_{sr} equals one, when layer $s = r$, and zero otherwise. It ensures that the coupling difference between assessed network and null network is only considered within the same layer.

δ_{ij} C_{jsr} considers the inte- layer coupling parameter. δ_{ij} equals one when node i=j, which ensures that only the node links to itself is calculated between layers when estimating inter-layer coupling parameters. C_{jsr} appraises the coupling between layer s and layer r for node j. The value of C_{jsr} indicates the strength of coupling across layers as the temporal resolution parameter. $\delta g_{is}, g_{jr}$ equals one, when node i in layer s and node j in layer r are in the same module, and zero otherwise. The optimization of Q_{ml} can be used to identify communities on varies scales over different combinations of spatial and temporal resolution. To avoid the deviation in multilayer modular analysis, I selected the common default values in my study, by setting the resolution parameter γ_s and C_{jsr} to 1 (Bassett et al., 2013; Wu et al., 2020). The network flexibility was calculated by computing the frequency of a given node which changes its modular affiliation across consecutive time steps.

To identify consensus-stable robust modules, consensus clustering was used when analyzing community structure so that the nodes of modules can be assigned into the same community across partition times. This representation of consensus community structure can also be used to analyze differences between the two populations. Firstly, I estimated the consistency of community partitions across participants by constructing the modular allegiance matrix M_{ij}, and then the modules were identified over a set of partitions across networks for each time point, frequency, subject and group. The modular allegiance matrix M_{ij} indicate the probability that nodes i and j are partitioned into the same community. Thereafter, the representative modules that were consistently present could be identified (Mucha et al., 2010).

To quantitatively measure the modular architecture of multilayer networks, the in-

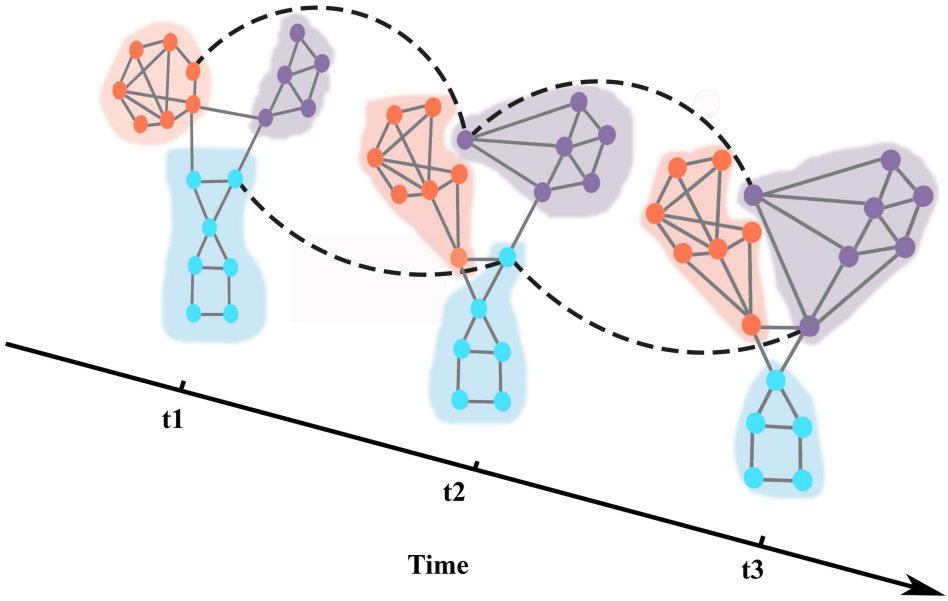

Figure 2.3: Schematic representation of a multilayer network. The colours refer to the community affiliation of nodes at different time points (temporal layers). Some nodes alter their affiliation to different modules across time (i.e., from orange to purple or from blue to orange). Nodes are coloured according to their optimal community distribution with maximal multilayer modularity index in which both connection topology within each layer and the coupling between neighbouring layers were detected.

teraction strength of modules in the brain were further evaluated based on the following formula:

$$I_{k_1k_2} = \left(\sum_{i\in P_{k_1} j\in P_{k_2}} M_{ij}\right) / \left(|P_{k_1}|\,|P_{k_2}|\right) \tag{3}$$

, where $I_{k_1k_2}$ is the interaction strength between module P_{k_1} and module P_{k_2}. $|P_{k_1}|$ is the number of nodes in module P_{k_1}. If $k_1 = k_2$, and$I_{k_1k_2}$defines the intra model interaction strength. If $k_1 \neq k_2$, the normalized interaction strength of different modules was calculated as the interaction strength of modules using the following computation:

$$I^{'}_{k_1k_2} = I_{k_1k_2} / \sqrt{I_{k_1k_1} I_{k_2k_2}} \tag{4}$$

2.3 Machine Learning and Deep Learning

The goal of machine learning (ML) is to generate algorithms using the dataset, associated features and weights that might be useful for the prediction to map features to the target. The generated algorithms can be used not only to represent the dataset, but also to make inferences about future data sets. Typical learning methods used in ML including supervised learning in regression and classification tasks, unsupervised learning in clustering, association or anomaly detection, semi-supervised learning and reinforcement learning. The commonly used classical machine learning algorithms consist of linear regression, logistic regression, decision trees, and random forests, some of which are specialized for classification, and some techniques can also be used for regression tasks.

Traditional machine learning has developed in decades and has been used in many aspects such as recommendations on websites and web searches. However, it is limited in processing natural data such as image or speech. Typically, ML requires appropriate

feature extractors through non-linear inspection that can be used to transform natural data into suitable feature vectors for pattern recognition. However, deep learning (DL) can directly process raw natural data from speech and audio files to image and video data (Babaee et al., 2018; Dourado et al., 2021; Fayek et al., 2017; Hossain and Muhammad, 2019). DL has been found to perform better than classical machine learning methods in large and diverse physiological signals (Faust et al., 2018).

DL is a subfield of machine learning, allows computational models with multiple levels of layers to discover the representations of large data sets in each layer. In the abstraction of multiple levels, DL learns how to change parameters to compute intricate structure of the input data through successive non-linear transformations (LeCun et al., 2015). Deep learning neural networks can act as approximators and represent a wide range of continuous functions, so they offer a promising alternative for addressing the high dimensionality of input data. For example, DL powers in aspects of genomics. It has been used to predict the effects of genetic variants on RNA splicing to analyze gene expression (Xiong et al., 2015). In addition, DL have shown light in neuroscience and psychology research such as enactive vision and mental representations (Perconti and Plebe, 2020).

2.3.1 Artificial Neural Networks (ANN)

Artificial Neural Networks (ANN) have become the most frequently mentioned term in deep learning. ANN are considered to be the most closely related to biological neural networks of humans, where nodes, named as perceptron in ANN, are recognized as cells and communication between cells, such as axons and dendrites, are perceived as connections of nodes.

ANN typically contain multiple layers of connected perceptron. The perceptron is the basis of ANN. It is proposed as an algorithm that can be utilized to separate space from numerous features and targets into lines, planes, or hyperplanes. The activation function can be applied for each perceptron to transform various inputs into output which can be use in next layer. In ANN, the information from the previous layer is collected and fed to the next layer, which is also known as feedforward neural network. The simplest ANN consist of three layers, including an input nodes layer, a hidden layer, and an output nodes layer. The ANN is deep learning neural networks if there exist hundreds of hidden layers (Fig. 2.4). There are sets of technologies for learning in DL neural networks. The computation performed by these designed stacked neural networks in DL enable recognition of patterns to generate the output.

Deep learning neural networks are composed of neurons and connections. Neurons act as processing units of the network architecture, specifying the learning objectives based on loss or optimization functions. The connections are trained by algorithms that optimize the objective function by iteratively updating the parameters of the network. Here four different architectures were tested in this thesis, feedforward neural network (FFNN), convolutional neural networks (CNN), recurrent neural network (RNN).

2.3.2 Feedforward Neural Network (FFNN)

In this section, I introduce some different types of deep learning models. The most basic model is a feed-forward neural network (FFNN). It is the simplest fully connected

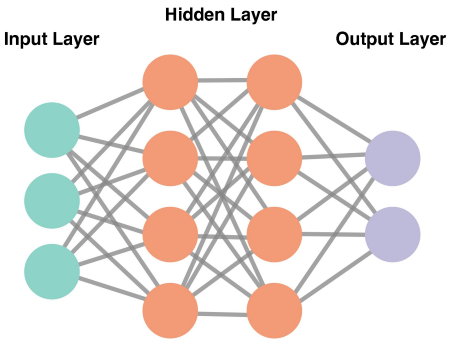

Figure 2.4: General schematic of an artificial neural network (ANN)- Feedforward Neural Network (FFNN).

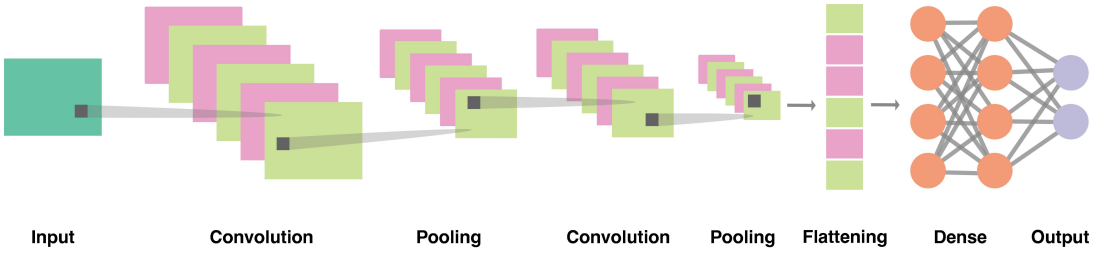

Figure 2.5: Architecture of a conventional convolutional neural network (CNN), which consists mainly of convolutional layers, pooling layers, fully connected dense layers, and some activation functions.

neural network that can leverage context. Three types of layers were organized: input, output and hidden layers. The input layer has the same number of neurons as the number of features in the data. The output layer outputs the number of categories or the results per neuron based on classification or regression. The hidden layer is located between the input layer and the output layer. The information flow is strictly unidirectional from the input layer up to the output layer, without feedback connections between layers. The structure of FFNN was presented in Fig. 2.4.

2.3.3 Convolutional Neural Networks (CNN)

Convolutional neural networks (CNN) extract local patterns by convolutional operators, which aim to exploit the structural information between adjacent pixels by performing minimal preprocessing on the image. A typical CNN consists of three types of neural layers: a convolutional layer, a pooling layer, and a fully connected layer. The convolutional layer learns features by convolving the local receptive field. The pooling layer is responsible for downsampling the spatial dimension of the input data. The fully connected layer maps multidimensional features into a one-dimensional feature vector. The structure of CNN is shown in Fig. 2.5. CNN has achieved considerable success in biomedical signal and computer vision. It has been proposed for identifying patients with depression from normal using 13 layers CNN (Acharya et al., 2018). In the early diagnosis of Alzheimer‘s disease, a deep CNN model was developed using structural MRI data (Liu et al., 2020).

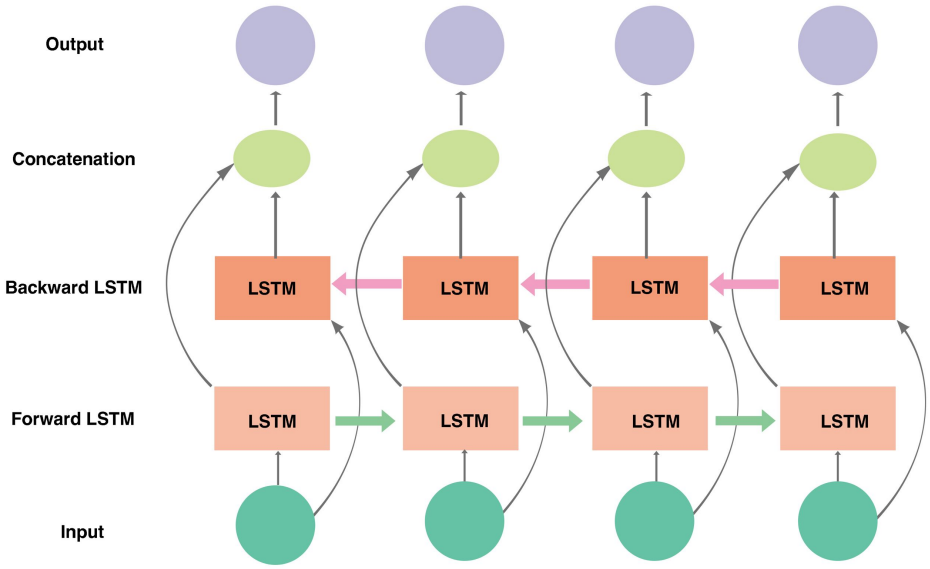

Figure 2.6: Overview of the bidirectional long short-term memory (LSTM) model.

2.3.4 Recurrent Neural Network (RNNs)

Recurrent neural network (RNN) has feedback architecture within or between layers that can dynamically learn long-term dependencies to improve the processing of individual bits of data. Long-short-term memory (LSTM) (Hochreiter and Schmidhuber, 1997) is the most popular RNN architecture. Unlike the basic RNN, LSTM adds three additional controllers: an input gate, an output gate and a forget gate. These controllers are able to decide which information needs to be retained or removed by controlling the activation signals. In this way, LSTM learns important features and is able to maintain memory over a long time. One popular variant is the Bidirectional LSTM (Bi-LSTM) which is capable of using information about events in both directions, which can capture both backwards and forwards information. There is a structure of Bi-LSTM as shown in Fig. 2.6. This memory based deep neural network has been developed in automatically detection of arrhythmias using electrocardiogram with an accuracy of over 99.0% (Yildirim et al., 2019). An LSTM classifier were constructed to decode gait patterns from the EEG to deal with walking activity during locomotion (Tortora et al., 2020). There was also a bidirectional LSTM to classify cancer hallmark text to distinguish cancerous cells from normal cells (Jiang et al., 2020).

In summary, this study used a variety of methods, ranging from data collection techniques to neural network modeling, to investigate in depth the complex dynamics of brain network function in patients with optic nerve damage and healthy controls, revealing the complexity of the human brain in the context of visual neurological injury.

Dynamic functional brain network changes were comprehensively analyzed by collecting visual field assessment results and electroencephalograms of visual evoked potentials from optic neuropathy patients and healthy subjects. And using rtACS, the possibility of visual recovery was investigated in terms of functional brain networks. Specifically, I used a series of EEG analysis methods and constructed the functional brain networks based on graph theory to fully analyze the role of FCN in visual function and visual re-

covery. The study also attempted to utilize deep learning techniques to reveal patterns and relationships in complex brain network data.

Overall, these approaches cover a wide range from data collection and preprocessing to cutting-edge neural network modeling, with the ultimate goal of advancing our understanding of visual processing and the potential for vision restoration in patients with optic nerve damage.

3 Global Alteration and Adjustment in Visual Evoked Brain Network

For centuries neuroscientists have explored how circumscribed brain centers support mental functions such as vision, language or cognition. This "localizationist" approach focused on how local neuronal cell assemblies or brain regions control specific sub-functions. But this localization cannot fully explain different behavioral phenomena such as rapid plasticity in normal learning (Mentis et al., 2003; Moll et al., 2005), transmodal plasticity (Pascual-Leone et al., 2005), recovery of function (Laurence and Stein, 1978), or receptive field plasticity following visual system damage which can happen even within minutes (Gilbert and Wiesel, 1992). It is the new network science which paves the way for a more global perspective of how neuronal information is integrated between regionally distributed local brain centers.

3.1 Introduction

Functional connectivity network analyses have become popular in recent years to unravel the spatial and temporal organization of local and global neural processing (Rossini et al., 2019). Typically, FCN analyses use resting-state data (Farahani et al., 2019), but rapid and transient changes of FCN (rFCN) were rarely studied in the human brain on a millisecond scale. Yet, the maximum speed of FCN dynamics needs to be known, because FCN provide the physiological support for top-down stimulus processing and synchronization of sensory, motor and cognitive functions. The synchronous mode uses a gain approach, weighting the anatomical connections to generate effective interaction patterns, where the phase relation supports interactions between neuronal assemblies as a function of brain regions (space), time, and specific frequencies (Womelsdorf et al., 2007). Although temporal dynamics of brain activities are often studied (Lankinen et al., 2018), little is known how fast multiple brain regions are "bound" in time through phase synchronization in the brain topological "workspace" (Singer, 2006).

Compared to 4-8 sec bolt response in magnetic resonance imaging (MRI), the EEG allows us to explore if and how fast FCN can synchronize, including events that have no (measurable) energy consumption (Rossini et al., 2019). For example, EEG recordings show phase synchronized patterns and temporal brain dynamics during face perception tasks (Jamal et al., 2015), and it can display unique, dynamic patterns of FCN changes, for example in auditory and visual oddball tasks (Karamzadeh et al., 2013), or during face and object matching tasks in autism spectrum conditions (Catarino et al., 2013).

While such studies confirm that individual brain regions can interact with each other in millisecond speed, rapid dynamics of whole brain FCN plasticity has not been explored. Yet, this is critical to fully understand how higher order "top down" cognitive influences can actively support, or interfere with, "bottom-up", afferent input (Gilbert and Li, 2013), especially in fast mental acts or behavioral tasks which happen at a split of a second such as temporal discrimination ($20 - 40$ms) or fast visual detection ($150 - 200$ms).

Also cognitive processing requires rapid and transient dynamic reorganization of brain functional networks (Bola and Sabel, 2015), so that topological rearrangements can enable the synchronization and integration of neural processing during different cognitive

modalities. But when neural synchronization is disturbed, they can lead to impairment or loss of functions. For example, optic nerve patients with vision loss show FCN disturbances in the resting state (Bola et al., 2014), and with neuromodulation using repetitive transorbital alternating current stimulation (rtACS) they can be partially restored which induces vision recovery (Gall et al., 2016). But it is unknown if, and to what extent, fast FCN reorganization exist and how they are affected by damage.

To characterize FCN, graph metrics were time-locked to visual stimulus onset and analyzed for each region of interest (ROI) on a time vector sub-divided in 8ms time-windows (see methods). Our graph metrics included global network topology measures, clustering coefficient (CC), characteristic path length (CPL), and small-worldness (SW).

3.2 rFCN Response to Visual Stimulus in Intact Vision Area (IVA)

In the present study, I used the EEG to study the brain of patients with optic nerve damage with high temporal resolution to estimate dynamic brain network reorganization with millisecond resolution. The visual evoked EEG recordings from patients were collected and analyzed to reconstruct the complex brain networks. My goal was to learn how the functional connectivity network of the brain responds to visual stimuli in the intact vision area.

The EEG analysis in this intact visual field region showed that patients had significantly greater global strength than controls ($t_{mass} = 1028$, $p = 0.008$) (Fig. 3.1A) and their node strength were stronger starting from around 350ms specifically in the beta band (Fig. 3.1B). In controls, in contrast, node strength showed much earlier activation at around 150ms after onset of the visual stimuli and this was only transient. Furthermore, while these nodes of control subjects were found mostly in the frontal lobe, in patients these nodes were distributed throughout the brain.

To learn if global rFCN dynamics are functionally meaningful, I compared FCNnetwork metrics between controls and patients. CC, CPL and SW increased at around 300ms in the network in both groups which corresponds to the cognitive stage of the P300 in VEP recordings (van Dinteren et al., 2014). In optic nerve damage patients, however, FCN had higher CC, longer CPL, but weaker theta-band SW organization during the different functional stages (Fig. 3.2). This indicates that neural processing during visual performance requires more steps in patients' theta network (lower processing efficiency). Of note, significant alterations in any other frequency networks were not observed.

3.3 rFCN Response to Visual Stimulus in Areas of Residual Vision (ARV)

Optic nerve damage can be a result of glaucoma, inflammation, trauma, ischemic or other pathologies which leads to optic neuropathy. Clinically, optic nerve damage is a frequent cause of vision loss and it is normally characterized by visual field defects and an abnormal papillary response (Martínez-Lapiscina et al., 2014; Medeiros et al., 2005). While some areas of the visual field are irreversibly blind, those regions which are partially damaged show some residual vision which can be reactivated to improve or restore visual functions (Maurer et al., 2005; Sabel et al., 2011b).

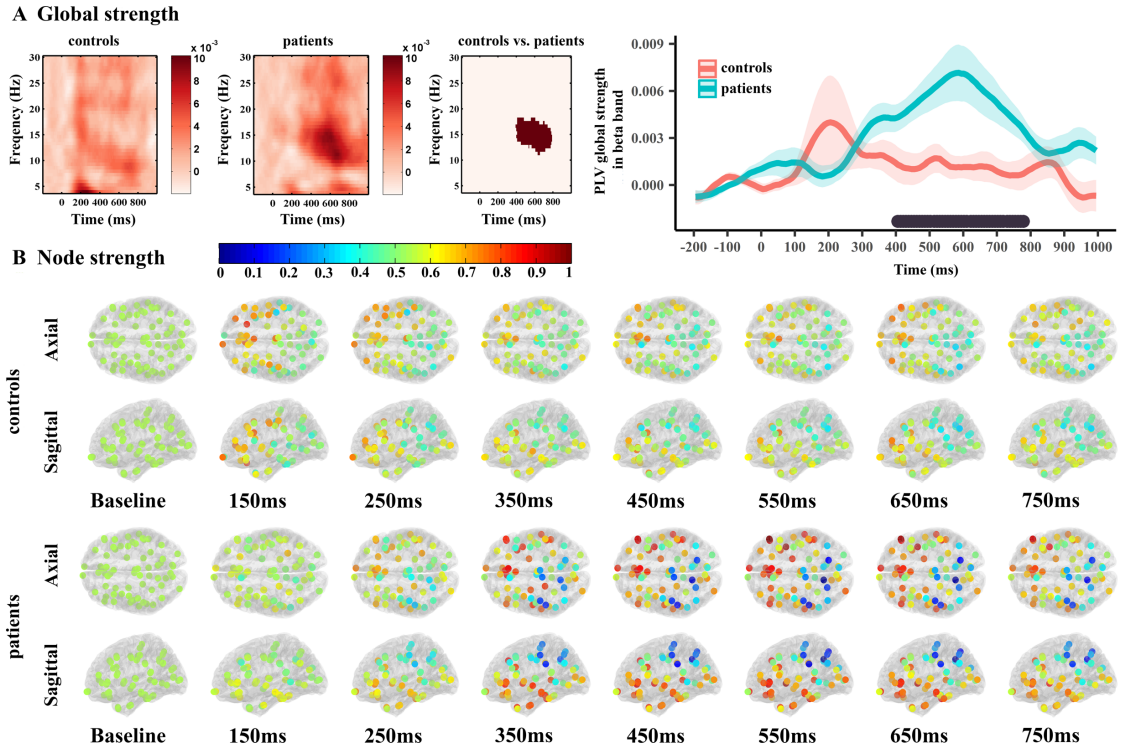

Figure 3.1: Group average values for global and node strength distribution between healthy and optic neuropathy patients. A: Global PLV strength as shown in time-frequency plot (left) and PLV strength changes over time plot in the beta band (right). B: Node strength distribution (topography) as a function of time after stimulus presentation. Baseline was defined as the average of the 200 ms epoch before stimulation, and post-stimulus node strength values are shown as averages of the respective interval (e.g the 150ms time point was the average node strength representing the interval of 150-200ms).

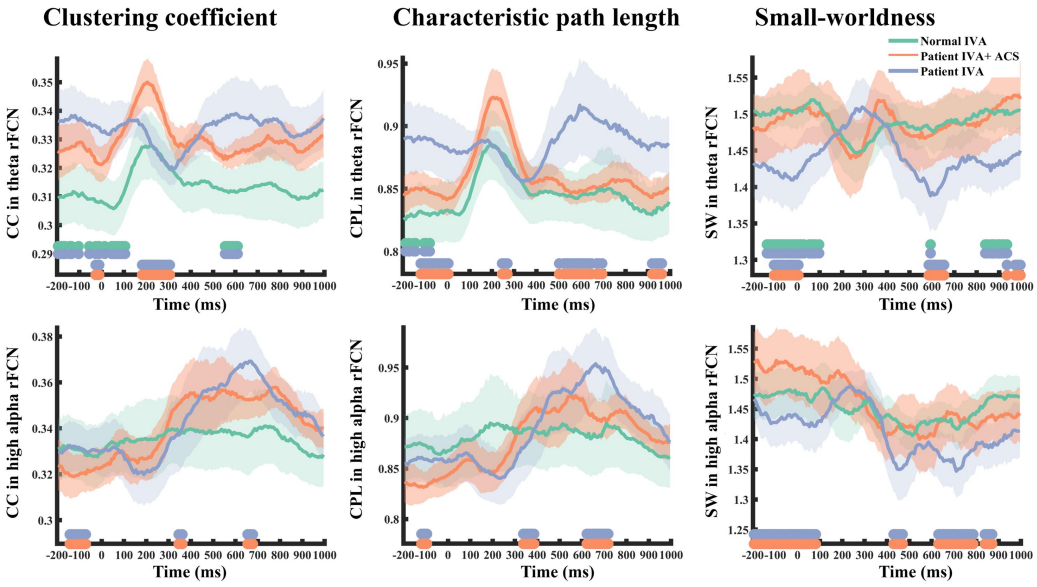

Figure 3.2: Transient dynamics of global rFCN parameters. Multiple global rFCN matrics change across time during visual processing in control subjects (green line) and patients with optic nerve damage pre- (blue) and post-rtACS treatment (red). The horizontal green-blue bars on the x-axis indicate time windows with significant differences between controls and patients; orange-blue bars mark significant differences of pre- vs. post- treatment ($p < 0.05$).

There are also other visual system diseases that affect the brain such as traumatic brain injury (McKenna et al., 2006), Dominant Optic Atrophy (DOA) and Leber Hereditary Optic Neuropathy (LHON). Here, the structural damage extends to the posterior optic pathways whereas in DOA patients, a more diffuse white matter damage was found (Messina et al., 2016). While, much is known about the primary pathology at the site of injury, little is known how this damage influences global brain interaction during cognitive processing especially in areas of residual vision.

I compared dynamic changes of network measures during visual processing in areas of residual vision in optic nerve damage patients: hit reactions to stimuli vs. miss conditions. The comparisons include multiple time and frequency dimensions. Time points from pre-stimulation at -200ms to 1000ms and all frequency points from 3.9Hz to 30Hz were involved (5760 total comparisons) to evaluate differences between groups using cluster mass permutation test. Further testing of specific frequency bands was also investigated between groups.

In areas of residual vision (relative defects), I studied how the brain of patients with optic nerve damage reacts to stimuli and how this relates to weighted brain network topology characteristics during the visual related cognitive processing.

By analyzing the network during hits and misses, the functional connectivity network showed stronger global PLV strength after a hit compared to misses (t_{mass} = 2258, p =0.0007) (Fig. 3.3A) specifically in the beta band from 170ms after stimuli onset (t_{mass} = 251, p =0.001). Node strength after stimuli onset revealed the following: activated network nodes were initially located in temporal and frontal regions around 250ms and then spread to occipital areas. Of note, at around 550ms, the node strength of motor areas was increased. This is the time where the subjects showed motor reaction pressing the response button (Fig. 3.3B).

In addition, when patients responded correctly to the visual stimuli (hits), the network presented higher clustering (t_{mass} = 625, p = 0.03) (Fig. 3.4A) and longer path length (t_{mass} = 1879, p = 0.002) (Fig. 3.4B) than when patient failed to respond (miss reactions). Specifically, after hits patients FCN had a high CC weighted network in the beta band at around 405ms (t_{mass} = 64, p = 0.03) after stimulus onset and a long CPL weighted network in both high alpha and beta band. But the difference showed up earlier in the beta band at around 198ms (t_{mass} = 40, p = 0.02) after stimulation and lasted much longer.

Furthermore, I observed a significant difference of small-worldness between hit and miss reaction (t_{mass} = 731, p = 0.02) (Fig. 3.4C). There is an appreciable smallworld-ness decrease after correct reaction to stimulation at around 630ms (t_{mass} = 52, p = 0.03) in high alpha band and 646ms (t_{mass} = 95, p = 0.006) in beta band. In contrast, for miss reaction, the SW value did not change significantly during whole visual related task.

3.4 Intact Area vs. Areas of Residual Vision

I then compared the network reorganization following hits in the intact visual field sectors and in areas of residual vision of optic nerve damage patients and quantified their network metrics. Global strength in hits was significantly greater in intact regions of the visual field than in areas of residual vision (t_{mass} = 570, p = 0.02) (Fig. 3.5A).

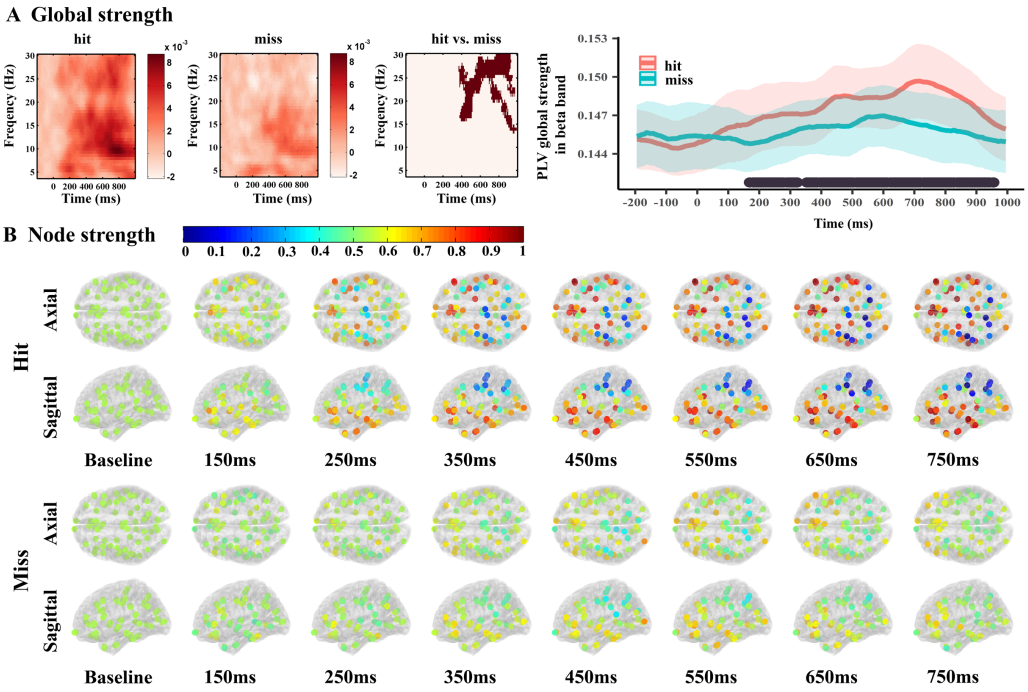

Figure 3.3: Global and node PLV strength changes during visual related task in areas of residual vision as a function of time for valid and missed reactions. A: Global strength distribution over baseline in time-frequency plot and global strength diversity in beta network. B: Topography of node strength changes over baseline in the beta band.

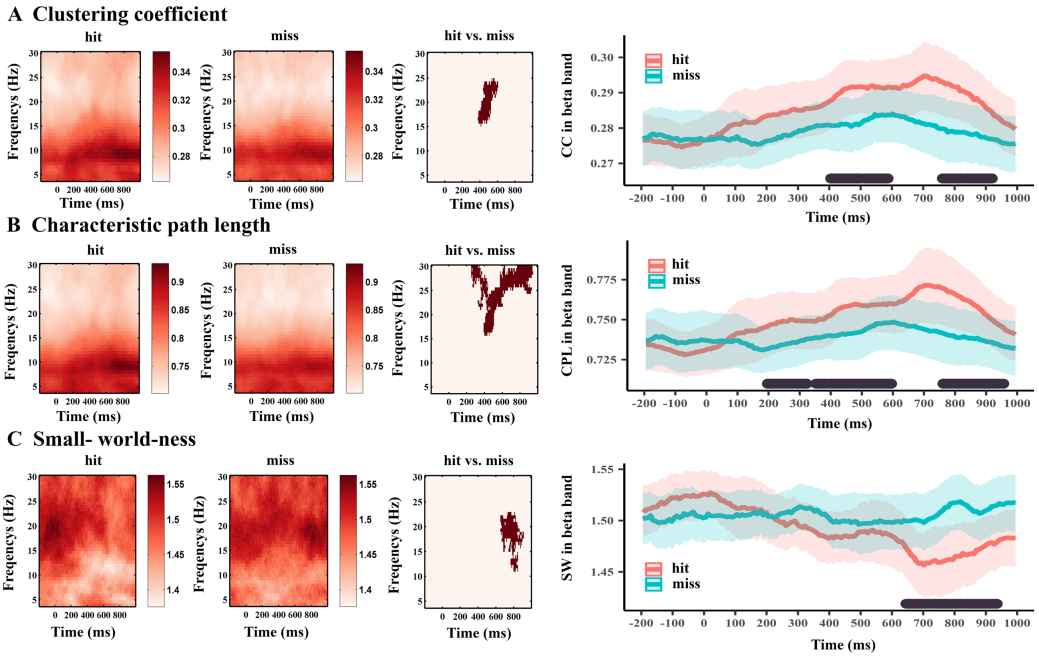

Figure 3.4: Global network parameters comparison between valid hit and miss response to stimulation in areas of residual vision in time and time-frequency plots. (A) Global clustering coefficient, (B) characteristic path length and (C) small-worldness.

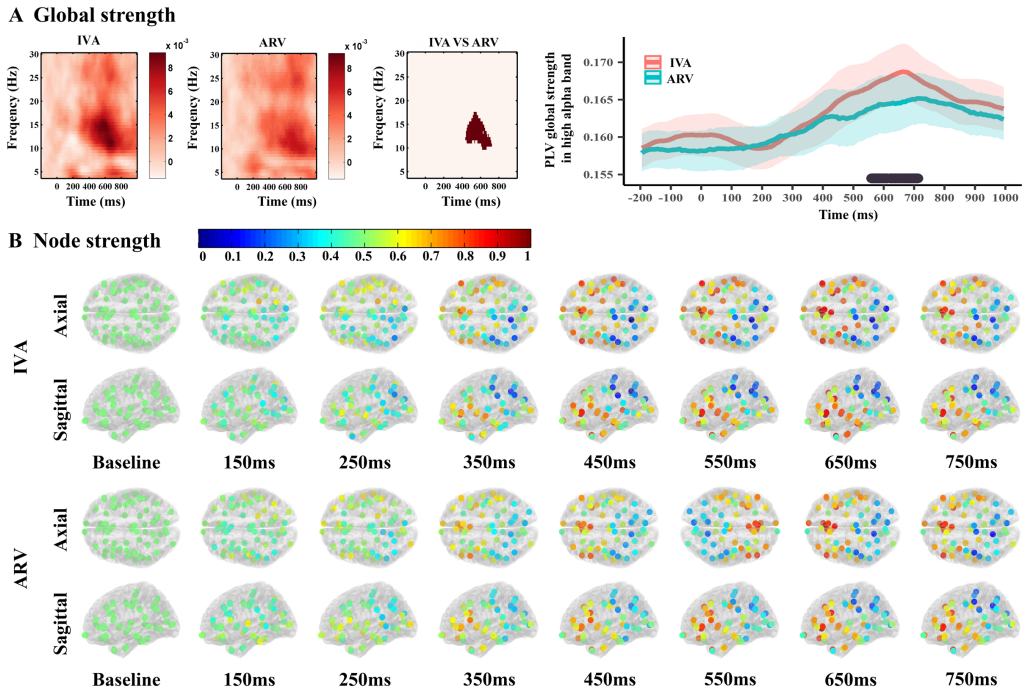

Figure 3.5: Global and node strength difference between intact visual field areas (IVA) and areas of residual vision (ARV) in the high alpha band as a function of time following stimulus presentation. A: Global strength in time and time frequency plots. B: Node strength changes over time.

Node strength analysis of hits (Fig. 3.5B) also revealed a more synchronized network during the cognition phase which included temporal and frontal areas, including motor area activation.

Hits during the cognitive processing stage exhibit higher CC in intact areas (t_{mass} = 2617, $p = 0.001$) (Fig. 3.6A) than in areas of residual vision in the theta, low alpha, high alpha and beta band. And the difference is apparent on both pre and post stimulation time points in all these four frequencies. In the high alpha band, at around -170ms (t_{mass} = 145, $p = 0.001$), CC of the intact visual field sector was higher before visual stimulation. Except for this pre-stimulation difference, higher CC emerges post stimulation at around 290ms and lasted until 818ms (t_{mass} = 223, $p = 0.001$). This was also noted in the theta, low alpha and beta band weighted network. For the CPL, there is also a difference in the hit-trials between intact visual field areas and areas of residual vision in high alpha and beta band (t_{mass} = 735, $p = 0.004$) (Fig. 3.6B). Patient´s hits in the intact visual field are associated with a larger CPL at around 550ms (t_{mass} = 59, $p = 0.01$) in the high alpha band and at about 500ms (t_{mass} = 40, $p = 0.03$) in beta band.

In the IVA, the small-world-ness (SW) in the weighted evoked response network was higher than in ARV (t_{mass} = 405, $p = 0.03$) (Fig. 3.6C). In the beta band, higher SW of IVA appeared in the pre-stimulus state at around -195ms (t_{mass} = 38, $p = 0.04$) to stimuli onset. After stimulation, the SW of IVA was also larger at 205-305ms (t_{mass} = 37, $p = 0.04$), and 786-942ms (t_{mass} = 49, $p = 0.03$). Similar to ARV, a decrease of SW was observed in the optic nerve damage patients' intact visual field areas.

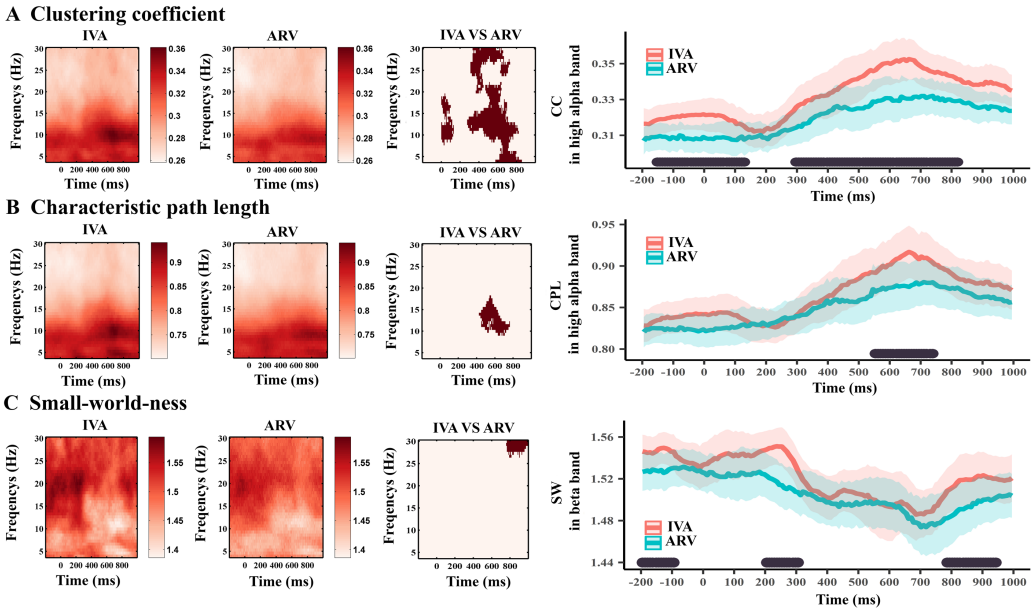

Figure 3.6: The functional network measures difference between intact visual areas and areas of residual vision during cognition. (A) Clustering coefficient distribution in time frequency plot (left) and changes over time in frequency band (right). (B) Characteristic path length and (C) small-world-ness.

3.5 Probing Global Network Adjustments using rtACS Neuromodulation in Patients

To test if the global network can be modulated in this structure, rFCN transients could be identified, this showed that rtACS can normalize FCN dynamics (Fig. 3.2). Specifically, rtACS led to significantly enhanced SW at baseline in patients (at the time just before stimulus presentation), and in the cognition and execution stage. rtACS enhanced the theta, low and high alpha networks, but it did not alter the beta network. There were no such activation changes in the placebo group. I conclude that neuromodulation with rtACS enhanced the balance between integration and segregation of global rFCN.

3.6 Discussion

Visual field loss is not only caused by damage to visual system structures, but also by alterations of brain resting state cortical networks outside of the visual system. However, not much is known about if and how local optic nerve damage affects dynamically global network reorganization on the time scale of milliseconds. To address this problem, I employed an evoked response design using a discriminate task as that involves multiple basic cognitive behaviors and cognitive processing to analyze dynamical cognitive topology arrangement in patients of optic nerve damage.

I found that on a global level that rFCN in patients had a greater degree of local integration with higher functional specialization (high clustering coefficient) than controls. This suggests reduced flexibility (i.e., greater stability or rigidity), possibly as a consequence of the loss of long-range interactions. My findings do not agree with resting-state FCN studies in other brain disorders where decreased local integration was interpreted as evidence of local clustering decreases in Parkinson patients (Olde Dubbelink et al., 2014) and in alcohol dependency (Sjoerds et al., 2017). A possible explanation for this discrep-

ancy is that optic nerve damage leads only to functional, not structural, deafferentation.

Increased clustering between the pairs of neighbors in patients' rFCN also signifies longer path length and poorer small-worldness in rFCN, a sign that neural information transfer needs more steps (greater processing cost), reducing processing speed. This interpretation fits my observation that longer reaction times correlate in patients with lower hub scores in many (but not all) ROIs. Increased path length was also reported in Alzheimer´s Disease (Cope et al., 2018) and Depression (Li et al., 2015). In sum, patients with optic nerve damage suffer a functional imbalance of specialization versus integration. These "Spacetime" disturbances reduce neural processing efficiency at both local and global levels throughout the brain. Comparison between correct visual responses and misses in ARV indicate that dynamic brain network changes are related to response fluctuations. Valid responses to visual stimuli induced strong specialization among subgraphs and longer path length in brain topological networks, demonstrating the vital role of functional brain network synchronization. As a previous study of brain synchronization in vision loss has found, I observed impaired brain synchronization which aggravates the consequences of reduced visual input (Bola et al., 2015). This shows that brain desynchronization affects not only the function of visual input but also the cognitive processing of visual information.

Furthermore, FCN cognitive topology in ARV reflects decreased optimal processing balance at around 200ms. This may present inefficient network structure during the cognition stage in patients. But during execution, when the response button is pressed at around 550ms, an increase of the small-world structure was observed. These network dynamics during valid responses exhibited FCN models during visual task in areas of residual vision. My FCN dynamics analysis provides a better understanding of the physiological mechanism of response fluctuations in areas of residual vision. Therefore, FCN response in areas of residual vision might be a target for measuring visual performance in patients with low vision.

My functional network analysis is the first EEG source space network study reporting the different topology remodeling during cognition between intact sectors of the visual field and areas of residual vision area on time scale of milliseconds. Such results might provide more information on restoration capacity of areas of residual vision (Poggel et al., 2004; Sabel et al., 2011b).

4 Modulate Local Core Hubs and Nodes After Optic Nerve Damage

This study attempts to delve into the rFCN at a millisecond resolution using event-related network analysis in both patients with optic nerve damage and healthy subjects. The investigation aims to uncover disturbances during rapid visual processing in these patients and to explore the modulatory effects of rtACS on rFCN structures, with a focus on the vision restoration potential. In addition to the dynamic aspects of the global FCN, the core hubs, which occupies crucial positions in the information transmission, and the functional alterations of each brain region after optic nerve damage were also a matter of interest. Furthermore, it is not known whether rtACS may induce the modulation of core hubs and node properties associated with vision recovery.

Therefore, in this section, I will focus on the variability of hub topology as characterized by hub scores (HS) and different node centrality metrics during normal visual processing and also in patients with optic nerve damage, as well as their plasticity induced by rtACS.

4.1 Introduction

To explored rapid FCN dynamics at millisecond resolution I now used "event related network analysis" (ERNA) (Bola and Sabel, 2015) in patients with optic nerve damage. Here, similar to visual evoked potentials, EEG recordings are time-locked to visual stimulus onset, and subsequent FCN graph analysis can show how topological 3D-"Space" (individual brain regions) is linked with the 4th dimension of "Time".

My analysis of rapid FCN plasticity extends prior studies of resting-state networks, which is the current standard to characterize the physiological basis of neurological function and behavior (Sporns, 2011). Using graph theory, I uncovered complex network features such as global clustering and efficiency, small-world attributes, and heterogeneous degree distributions (Sporns). FCN alterations during resting state were reported in different neurological and psychiatric disorders, including depression (de la Cruz et al., 2019), and partial optic nerve damage (Bola et al., 2014) which revealed lower FCN coherence, less dense clustering, loss of small-worldness, and long-term reorganization. But unlike such resting-state studies, rFCN analysis can inform us of topological centrality and node activity changes as a function of time, indicating how fast the brain network can change in response to visual stimulation and in which time range such FCN plasticity happens.

In the present study I hypothesized that patients with optic nerve damage suffer disturbances in rapid visual processing and that rtACS can modulate topological networks structures and induce vision restoration. To this end, I first determined brain regions with the highest level of synchrony ("hubs") and functional connections between them before and after stimulus onset, comparing network dynamics in normal subjects and patients with vision loss at millisecond resolution. I next wished to learn if FCN metrics correlate with normal and abnormal visual performance. Finally, I investigated the effects of "neuromodulation" with rtACS to explore the functional relevance of fast FCN changes for "visual performance". Specifically, I hypothesized that hubs and their connections (i) can be monitored at millisecond resolution, (ii) they can vary systematically in their strength, stability and dynamics, (iii) are disorganized in patients with low vision, and (iv) they can

be modulated with rtACS which correlates with vision recovery.

4.2 Brain Spacetime in Normal Subjects

In control subjects with normal vision 20 FCN 'hubs' could be identified in the high alpha band in the default mode network (DMN), attention network (AN), salience network (SN) or execution control network (ECN) (Fig. 4.1). Surprisingly, primary visual cortex and visual-association areas had no hubs. Hub distribution among individual rFCN (Fig. 4.1A) and the averaged rFCN (Fig. 4.1B, C) were similar, but hub strength was quite different between individuals.

Although overall hub-topography was relatively stable, hub-strength and connections between hubs were highly dynamic during the one-second time vector following stimulus onset. Inter-hub connections changed their strength in tremendous (millisecond) speed. As (Fig. 4.2) shows, how hubs´ strength and connections can rapidly evolve and/or dissolve. After stimulus onset, the average rFCN had more connections compared to baseline. Here, the phase synchronized strength increased at around 300ms. At around 600ms, when the response button was pressed, the connections were densely connected. This pattern suggests that rFCN dynamics are behaviorally meaningful. Yet, the fluctuations of total hub scores show a typical oscillation pattern with peaks that are comparable to those found in visual evoked potentials (VEPs) (such as N100 and P300) (Fig. 4.1D). To facilitate interpretation, FCN transients were divided into different functional stages of neural processing that were known from visual evoked potentials: "baseline", from -200ms to 0ms ([-200,0]ms), "sensation/perception" ([0,200]ms), "cognition" ([200,400]ms), "execution" ([400,700]ms) and post-execution ([700,1,000]ms).

Rebustness of hub selection threshold was demonstrated by comparing my results with 15% and 25% thresholds, both of which showed similar results.

4.3 Brain Spacetime in Patients - Realignment of Node Centralities

Node activity changes over time were found in node degree, node betweenness, node closeness and node clustering coefficient, with transient engagements of different brain regions in space as a function of time. Compared to controls, patients had local disruptions in both hub and non-hub regions: three hubs showed transiently lower betweenness during visual processing in patients: left medial orbital frontal cortex at around 290 to 554ms (t_{mass} =88, $p = 0.02$), left superior temporal gyrus [478,686]ms (t_{mass} =67, $p = 0.01$), and left temporal pole in time ranges of [-94,97]ms (t_{mass} = 63, $p = 0.01$), [246,470]ms (t_{mass} = 97, $p = 0.004$), and [514,738]ms (t_{mass} = 77, $p = 0.007$) (Fig. 4.3A).

Regarding non-hubs, node activities of five regions were transiently lowered in patients, reflecting less synchronization compared to normal visual processing. Three regions located in the visual network (VN), including left cuneus cortex (CC: [100,500]ms, t_{mass} =136, $p = 0.01$), left lateral occipital cortex (CC: [-195,5]ms, t_{mass} = 68, $p = 0.02$) and left pericalcarine cortex (Degree:[82,345]ms, t_{mass} =88, $p = 0.02$; Betweenness:[361,486]ms, t_{mass} =32, $p = 0.03$), two regions were located in attention network (AN) and default mode network (DMN) respectively, including right supramarginal gyrus (Degree:[-10,230]ms, t_{mass} =82, $p = 0.02$), and left frontal pole (CC:[-163,-87]ms, t_{mass} = 22, $p = 0.04$; [37,97]ms, t_{mass} = 17, $p = 0.05$; [206,361]ms, t_{mass} = 47, $p = 0.02$) (Fig.

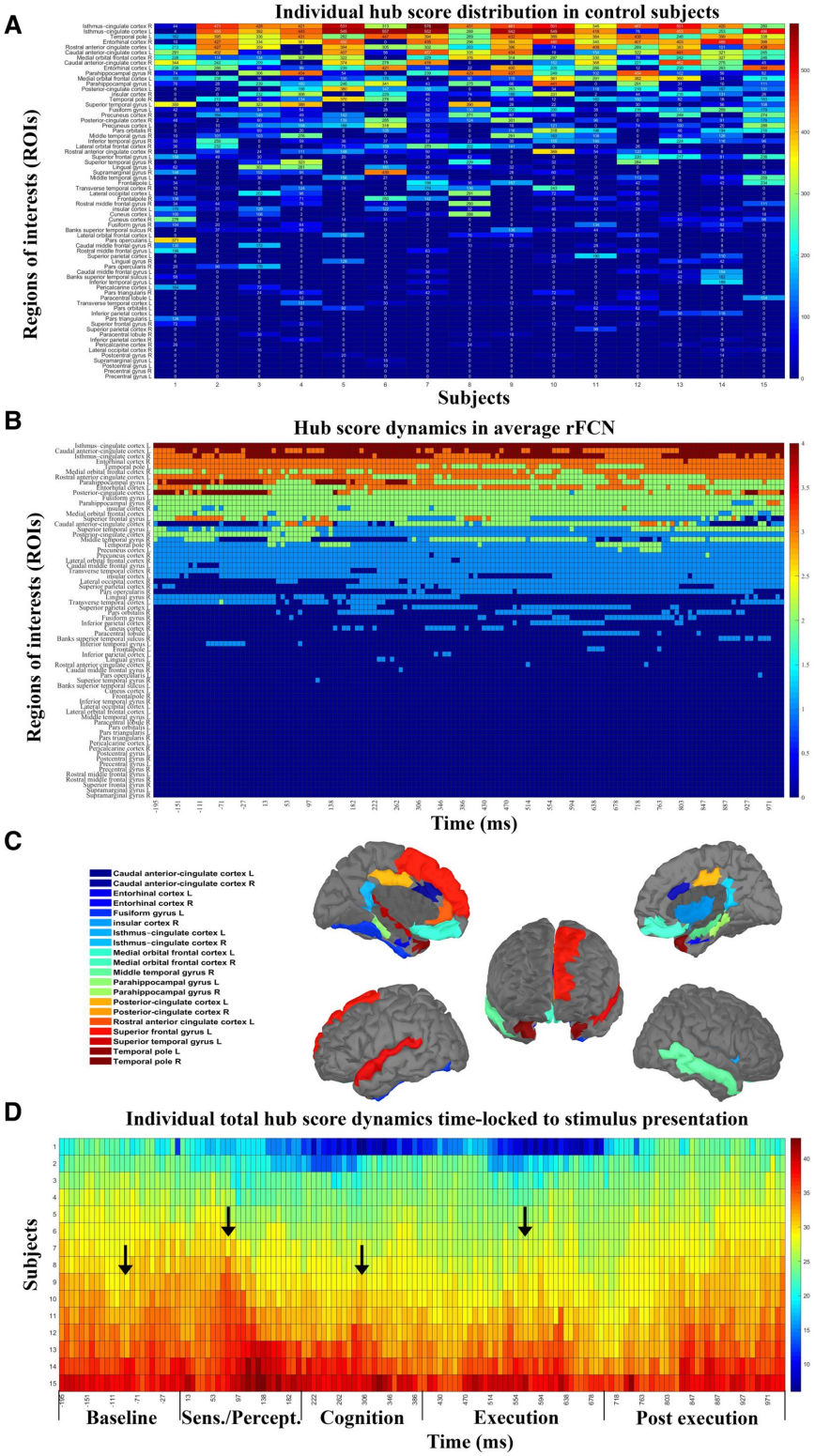

Figure 4.1: Hub score distribution and changes across time in high alpha FCN.
A: Hub score distribution in networks of individual control subjects during visual processing. Each value shows the sum hub score (0-4) during the recording epoch of -200 to 1000 ms for the respective brain areas. The regions are sorted from small to large. Control subjects varied in their individual hub localization, hub number and hub strength.
B: Transient hub score distribution of averaged healthy brain networks. Hub scores were computed for each region of interest (ROI) at each time point. If a region had a hub score >= 2 and a duration of >= 50 ms without interruption throughout the visual process, this node was identified as a hub. ROIs were sorted according to hub strength, differing in their hub (synchronization) strength and stability across time (scale shows averaged hub score 0 to 4 during visual processing).

Figure 4.1: C: In normal subjects I identified rFCN 20 ROIs which were hubs in the high alpha-band during the visual task in cingulate (n=7), temporal (n=9) and frontal cortex (n=3); and in the insular region (n=1).
D: Total hub score changes across time for all control subjects for the 20 hubs. It shows phases of hub score strength fluctuations across time. To facilitate interpretation, FCN transients were divided into different functional stages of visual processing: "baseline", from -200ms to 0ms ([-200,0]ms), "sensation/perception" ([0,200]ms), "cognition" ([200,400]ms), "execution" ([400,700)ms) and "post-execution" ([700,1,000]ms). Of note, peaks of hub strengths correspond to those typically found in evoked potential recordings (e.g., N100, P300).

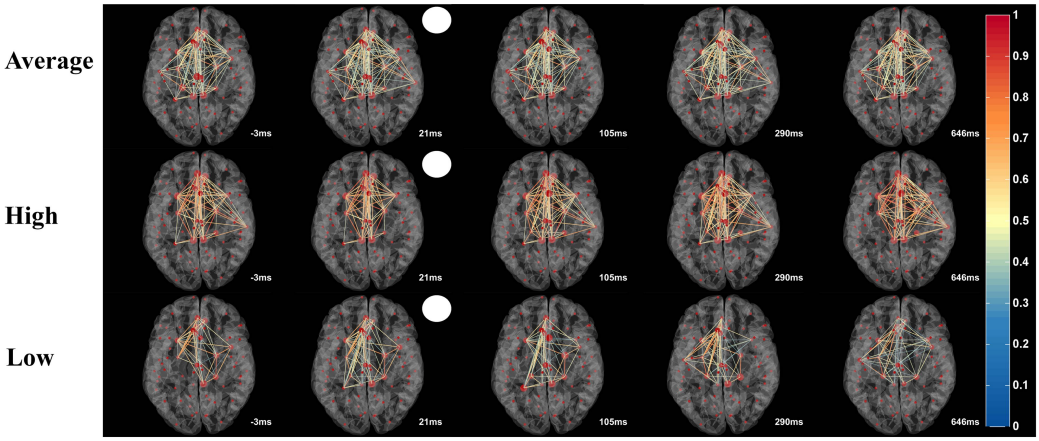

Figure 4.2: Imaging "Brain Spacetime" in visual processing. Transient network formations during visual processing displayed in time-slices as a function of visual stimulus onset (white circle) in averaged normal rFCN. Hubs (big red dots) represent ROIs with high synchronization (hub scores 2 to 4, displayed by hub size). Links between the hubs were color-plotted as a function of their weight from 0 to 1. The top row shows the averaged hub locations and their inter-hub connections in normal brains. The lower rows show two representative subjects with different levels of network synchronization (high and low).

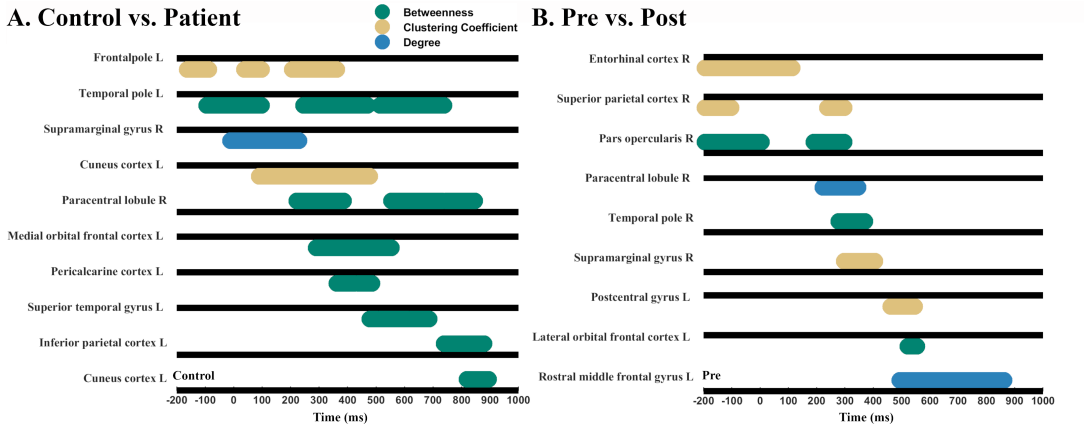

Figure 4.3: Significant node centralities as a function of the network state. Significant node centrality dynamics for different brain regions as a function of time in reference to stimulus onset (0 ms) during the visual detection task. The black line is the respective reference value for the control group (A) or the pre-rtACS group (B). The colored horizontal bars display time windows of significant differences between groups ($p < 0.05$) (green: betweenness; yellow: clustering coefficient; brown: degree). Whereas activation increases are plotted above the respective reference line, activation decreases are plotted under the line.
A: shows the differences of local hub properties between controls and patients which were mainly observable for "betweenness centrality" which was higher in controls than in patients. But three non-hub regions in patients (hub score< 2) show significantly stronger betweenness than controls. Other non-hubs of patients showed significantly weaker local activation in multiple node centralities.
B: Effects of rtACS neuromodulation on rFCN dynamics. Brain regions showing significant differences of local FCN attributes after rtACS treatment ($p < 0.05$). While node centralities of some brain regions increased following rtACS neuromodulation, others decreased.

4.3A). But there were also three non-hub regions in patients which showed transiently stronger betweenness in patients during visual processing in the right paracentral lobule ([222-385]ms, t_{mass} = -50, p = 0.02; [550-730]ms, t_{mass} =-68, p = 0.01), left inferior parietal cortex ([738-878]ms, t_{mass} = -48, p = 0.01) and left cuneus cortex ([818-894]ms, t_{mass} =-25, p = 0.05) which signifies 'compensation' (Fig. 4.3A).

4.4 Probing Spacetime Causality of rtACS Neuromodulation in Patients

More detailed FCN dynamics can be obtained when the time-vector is considered which shows great variability. Two hubs were transiently strengthened in degree or betweenness after rtACS in patients: the left superior temporal gyrus (Degree: [794,870]ms, t_{mass} =26, p = 0.03), which had a lower betweenness in the attention network than controls, and the right temporal pole (Betweenness: [278,369]ms, t_{mass} =36, p = 0.03), showing a synchronous enhancement, while before rtACS, betweenness of the left temporal pole was weaker. Another hub, the right entorhinal cortex, showed a significant decrease in its clustering coefficient (CC: [-195,113]ms, t_{mass} =-137, p = 0.001). In sum, rtACS modulated local connection patterns of hubs.

After rtACS, node centralities were also changed in several non-hub brain regions. Specifically, four non-hub nodes in the attention network were more enhanced as revealed by multiple node centrality metrics: left pars triangularis (Betweenness: [-195,-127]ms, t_{mass} =24, p = 0.04; [900,1000]ms, t_{mass} =42, p = 0.004), right pars opercularis (Betweenness: [-195,5]ms, t_{mass} =78, p = 0.02), left rostral middle frontal gyrus (Degree: [494,862]ms, t_{mass} =145, p = 0.01) and right supramarginal gyrus (CC: [298,405]ms, t_{mass} =71, p = 0.005). In addition, CC was transiently increased after rtACS in the right pericalcarine cortex ([73,169]ms, t_{mass} =43, p = 0.04) in visual network and left precentral gyrus (Betweenness: [602,638]ms, t_{mass} =16, p = 0.05) and in sensory-motor network (Fig. 4.3B).

But there were also 6 transient non-hub deactivations after rtACS treatment: two were in the attention network, including right pars triangularis (Degree:[602,786]ms, t_{mass} = -65, p = 0.02; [838,942]ms, t_{mass} = -42, p = 0.03) and the right superior parietal cortex (CC:[-195,-102]ms, t_{mass} = -45, p = 0.001; [237,297]ms, t_{mass} = -21, p = 0.03), and two in the default mode network, including left lateral orbital frontal cortex (Betweenness:[522,554]ms, t_{mass} =-17, p = 0.04), right lateral orbital frontal cortex (Betweenness:[454,562]ms, t_{mass} = -45, p = 0.02) and two in the sensory-motor network, including right paracentral lobule (Degree:[221,345]ms, t_{mass} = -52, p = 0.02), and left post-central gyrus (CC: [462,546]ms, t_{mass} = -34, p = 0.03)(Fig. 4.3B).

Thus, rtACS neuromodulation altered patients' ability to transiently synchronize oscillatory activity throughout the brain, affecting the reorganization of the attention network, visual network, sensory-motor network and default mode network.

4.5 Correlation between FCN Parameters and Visual Performance

To explore if FCN attributes correlate with vision performance, I calculated the Pearson's correlation of FCN metrics with age, reaction time and number of hit trials in both healthy controls and patients with optic nerve damage. I found that better visual detection performance was associated with transiently elevated hub scores (synchronization)

and increased SW (greater balance of integration and segregation). Specifically, the transiently higher hub scores in patients at 250-350ms correlated with faster reaction times, but this correlation was not present in normal subjects. After rtACS treatment, increased SW during -100 to 100ms (baseline and early sensory processing) was also positively correlated with the increased number of visual detections (hits). In normal subjects, SW was negatively correlated with age (Fig. 4.4A-D), but SW was not associated with reaction time or number of hit trials. Follow-up visual field tests were conducted after 8 weeks treatment and were found to be stable for at least 2-months. This result demonstrates the stability of the visual field parameters and their correlation with rFCN metrics. In addition, it has been shown that metrics of human brain networks exhibit typical test-retest reliability in the relevant graph-theoretic analysis of human brain networks and do not interact with time, highlighting the stability and reliability of these measured indicators (Vecchio et al., 2020).

I further analyzed the pre-task network status and found a significant correlation between pre- and post-task performance on multiple network parameters. It revealed that the maximum of global parameters in the post-task network were positively correlated with the pre-task network state in different frequency bands, including low alpha, high alpha, and beta, for both the control and patient groups (Fig. 4.4E, F). Perception in the brain can be viewed as a highly selective process, where top-down stimuli processing can create dynamic predictions about forthcoming events in stimulus-evoked and ongoing temporal activity (Engel et al., 2001).

This supports the notion that brain states at the time of visual stimulus onset influence final task performance. It provides remarkable insights into brain state-dependent, yet task-related, dynamics of rapid brain network reorganization.

4.6 Discussion

I visualized for the first time behaviorally meaningful brain FCN dynamics in the millisecond resolution during visual processing and recovery as a function of 3D-topology "Brain-Space" in the 4th dimension of "Time", 4D- "Spacetime". Rapid and transient FCN hub and node interactions evolved and dissolved within milliseconds, and this rapid FCN plasticity was associated with different phases of visual processing, co-varying in patients before and after rtACS neuromodulation-induced recovery.

I plotted 8ms EEG epochs to quantify fast and transient FCN plasticity in normal subjects and in patients with visual system damage. Using ERNA (Bola and Sabel, 2015), I now showed that "FCN transients" are associated with different phases of visual processing in normal subjects and are altered in patients before and after vision recovery. Apparently, rFCN reorganization in patients is not as flawless as in normal subjects, especially in hub regions of the visual network. But rtACS induces rFCN recovery of hubs and reorganization in the attention and vision network. However, patterns of neural FCN phase synchronizations are rather complex, in (brain space) location, strength and timing.

I identified 20 hubs in control subjects, of which 10 belong to the default mode network (DMN) (Raichle, 2015). These 10 hubs of a rather stable network of anatomical regions are believed to support different functions such as internal modes of cognitive (Buckner et al., 2008) or episodic memory processing (Greicius et al., 2004). Six hubs belong to the

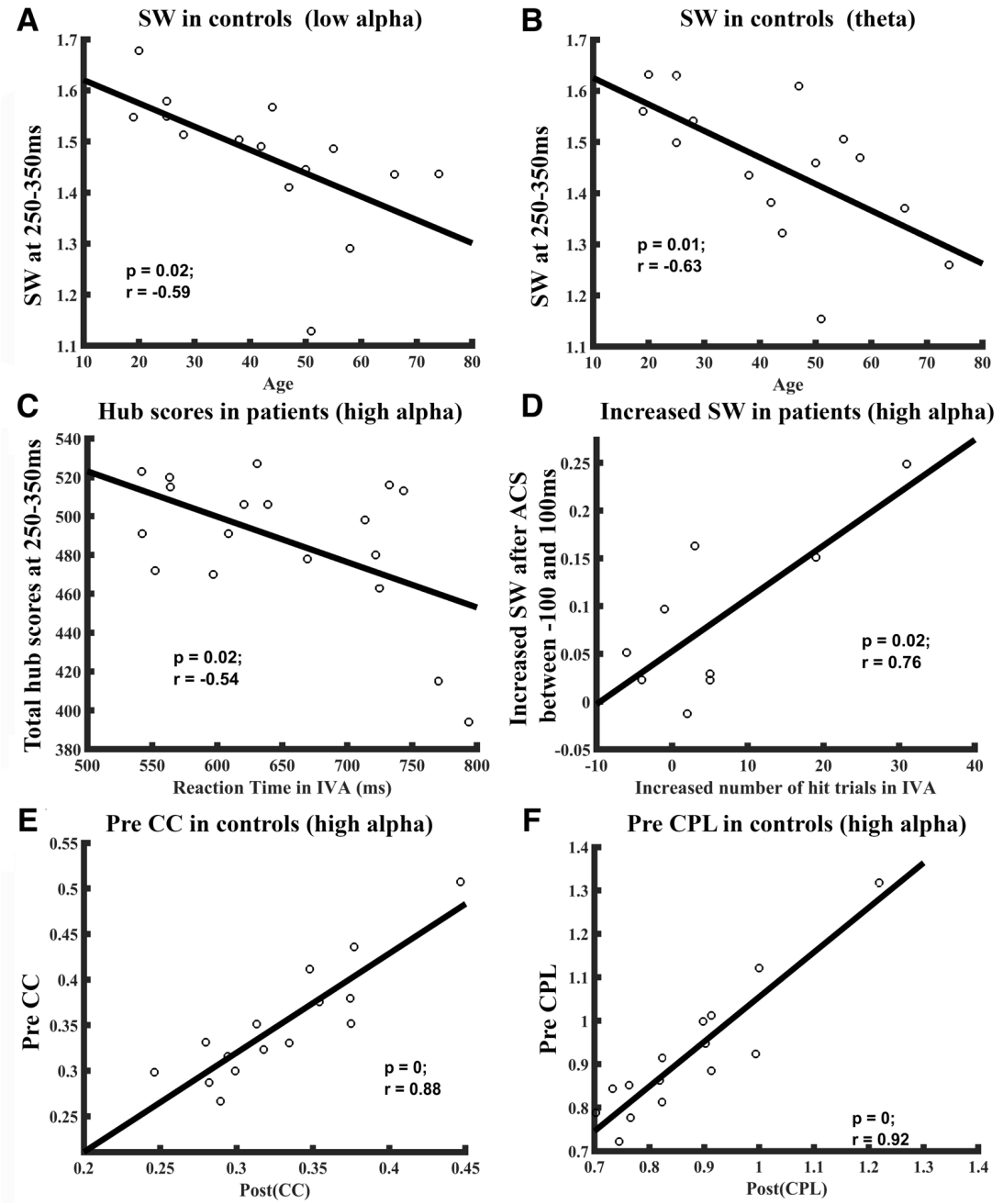

Figure 4.4: Visual detection performance in patients correlate with network metrics. Parts b-g: In normal subjects, small worldness (SW) was negatively correlated with the subjects´ age. Older subjects had weaker SW attributes during 250-350ms following stimulus presentation in low alpha (A) and theta (B) rFCN. In optic nerve damage patients, higher total hub-score at 250-350ms time window were correlated with the shorter reaction time (C). In patients after rtACS treatment, the increased SW during -100 to 100ms was positively correlated with the increased number of hit trials in the intact visual field sector (D). In addition, the maximum of clustering coefficient (E) and characteristic path length (F) in the post-task (250 to 650ms) network were both positively correlated with the pre-task (100ms before stimuli) network state. This means that rtACS optimized the rFCN of patients, i.e., better vision was associated with a higher hub score and increased small worldness. And brain states at the time of visual stimulus onset influence final task performance.

salience network (SN), which plays a key role in attention and the detection of behaviorally relevant stimuli by way of coordinating neural resources (Uddin, 2015). My study confirms that DMN hubs are rather stable in location, but I now unveiled that their strength, and the connections between them, are highly dynamic, establishing and dissolving during visual processing in the millisecond range. Such transient DMN hub activations possibly provide a network-state reference frame for temporal binding of visual processing with other, non-visual processes such as emotions, expectations, visual memories etc. Clearly, the DMN is not a passive "internal" network, but it influences, or is influenced by, sensory, cognitive or motor execution tasks. This is in line with the argument that the DMN plays a role in task relevant processing (Vatansever et al., 2015).

The question arises why hub scores are stable even though their connections rapidly change. As Fig. 4.2 shows, the inter-hub connections among hubs are highly dynamic as shown with 8ms resolution. Thus, although the connection between two hubs may appear to have disappeared, each hub quickly establishes connections with other hubs again. This rapid presence and absence of connections can result in the hub-score, and this can, in fact, remain relatively stable at a resolution of 8ms. Furthermore, I only analyzed stronger connections of hubs, but hubs can also have many weaker-type connections as well; it is the sum of all connections – stronger or weaker ones – that contribute to the hub score.

These 20 hubs play a key role not only in normal visual processing but also in patients with visual system damage. Here, three hubs were disrupted in their betweenness centrality, and some "non-hub" regions had weaker local activations in the visual and attention network. In view of the special role of frontal-occipital network interactions in visual processing (Bola et al., 2014), I believe that such network disturbances cause interruptions during vision related cognition due to FCN reorganization in key hubs, even if these brain regions are anatomically "intact". This might help explain subtle visual disturbances or pseudo-hallucinations in low vision patients (Poggel et al., 2007). Furthermore, two non-hub regions that belong to the visual and attention network showed stronger betweenness during visual processing in patients: the left inferior parietal cortex and left cuneus cortex ROIs. On one hand, this illustrates the disruption of hub regions and peripheral visual and attention networks in patients' rFCN, but - on the other hand - it also documents compensation in non-hub regions to adapt to the loss of interactions in patients during visual processing.

To learn if changes on rFCN are associated with different behavioral states, I studied the dynamics of rFCN following neuromodulation using rtACS treatment to study if this impacts vision recovery. rtACS is a non-invasive method which can modulate ongoing brain activity rhythms, it enhances alpha activity in normal subjects (Kasten et al., 2016), and in patients with optic nerve damage (Sabel et al., 2011b), it induces "after-effects" that outlast the stimulation period (Sabel et al., 2020a). Repeated rtACS modulates resting-state FCN re-synchronization, enabling more effective information transfer both in normal subjects (Ali et al., 2013) and in patients (Bola et al., 2014). My rFCN findings confirm this conclusion and show that rtACS normalizes integration within subsystems and improves small world organization at rest (baseline), early sensory and late cognition stages in patients. The peripheral attention network and visual network also showed significant enhancement after rtACS, and the default mode network and some regions of visual network reorganize in their hub score dynamics during vision processing. In sum, I observed rapid FCN plasticity both in normal subject and in patients as supported by

many transient FCN patterns especially in the alpha-rhythm. In fact, visual performance correlated significantly with greater alpha network synchronization, and both reaction time and visual detection improved after alpha rtACS stimulation, which, in turn, significantly correlated with alpha PLV networks. Therefore, I interpret visual improvement as a sign that alpha frequency oscillating networks induce activation, not inhibition, of visual processing.

The alpha rhythm has long known to be a fundamental mechanism of perception and cognition, affecting multiple top-down cognitive processes (Helfrich et al., 2014). Therefore, I focused analysis on the alpha PLV networks. While alpha oscillations are functionally distinct, I cannot tell if they serve an inhibitory or active purpose. In some tasks alpha oscillations may support inhibition of task-irrelevant neuronal processing on amplitude dynamics in several EEG and functional MRI studies, yet others suggest that alpha phase dynamics support activation in task-relevant functions like attention (Lobier et al., 2018), working memory process (Crespo-Garcia et al., 2013) and executive functions (Haegens et al., 2011).

While my research focused upon alpha frequency network modulations, I recognize that neural processing involves simultaneous oscillations in multiple frequencies, not just alpha. For example, beta oscillations represent coordination and adaption between neurons in the motor system (Buzsáki et al., 2013), and theta oscillations largely serve to structure recurrent interactions of neurons during working memory (Lee et al., 2005).

Other types of phase synchronization across frequencies exist, like cross frequency coupling (CFC) (Canolty and Knight, 2010) to integrate neuronal activity across different spatial and temporal scales. The relation and statistical dependence across frequencies awaits further experimental evidence due to the complexity of the different varieties of CFCs, like phase-amplitude CFD, phase-phase CFC and amplitude-amplitude CFC.

Nevertheless, my observation of functionally relevant millisecond dynamics of FCN has broad implications of how neural information is synchronized in the dimensions of neural 3D-SPACE and the 4th dimension of TIME in visual processing and recovery. I propose that "Brain Spacetime" as a fundamental principle of the human mind not only in vision cognition, but also in vision restoration. Specifically, I showed that nodes and their connections (i) can be monitored at millisecond resolution, (ii) they vary in strength, stability and dynamics over time, (iii) they are disorganized in patients, and (iv) neuromodulation with rtACS modulates temporal processing of rFCN which correlates with vision recovery.

5 Modularity Dynamics of Brain Networks Following Local Damage

Using dynamic modular analysis, I studied several questions about multilayer modularity of visual evoked functional networks in both normal controls and optic nerve patients: (i) Are there any communities in visual processing which more preferably connect within modules? (ii) If so, how do these communities modulate visual processing in optic nerve damage patients? (iii) Does rtACS treatment (neuromodulation) affect the multilayer modular architecture? I addressed these questions by quantifying putative modules at the multi-layer level as induced by visual stimulus presentation.

5.1 Introduction

Damage of the brain has not only local effects at or near the lesion site, but it also impacts distant regions in the brain functional connectivity networks (FCN) on a global level. Indeed, vision loss and blindness after optic nerve damage is not just the result of the primary cell loss in the retina, but it has also secondary and tertiary functional deafferentation effects on visual and non-visual brain regions (Bola et al., 2014; Wu and Sabel, 2021). To better understand the nature of neurological deficits and post-lesion dynamics (progression or recovery), I need to know if and how different nodes synchronize their neural interactions to form functional communities ("modules") and find out if this modularity can be modified after treatment. This can be studied most elegantly using the local lesion paradigm of partial optic nerve damage.

Modularity describes the modular organization of brain networks (Newman, 2012), where communities of nodes preferentially interact with each other to form strongly connected subgroups. Modules can engage in data analysis with high dynamic complexity, and the principle of a "modular architecture" reduces the wiring cost in neural information processing (Raj and Chen, 2011). Indeed, there is a correspondence between performance of higher order processing and reconfiguration in topological community structure or intermodular communication (Kitzbichler et al., 2011).

There is evidence that brain FCN modularity is a functionally meaningful parameter of "spacetime in the brain". For example, modularity was recently proposed to be a biomarker of plasticity associated with interventions that can drive cognitive plasticity (Gallen and D'Esposito, 2019), and schizophrenia patients show alterations of network flexibility in the dynamic reconfiguration of community structure during working memory (Braun et al., 2016).

Especially "multilayer modularity" is an important principle for our understanding of temporal dynamics of FCN reorganization during complex cognitive functions. A time-resolved community analysis of functional networks requires the identification of modular structures across multiple time slices, and especially the multilayer modular analysis is a useful method to examine temporal dynamics of networks (Mucha et al., 2010). For example, it was used for the study of learning-induced evolution of connectivity patterns over the course of four training sessions (Bassett et al., 2015). Network architecture patterns where also reported to change across the human life span, showing that ageing leads to reorganization of modular structures and inter-hemispheres redistribution of neural processing

(Puxeddu et al., 2020). Others studied the modular structure across different depths of consciousness during anesthesia and found a hierarchical fragmentation of dynamic network and disturbance of temporal interactions between cortical modules (Standage et al., 2020). While it is known that dynamic reorganization of network patterns can rapidly change, the dynamic multilayer modular topology changes on the time vector has not been studied in optic nerve damage patients.

To achieve a more precise brain spacetime description of FCN modularity dynamics, I now employed a simple visual detection task where, similar to visual evoked potential (VEP) recordings, the precise onset-time is known. I used this approach to study normal subjects and patient with optic nerve damage, where I could correlate visual detection performance with alterations in modular dynamics. In addition, I used treatment of the patients with transorbital alternating current stimulation (tACS) to study how visual dynamics (here: vision recovery) and FCN modularity correlates.

The transcranial electrical stimulation induced primary and secondary vascular response has been observed in various studies (Sabel et al., 2019). And there is a suggestion that vascular parameters are modified to match the neural activity of the stimulated brain networks (Bahr-Hosseini and Bikson, 2021). rtACS was previously shown to modulate (improve) visual function and altered FCN reorganization (Schmidt et al., 2013; Bola et al., 2014). In the current study, I used data collected earlier and published by Sabel (Sabel et al., 2011a). In this earlier study, the improvement in visual function and the enhancement of alpha brain oscillation was identified (Gall et al., 2011; Sabel et al., 2011a). I subsequently linked individual responses and vision recovery with rtACS-induced alteration in brain functional connectivity networks between individual brain regions (Wu and Sabel, 2021). In the present study, I studied this brain network plasticity in greater detail by exploring network nodes and their clustering of communities before and after neuromodulation with rtACS.

Therefore, I set out to describe the community structure and multilayer brain network changes to explore how modification of the modulation of strength of intra- and inter-module interactions with rtACS brain stimulation impacts visual performance.

As I have shown, functionally separated modules of multilayer brain networks respond to visual stimulation and inter-module interactions relate to visual performance. I found that rtACS promotes both global optimization of modular organization and local activation of pathways associated with attention network, providing a new understanding of the role of multilayer modular architecture in visual processing.

5.2 Multilayer Modularity Diagnostics

The examination of the null model in multiple layer networks is necessary, because it helps defining the fundamental basis for the community detection, permitting the principle identification with statistical significance in the diagnosis of network communities.

To determine whether the real network shows community topology, I firstly investigated statistical differences between real networks and surrogate null models which were constrained by properties of the empirical network. Three appropriate null models were generated including connectional null model, nodal null model and temporal null model as proposed by Bassett (Bassett et al., 2013). The connectional null models were constructed

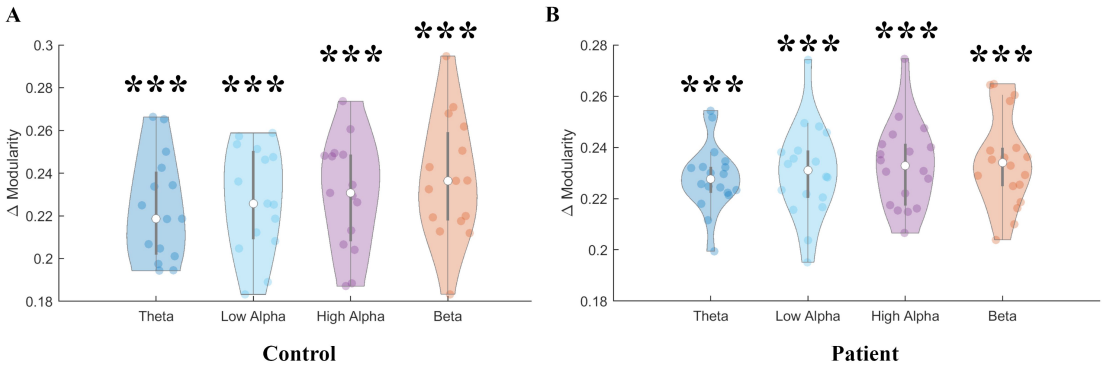

Figure 5.1: Comparison of real networks versus connectional surrogate null networks using the optimized module quality function for both normal (A) and patient (B) groups. The x-axis displays the frequency bands, the y-axis shows the difference between the null model and the real FCN modularity. The "Violin plots" indicate interquartile range and kernel density at 95% confidence interval. Compared to the null model, both controls and patients with optic nerve damage displayed heightened community topology in all frequency bands.

by reshuffling the links between nodes in each layer while maintaining the weight, degree and strength distribution as the empirical network. While the nodal null model scrambled inter-layer links that connected a single node in one layer to another layer, the temporal null model randomly permutated the order of the network layers. Then, for each subject, I subtracted the optimized multilayer modularity for the surrogate networks from that of the original networks in each frequency, and subsequently I tested difference values against 0 with a one sample t-test.

The optimized multilayer modularity was characterized by the multilayer "modularity index Q". The maximization of Q allows partitions of optimization considering both intra-layer connection and inter-layer coupling in a multilayer network.

I found that the dynamic networks of both controls and patients with optic nerve damage showed a large difference from the null model and displayed heightened community topology in all frequency bands (Fig. 5.1). This verifies the existence of the modular structure in the visual evoked functional networks. Comparison of the real network with nodal and temporal null models showed similar results (Fig. 5.2).

5.3 Multilayer Modular Organization

Because the brain FCN can dissolve and evolve rapidly (Wu et al., 2020), I need to characterize such dynamic fluctuations on the time vector. Specifically, I would expect that the organization of the modular structure also displays apparent changes in the temporal dimension which might be functionally meaningful.

To adequately explore this multilayer modular organization, in addition to the multilayer "modularity index Q", the parameter of "flexibility" was characterized under multiple conditions. "Flexibility" represents how often a given node changes its modular affiliation across consecutive time steps. In dynamic multilayer networks, each layer corresponds to one time point.

My results showed that in intact visual field regions, the modularity and flexibility of patients' FCN did not differ significantly from that of the normal controls (Fig. 5.3A).

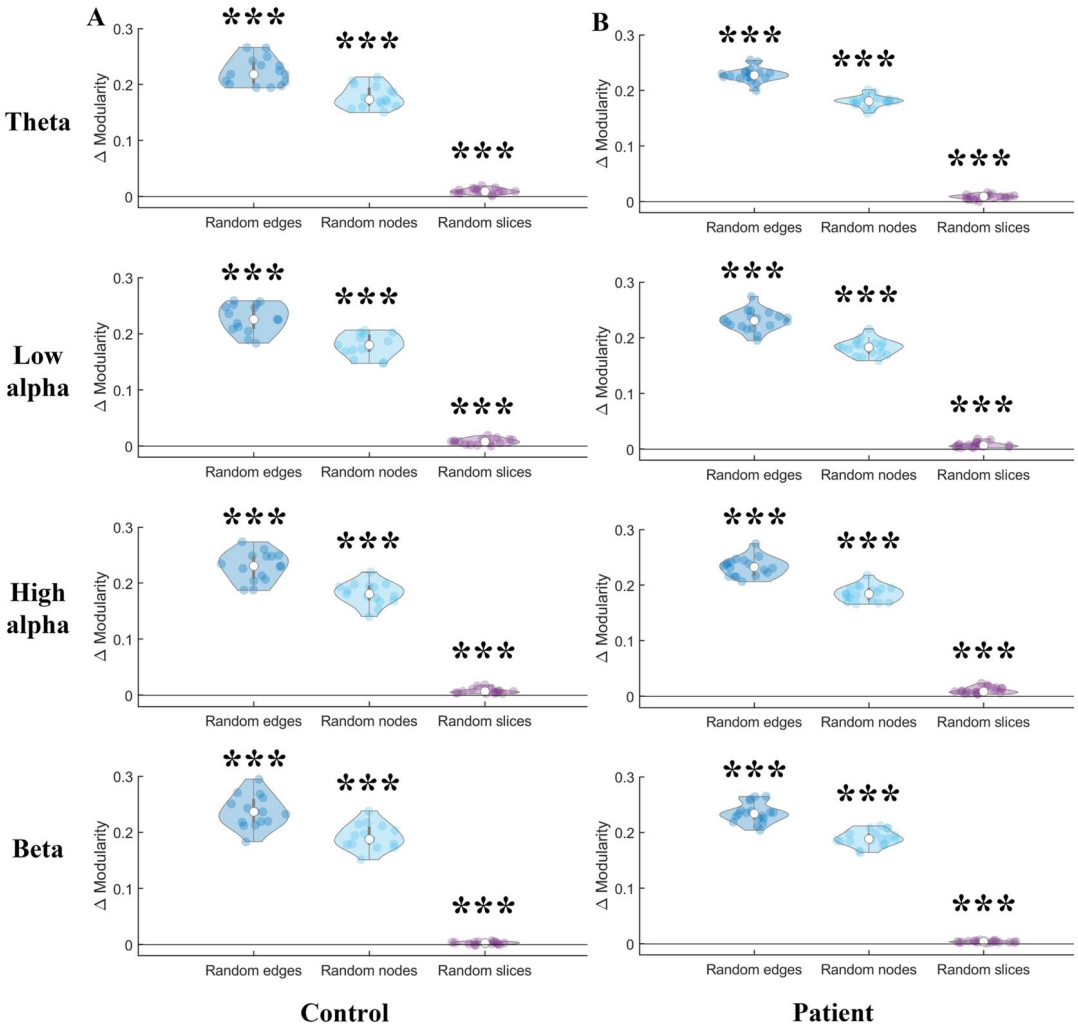

Figure 5.2: The presence of modular structure was statistically quantified by comparing the real and surrogate null networks of controls and patients. Three appropriate null models were generated, including connectional null model (random edges), nodal null model (random nodes) and temporal null model (random slices). The connectional null models were constructed by reshuffling the links between nodes in each layer while maintaining the weight, degree and strength distribution as the empirical network. While the nodal null model scrambled inter-layer links that connected a single node in one layer to another layer, the temporal null model randomly permutated the order of the network layers. Then, for each subject, I subtracted the optimized multilayer modularity for the surrogate networks from that of the original networks in each frequency, and subsequently I tested difference values against 0 with a one sample t-test. The brain FCN of both controls (A)and patients with optic nerve damage (B) exhibited the modular structure in all frequency bands of visual cognition. Statistically significant differences: *** $p < 0.001$.

Furthermore, there was no significant difference between the rtACS and sham group before treatment (Fig. 5.4A). However, after receiving rtACS, the modularity of the patients was significantly increased in the high alpha FCN, while the flexibility of the beta network was significantly decreased (Fig. 5.3B). The sham group, on the other hand, did not show any difference before and after treatment (Fig. 5.4B).

Thus, rtACS treatment induced changes in the multilayer community structure as follows: after rtACS the multilayer modular topology shifted towards a more optimized and stable modular structure, while the sham group showed no such differences of the multilayer modular structure.

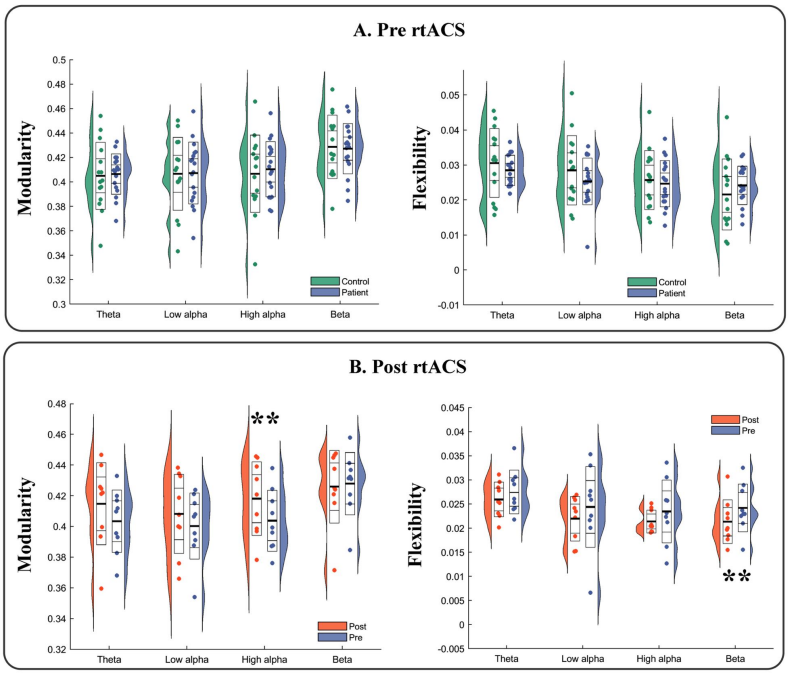

Figure 5.3: Modularity of multilayer networks for visually evoked brain networks. A: Before treatment, the modularity and flexibility of patients' FCN did not differ significantly from those of normal controls. B: However, after treatment with rtACS, patients showed a significant increase in the modularity of the high alpha FCN (left), and a significant decrease in the flexibility of the beta network (right). Statistically significant differences between conditions: ** $p < 0.01$, *** $p < 0.001$.

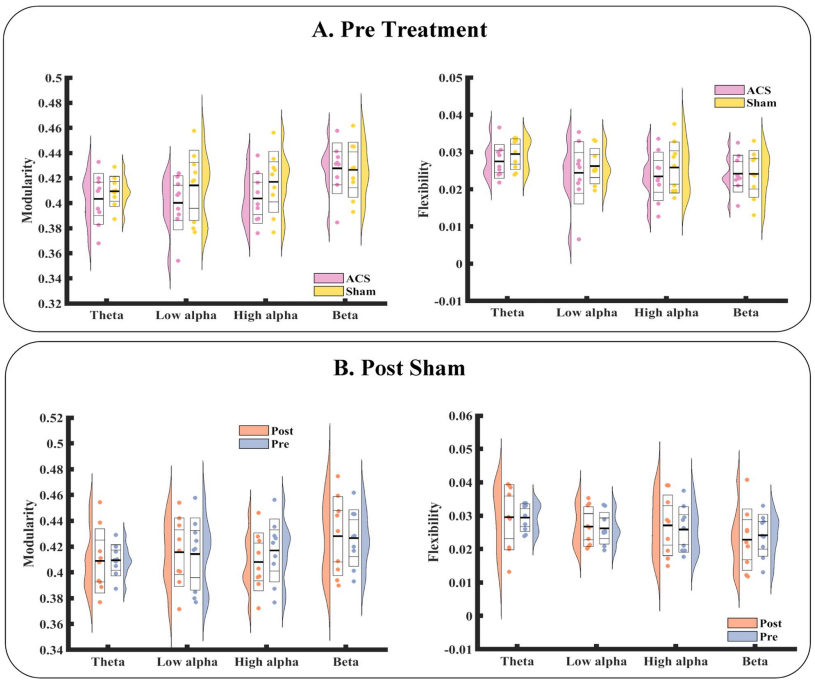

Figure 5.4: Comparison of FCN modularity and flexibility during visual processing in rtACS and sham patients group. A: Before treatment, the modularity and flexibility of the FCN in the rtACS group were not significantly different from those in the sham group in all frequencies. Modularity and flexibility were calculated for the multilayer network formed throughout the visual processing. B: Characteristics of modules were computed to compare the effects of the sham treatment. In the sham group, modularity and flexibility of the FCN in all frequency bands did not show significant changes before and after treatment.

5.4 Representative Partitions in Dynamic Multilayer Networks

Multilayer module analysis can obtain a set of partitions by repeatedly applying modularity maximization algorithms. Considering the degeneracy of community detection algorithms, the examination of consensus partitions that can reveal the consistency of module affiliation of nodes in multiple partitions helps generate a common representative partition of the community structure. Using these measures, I evaluated the consensus architecture in visual processing.

One of my first question was the following: "Are consensus modules expressed during visual processing?" To answer this question, I extracted the consensus brain network communities that were consistently active during the whole visual process using the clustering approach. A module allegiance matrix was estimated for each pair of brain regions, with each element representing the probability of two nodes being classified into the same community in FCN over all time layers, frequencies, subjects and group conditions (Mucha et al., 2010).

I observed that the brain networks of our subjects have four identifiable communities, where different regions preferentially interact with each other during visual processing (Fig. 5.5A). The module allegiance reveals the extent to which these brain areas are consistently grouped into the same module (or "community"). I refer to these four putative functional modules as "motor", "attention", "visual" and "other" modules (Fig. 5.5B).

5.5 The Architecture of Multilayer Networks in Optic Nerve Patients

To further understand how consensus brain modules were distributed and reorganized before and after treatment in patients with optic nerve damage, I constructed module allegiance matrices for each group. I observed greater inter-regional allegiance within modules of patients, which clustered more persistently than normal subjects throughout visual processing especially in attention and other modules. However, allegiances were stronger after rtACS treatment, whereas they did not change much in the sham group (Fig. 5.6).

5.6 Interaction Strength Correlates with Performance

To further quantify the modular architecture of multilayer networks, I next evaluated the interaction strength of modules in the brain. The interaction strength of both intra- and inter-modules in motor, attention, visual and other modules were estimated at individual subject level per group. Next, I investigated whether such interaction strength of modules could explain the different behavioral performance in the visual detection task among individuals. To this end, I calculated Spearman rank correlation coefficients between the interaction strength of the modules and the number of trials detected during visual processing and individual reaction time. The correlation coefficients were not corrected for multiple comparisons as my study was of exploratory nature. If I included the total number of interaction strengths and the variable of visual behavior for multiple corrections, I believe this to be too stringent for the statistics of a relatively small sample of an exploratory study and miss findings that might be clinically relevant.

Normal subjects showed stronger interaction strength between motor and visual net-

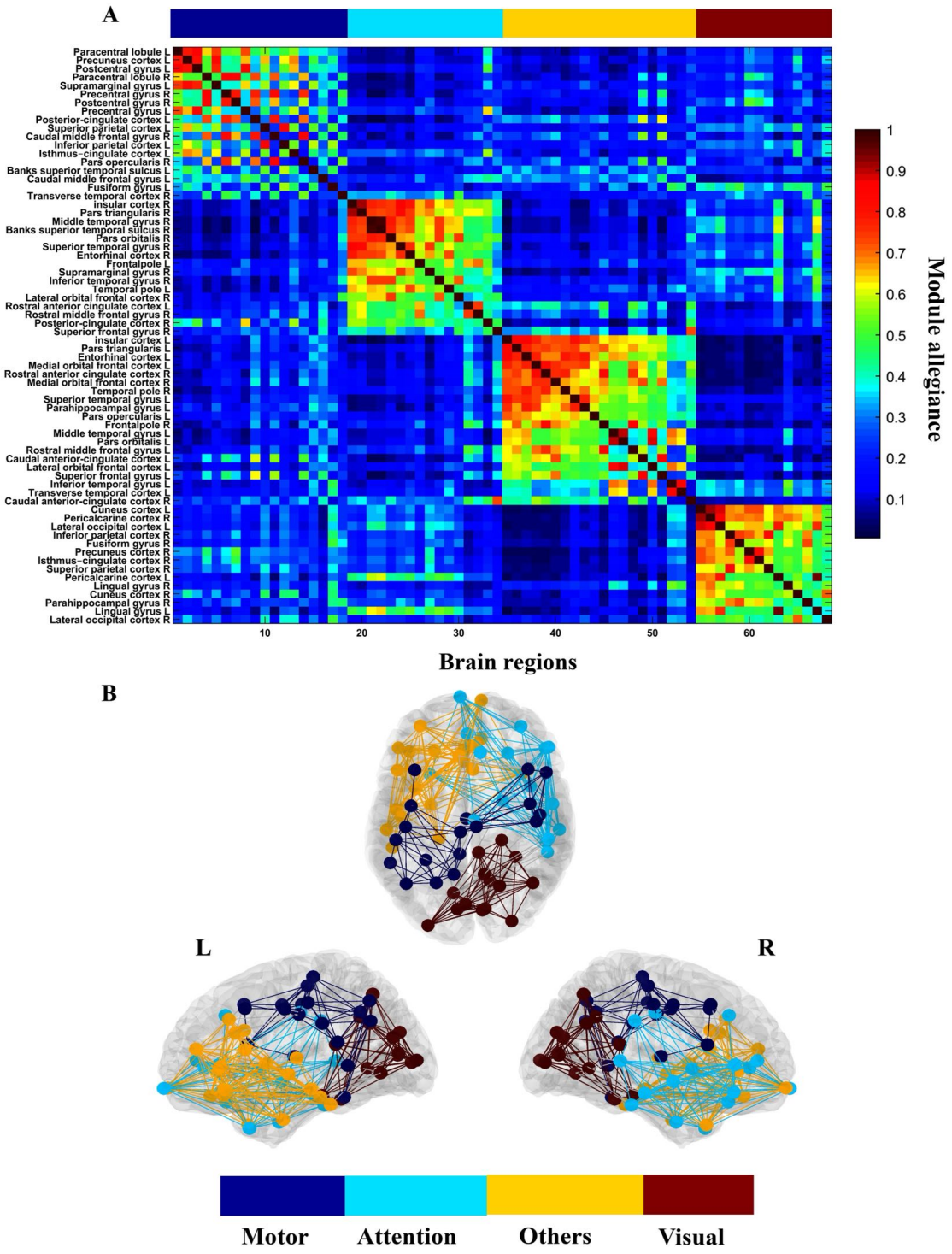

Figure 5.5: Representative partitions of multilayer networks during visual processing. A: Four consensus brain network communities that were consistently active during the visual process were identified in the brain networks using the clustering approach. Each element of the module allegiance matrix represents the probability of two nodes belonging to the same module across all time layers, frequencies, subjects and group conditions. Brain regions of each module are shown in descending order according to their strength of module association. B: Visualization of representative partitions of the brain surface. Four communities were putatively identified which are proposed to support different functional modalities: "motor", "attention", "visual" and "other" modules.

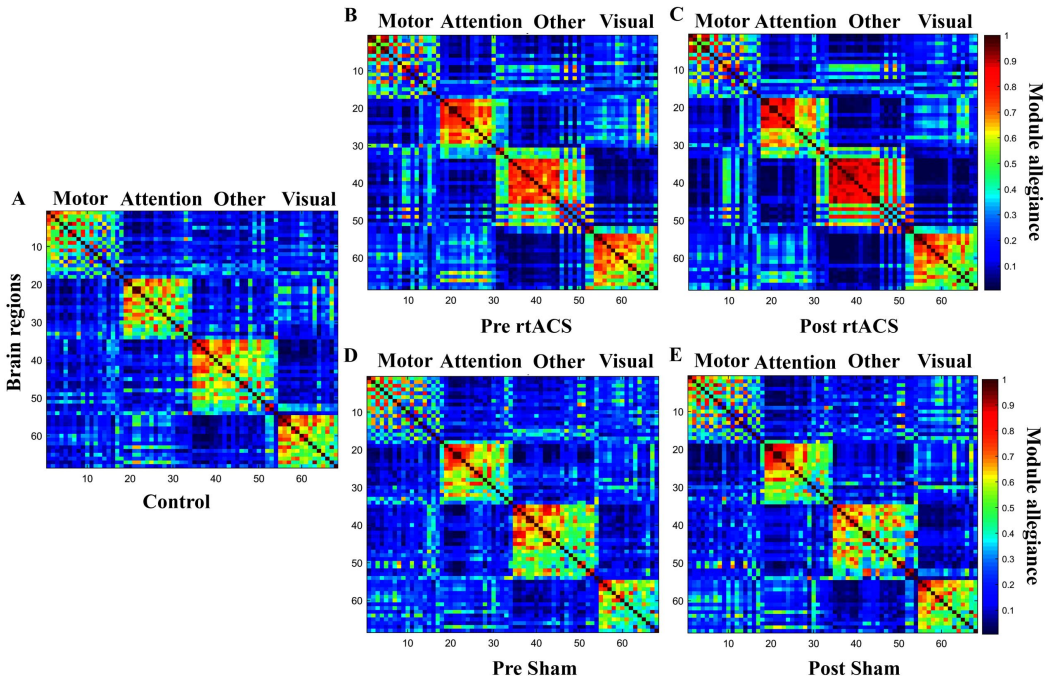

Figure 5.6: Modular allegiance between groups during visual processing. The communities were plotted based on consensus representative partition. The order of brain region names is consistent with Figure 5.5. A showed the strength of interregional allegiance in normal subjects. B-D represented the distribution of module allegiance values for patients before and after rtACS (B, C) or sham (D, E) treatment. Patients had greater interregional allegiance within modules and clustered more consistently than normal throughout visual processing, especially in attention and other modules. Allegiances were stronger after rtACS treatment, whereas they changed little in the sham group.

work and this correlated with the greater number of correct responses in the visual task (hit trials). In addition, the attention-motor and attention-visual networks integration intensities were associated with an increased number of hits (Fig. 5.7A), which was evidenced that neural processing and task performance (visual detection) required the functional coordination between visual-motor, attention-motor and attention-visual modules. While this conclusion seems obvious, the result highlights the functional validity of our FCN community approach which makes this interaction measurable. In optic nerve damage patients, faster reaction time was associated with greater interaction strength of motor-visual modules, showing similar results to normal subjects. However, the strength of interactions between motor-other and visual-other modules were negatively correlated with reaction time, not the attention related connections (Fig. 5.7B). In optic nerve patients apparently, "other networks" became more engaged in visual processing, leading to a strong integration of visual and motor module with other modules, i.e., a global brain FCN adaptation or engagement.

The recruitment of intra-modules was not significantly correlated with individual visual performance. This suggests that interaction strength between modules had a more pronounced effect on subjects' behavioral performance than the integration within modules. This implies that better or worse vision is supported by the global brain FCN synchronization, and not just the strengthening of neural processing in local (visual) regions.

The differences in interaction strength of modules between pre- and post- rtACS showed that changes of the interaction strength between motor-attention and attention-

other modules were positively correlated with changes in the number of correctly detected stimuli (Fig. 5.7C). However, patients of the sham group did not show this association.

5.7 Discussion

Damage of the brain has both local effects at or near the lesion site and it affects remote regions of the brain functional connectivities network (FCN). Using partial optic nerve damage as a model, the present study explored how the multilayer network module architecture responds to visual stimulus presentation in normal controls and in patients with optic nerve damage, particularly with respect to the extent to which modules interact within and between each other. In this way, I was able to highlight the modular architecture of dynamic multilayer network under different conditions and study the impact of rtACS neuromodulation on the community structure of such dynamic networks.

I firstly confirmed the existence of a pronounced modular structure in the visually evoked functional networks comparing our data with the modularity index of random networks. As I demonstrated, the brain operates as a modular system to control functional separation and integration of the modular topology to ensure flexibility and reliability of the brain FCN. This is because independence between subsystems helps neural connections reduce the risk of major dysfunction of the entire network system due to defects in local areas. Consistent with previous findings (Variano et al., 2004; Sporns and Betzel, 2016), the hierarchy of modules added resilience and robustness of the network to random perturbations. In particular, in both normal controls and visually impaired patients our modular architecture analysis revealed visual, attention, motor and other communities which formed functionally separate modules during the whole visual processing within one second after stimulus presentation.

My findings of modular structure in the FCN of the brain are in line with other studies on the brain's structural and functional wiring network in cognition (Cohen and D'Esposito, 2016; Sporns and Betzel, 2016). It is also in line – though on another level - with other examples of modularity in other biological analyses. For example, modularity is found in gene expression patterns and in cytoarchitecture. Specifically, a group of genes with a similar expression profile is considered to be functionally related (Saelens et al., 2018), and transcriptomes of co-express genes modules can be used to distinguish major cell classes of the human brain (Oldham et al., 2008). And modular organization of cellular networks has been identified for protein interaction and protein complexes (Rives and Galitski, 2003).

My study shows that global modular properties were not statistically comparable between healthy subjects and patients in the "intact" sector of their visual fields. This suggests that the overall multilayer modular structure for visual processing was not affected. Furthermore, and in agreement with previous studies, the interaction strength of intra-modules was not significantly correlated with individual parameters of behavioral parameters, here visual performance. According to theoretical tenets concerning the human brain network architecture, activities within modules do not increase when processing cognitive tasks that requires coordination of multiple brain functions. My observations are in line with this argument that each module performs distinct cognitive function relatively autonomously from other modules. Specifically, when processing cognitive tasks requiring the coordination of multiple brain functions (functionally specific sub-networks), activities

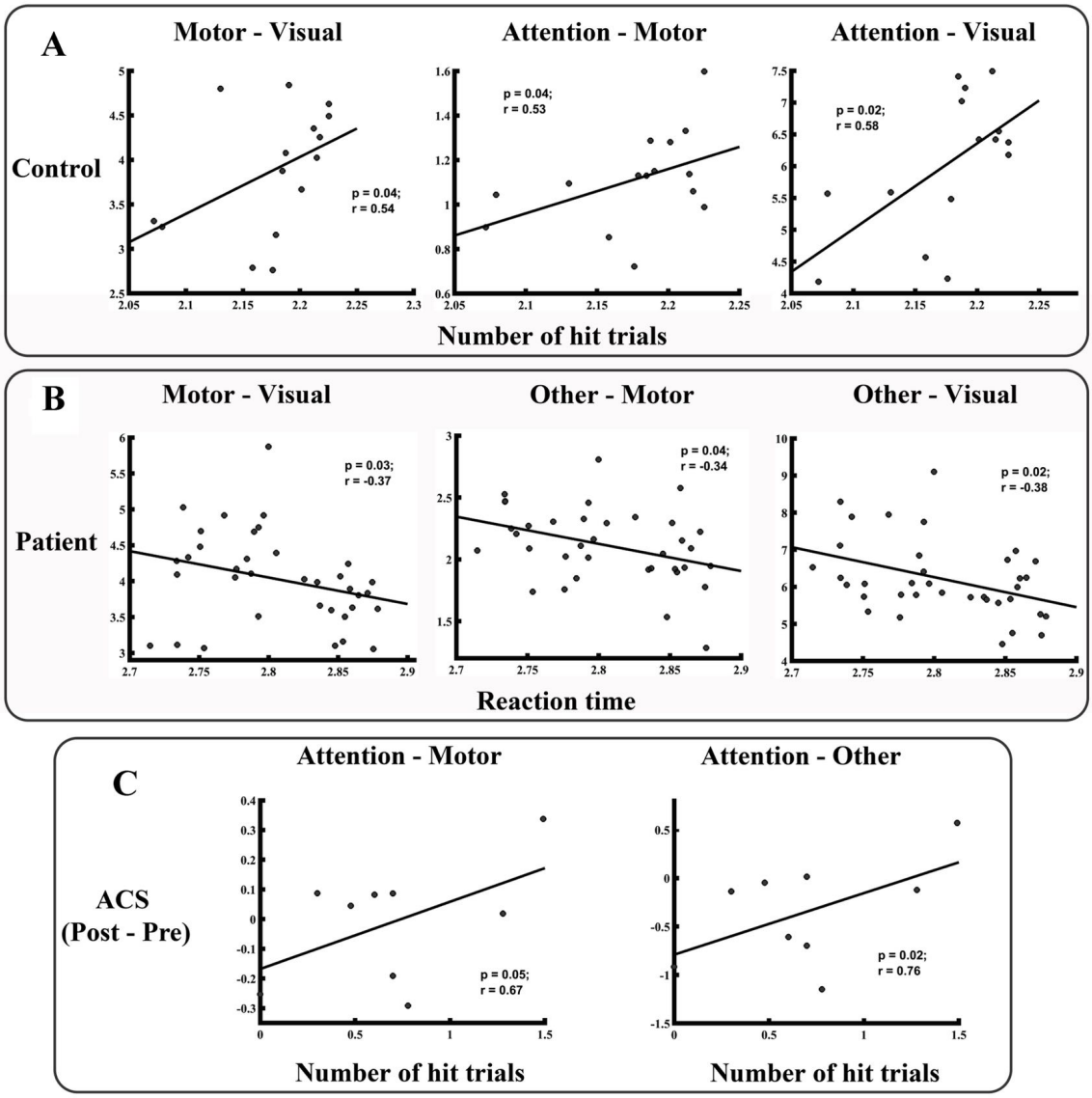

Figure 5.7: Schematic diagram of visual field distribution and correlations of interaction strength of modules with behavioral performance. A: Scatter plot of the number of detected stimuli and their relationship with the interaction strength of the motor-visual, attention-motor and attention-visual modules in normal subjects. B: In patients with optic nerve damage, the interaction strength between motor-visual, other-motor and other-visual were shown as a function of individual reaction time in all patients before and after the treatment together. C: After rtACS treatment, changes in the interaction strength between the attention-motion and attention-other modules were positively correlated with changes in the number of correctly detected stimuli. The number of trials practiced and response times shown here using logarithmic scales.

within modules do not increase, but the connector nodes between modules communicate more with each other (Bertolero et al., 2015).

Indeed, in the absence of statistical differences in overall multilayer network modules between healthy controls and optic nerve patients, I found that local interactions between modules were correlated with their behavioral performance. Specifically, in normal subjects, better vision (processing speed/ reaction time) was associated with greater visual-motor, motor-attention and visual-attention interactions. However, in patients the stronger integration strength between visual-motor, motor-other and visual-other was associated with superior behavior performance which suggests that the strength of interaction between modules had a more pronounced effect on subjects' behavioral performance than the integration within modules. This is a hint that in our patients, other modules assume more responsibility for inter-modules connections in visual perception, especially taking over some of the inter-modules connectivity functions that should have been performed by the attention-motor and/or attention-visual modules.

I wish to point out that our naming of four representative communities is implicit and does not properly reflect the structural-functional complexity of the network. Yet, it is a first and useful step on approximation to help interpret the modular interactions and dynamic reconfigurations before and after neuromodulation following rtACS treatment. Future studies should explore in greater detail the more covert neuromodulatory mechanisms within these modules.

But how does local optic nerve damage affect global multilayer module structure and interaction? Ever since the work of C.v. Monakow (Monakow, 1914) clinical neurologist know that pathology in one region can cause impairments in functionally deafferented, remote brain regions (Catani et al., 2012). These changes are well beyond the secondary degeneration in the optic tract and the brain´s striate cortex following retina or optic nerve damage (Beatty et al., 1982; You et al., 2012). This functional interaction with remote brain areas, or the lack of it, can either be maladaptive, amplifying the functional problem, or it can be an adaptive compensation of neural interactions between communities in patients with optic nerve damage (Fornito et al., 2015). Indeed, modules of the multilayer module architecture may become more (or less) engaged in optic nerve damage patients, contributing to visual tasks through inter-module connections or disturbing vision.

The other key finding of the present study was that the modular structure could be neuromodulated with non-invasive brain stimulation. I observed that after rtACS treatment, the global modularity index of the optimal network partition was significantly improved. The modularity of multilayer brain networks quantifies how well a multilayer network is organized into densely connected communities. Others have also observed modularity alterations in neurodevelopmental pathological conditions. For example, individuals with the autism spectrum disorder have functional networks with reduced modularity and lowered local efficiency (Rudie et al., 2013), and modularity is reduced in childhood-onset schizophrenia (Alexander-Bloch et al., 2010).

The conclusions of my current findings are in agreement with our previous observations that rtACS influences the organization of functional brain networks in promoting global neural activation, strengthening both short- and long-range synchronization of brain networks (Bola et al., 2014). It is known that rtACS can manipulate human rhythmic brain activity in a phase-specific fashion (Fiene et al., 2020). My result of a strengthened global

modularity index after rtACS treatment suggests that neuromodulation can induce a more optimal balanced multilayer modular structure that benefits visual processing. This is in line with similar observations that obsessive compulsive disorder patients exhibit significantly elevated modular organization after pharmacological treatment (Shin et al., 2014).

My observation in optic nerve patients that rtACS treatment decreases the flexibility of the multilayer network in beta oscillations suggests that neuromodulation can induce a more stable community structure. Network flexibility is a metric reflecting the tendency of a given node to change its modular affiliation over time. Recent work on learning-induced functional connectivity pattern shows an apparent flexibility in the early phases of training, but less change of their module affiliation in later phases (Bassett et al., 2011). It has also been noted that lower brain flexibility correlated with the stronger psychological resilience, i.e., the ability to adapt to stress, adversity, and negative events (Paban et al., 2019). When interpreted in the context of these studies, my results suggest that on a global level of FCN analysis, rtACS induces more proficient and balanced multilayer modular structure and prompts greater specialization of corresponding neurons within the same module. Specifially, the strength of allegiance of all modules increased after rtACS treatment. Of note, stress resilient optic nerve patients are more likely to benefit from rtACS treatment (Sabel et al., 2020b), and when taken together with the current finding, I speculate that their greater stability of FCN community structures might make them less vulnerable to stress and adversities in daily life.

Importantly, in patients rtACS increased interaction strength in motor-attention, and attention-other modules and this correlated positively with improved stimulus detection. This indicates that rtACS is able to modulate the interaction of pathways which are associated with the attention module during visual processing. According to a previous study, rtACS appeared to exert a sustained stabilizing effect on visual attention (Clayton et al., 2019) and rtACS is known to induce neural oscillations related to selective endogenous and exogenous attention (Hopfinger et al., 2017). Considering the vascular response associated with neuronal activation (Phillips et al., 2015), I propose that rtACS may induce the neurovascular coupling and immediate vasodilatory in attention related pathways. Further studies are warranted to investigate the mechanisms underlying this modularity dynamics.

Also in stroke patients, increased attention has both an acute and a chronic influence on visual performance: acute attention improves short-term residual vision (Poggel et al., 2006) and when used in combination with vision restoration training, visual field recovery is potentiated (Poggel et al., 2004). Thus, reorganization of the multilayer modular FCN structures may be the neurophysiological contributor, or mechanism, of how attention can activate residual vision in patients with visual system damage (Sabel et al., 2011b). I propose that this mechanism of intra- and inter-module interactions has important implications not only for the visual domain but also for training, recovery and plasticity of other functional modalities as well. Therefore, further exploration of the spacetime of multilayer brain network reorganization is promising to better understand normal brain function and the role of FCN plasticity in the pathology and recovery/restoration of neural functions of different brain disorders, not just those affecting the visual system.

Recent studies of electric brain oscillations during rtACS provided a possible option to directly evaluate the effects of rtACS on network modularity (Haslacher et al., 2021, 2022). By simultaneous collection of EEG during rtACS, msec. modularity assessment

and msec. precise modulation of brain oscillations during rtACS became feasible. It allows the investigation of msec. inter-modules interaction induced by rtACS and to tune rtACS stimulation parameters to the target brain oscillations in real-time. It could be a basis to further develop closed-loop adaptive brain stimulation protocols.

My study is the first to use multilayer modularity to analyze functional brain networks and network plasticity in neuromodulation using non-invasive brain stimulation in patients with optic nerve damage. By exploring intra- and inter-module interactions and their correlation with normal and abnormal vision, it is possible to identify representative consensus partitions of complex brain networks in a multilayer modular manner and this can be modulated by non-invasive brain current stimulation. I propose that modularity diagnostics of dynamic multilayer organization may help us to better understand the neural basis of normal and abnormal brain functions, not only in visual processing but also in other functional modalities. Multilayer modularity analyses thus provide a novel heuristic and comprehensive framework for understanding – and modulating – the potential of the human mind.

6 Deep Learning of Brain Spacetime: Predicting Outcome of Vision Restoration following Non-invasive Brain Stimulation

Vision loss following optic nerve damage does not only impair visual field function in patients. But it also alters "Brain Spacetime", i.e., the dynamics of functional brain connectivity networks that support cognitive processing. As I showed repeatedly, non-invasive transcranial alternating current stimulation (rtACS) can enhance residual visual capacity of the brain, opening a new window of opportunity through plasticity of the brain. However, treatment efficacy varies considerably between subjects and the treatment outcomes remains unpredictable.

In order to identify vision recovery predictors (VRP), existing EEG data from optic nerve patients were analysed and trained using deep learning. I tried to identify individual brain network responses from EEG that signify "vision recovery" using deep learning algorithms. To this end, I developed a vision recovery prediction model for post-rtACS effects by training the node centralities of the functional brain networks during visual cognition of optic nerve damage patients.

6.1 Introduction

Visual impairments can significantly impact the quality of life and independence of individuals. Vision restoration has been a topic of much interest in the fields of neuroscience and medicine (Quintero et al., 2022). This study was undertaken because early diagnosis and prognosis of vision improvement plays a pivotal role in effective clinical management and patient care.

It has been shown that vision loss resulting from optic nerve damage not only disrupt the conventional understanding of visual field function in affected patients but also exerts a profound influence on what can be referred to as "Brain Spacetime" (Wu and Sabel, 2021). This term encompasses the intricate dynamics of functional brain connectivity networks that underlies various aspects of cognitive processing. Our research has consistently demonstrated that non-invasive transcranial alternating current stimulation- rtACS holds the potential to reactivate the residual visual capacity within the brain, effectively opening a novel gateway to harnessing the brain's inherent plasticity.

In my previous study, I observed that the rtACS intervention optimizes brain network reorganization during visual processing and facilitates interactions between distinct modules of the brain network, thereby promoting recovery of vision in patients with optic nerve damage (Wu et al., 2022). Such findings not only highlight the extraordinary adaptive capacity of the human brain, but they also exemplify the relevance of brain network characteristics for vision recovery. However, a great challenge is that the efficacy of the rtACS treatment varies considerably between individuals and the outcomes of such intervention remain unpredictable.

To refine treatment strategies, I need to understand the subtle interactions between rtACS, brain network plasticity, and individual patient characteristics in order and only then I can fully realize the potential of rtACS as a means of restoring visual function in

patients. Therefore, I aimed to develop a predictive model for visual recovery after rtACS using FCN features. Over the years, deep learning techniques have made significant advances in a number of areas such as computer vision and medical diagnostics, especially using biological data (Eraslan et al., 2019; Høye et al., 2021). Biological data like protein structure, gene expression or medical imaging help to understand physiological and functional details of the life sciences. For the last decades, the rapid advances in data science and artificial intelligence provides powerful technical support for our understanding of these biological data. In addition, analytics in medical applications have contributed to the detection and classification of brain disorders (Burgos et al., 2021; Lin et al., 2021).

In addition to medical diagnosis and research, neuroimaging data can help solve real-world problems in neuroscience. A range of new technologies and a significant increase in computing power have made it possible to gain a deep understanding of biological data, particularly brain activity. The brain activity can be acquired in several ways, such as non-invasive neuroimaging data, or invasive brain computer interface (BCI)(Merk et al., 2022), which requires the implantation of electrodes in visual or motor areas under the scalp, or partially invasive electrocorticography (ECoG), which is placed on the surface of the brain (Habets et al., 2018; Luo et al., 2022). Unlike the non-invasive recordings, invasive BCI can capture the activity of single neurons. They can provide more accurate readings of brain signals, including side effects after surgery such as scar tissues or body rejections (Abiri et al., 2019).

In most cases, the non-invasive neuroimaging data were recorded from electroencephalogram (EEG), functional magnetic resonance imaging (fMRI), magnetoencephalography (MEG), or functional near-infrared spectroscopy (fNIRS) (Simon et al., 2021). Various applications of these neuroimaging data have also been linked to deep learning inside and outside of the clinical field. For example, brain disorder could be diagnosed using DL based on fMRI images, such as Alzheimer's disease, Parkinson's disease and schizophrenia (Li et al., 2020; Noor et al., 2020; Yin et al., 2022). In the field of EEG, an epileptic discharge detector was proposed based on EEG-fMRI deep learning to delineate the epileptogenic zone (Hao et al., 2017).

The EEG measures slight voltage changes through electrodes on the scalp of the brain. Because of its flexibility and ease of use, EEG is commonly used to study a series of brain processes. It has a high temporal resolution for real-time monitoring of brain activity, as the timing of parallel/serial synaptic potentials is very fast, indirectly reflecting information flow and signal propagation across the various neuronal assemblies (León et al., 2020). However, this character also leads to the problem of poor signal-to-noise ratio in EEG. Therefore, for decoding of EEG based brain signals, many machine learning algorithms have been investigated, especially deep learning neural networks. For example, deep neural networks can build robust and high accurate BCI models for the classification of motor imagery (MI) EEG signals, which have significant applications in neurorehabilitation (Al-Saegh et al., 2021).

This paper introduces a novel deep learning-based vision recovery prediction model, which leverages EEG-based node centrality of functional brain networks to predict visual field improvement in patients.

6.2 Datasets and Preprocessing

Data were obtained from our previous trial with 20 patients suffering optic nerve damage. Two of the subjects did not receive tACS stimulation, making a total of 18 subjects with data included. Information about the subjects' details was shown in Table A.1. EEG data and visual field information were collected from each subject while they performed a visual discrimination task before receiving rtACS treatment.

Perimetric visual field was diagnosed first with the computer-based high-resolution perimetry (HRP). The subjects had to press the space bar once a light stimulus was observed or when the color of the fixation point changed. In areas where all stimuli were correctly detected in the same position was defined as intact area (plotted in white in Fig. 2.1) and three missed stimuli were taken as signs of absolutely impaired areas, plotted as black. Other positions were marked as grey area. In this way, three visual field areas were identified: intact vision area, partially damaged and absolutely impaired areas. The partially damaged areas were identified as "areas of residual vision".

For each subject, eight different positions were selected to present stimulation individually based on visual field diagnose result to collect visual evoked potentials EEG recording. One position was always in the intact area and one position always in the completely impaired area. Six positions were placed in grey areas, i.e., at points with HRP detection accuracy was between 33 to 66%.

Visual evoked EEG data were then collected during the visual processing in these distinct areas. During VEP, Stimuli were presented for 400 ms followed by a variable inter-stimulus interval ranging from 1300 ms to 1700 ms. Then the EEG data were preprocessed and source reconstructed on the cortex using Desikan–Killiany atlas 68 regions of interests (ROIs, 34 in each hemisphere). In this way, the source brain activities were filtered and decomposed into five frequency bands using the Hilbert method. Functional brain networks were then constructed by measuring oscillatory synchronization on each trial in each frequency band.

Subsequently, the Hilbert transform was employed to obtain discrete time analytic signals across five distinct frequency bands, encompassing theta, alpha, low alpha, high alpha, and beta, as previously described (Le et al., 2001). The investigation then focused on the evaluation of coherence and phase synchrony from Hilbert transformed signals, both of which are fundamental mathematical approaches for quantifying the frequency and phase correlations within brain activity recorded from two or more brain regions. More precisely, four network construction metrics were examined, specifically the phase locking value (PLV), coherence (COH), imaginary part of the phase locking value (iPLV), and imaginary part of coherence (iCOH).

Node centralities, which were typically used to assess the different impacts of nodes on network function, including degree, eigenvector centrality, betweenness centrality, closeness centrality, and clustering coefficient were extracted based on brain networks and then fed into deep neural networks afterwards. After receiving rtACS treatment, the visual field was evaluated again for each subject to calculate recovery of vision. Here, the characteristics of node centralities during the visual discrimination task, of size 68*5 were considered as inputs to the neural network. Among them, 2205 and 2507 trials were available for IVA and ARV, respectively. The output is the percentage change over the baseline of the

stimulation detection rate. The goal is to predict the percentage of vision recovery.

The node attributes are shown in Fig. 6.1. Vision improvement, i.e., stimulus detection enhancement rate after rtACS treatment, was considered as the label of vision recovery. The developed deep neural network algorithm processed the input data and optimized the weights and bias by learning and adjusting them to continuously reduce the error or loss to build the recovery prediction model for post-rtACS effects.

6.3 Deep Learning Algorithms and Models

In this study, two deep neural network modals, FFNN and bidirectional LSTM, were tested to accomplish the vision recovery prediction model for post-rtACS effects.

The feedforward neural network is modeled with an input layer, two hidden layers containing 68 and 34 neurons, respectively, and an output layer. The output is a prediction of rtACS induced visual recovery outcome in optic nerve damage patients. Each neuron in the FFNN model is connected to the neurons in the previous layer. Sigmoid were used as an activation function. The FFNN structure in this study is shown in Fig. 6.1.

Bidirectional long short-term memory (Bi-LSTM) is a recurrent neural network, that can deal with long term dependencies by memorizing useful information from the inputs and is capable of being trained information from backward and forward directions simultaneously, thus providing better predictive performance. As shown in Fig. 6.2, the Bi-LSTM prediction model consisted of two directional LSTM layers with 68 neurons. The final output is a neuron representing the probability of visual field recovery in patients with optic nerve damage.

The neuron count was determined based on prior experience with deep learning models for EEG signal feature extraction, as demonstrated in studies such as (Khan et al., 2022) for recognizing human emotions through EEG spectrogram images and (Das et al., 2019) for EEG-based person identification. An initial kernel count of 34 was chosen to construct a 3-layer CNN.

6.4 Training and Evaluation Metrics

The input data was split into 70% training data and 30% test dataset with 3-fold cross-validation for the training data. If the training performance does not improve significantly as the training epoch increases, there is a risk of overfitting, which can lead to negative performance on the test data. This risk is especially high when there are only a small number of training samples and a large number of parameters to be learned. Therefore, a number of regularization methods have been proposed to optimize training of the model, such as dropout and batch regularization. The parameters of all neurons are used in the prediction stage, while only the parameters of the retained neurons are updated in the training stage using dropout. Here, I also applied dropout method with a 0.5 ratio to randomly ignore neurons and connections to avoid overfitting the data.

An Adaptive moment estimation algorithm (Adam) optimizer, which is an extension of the stochastic gradient descent algorithm, was used to train the model. The batch size is 50, the learning rate is 0.001. The prediction performance of each model was evaluated based on the error. This error was quantified using the mean squared error (MSE). MSE

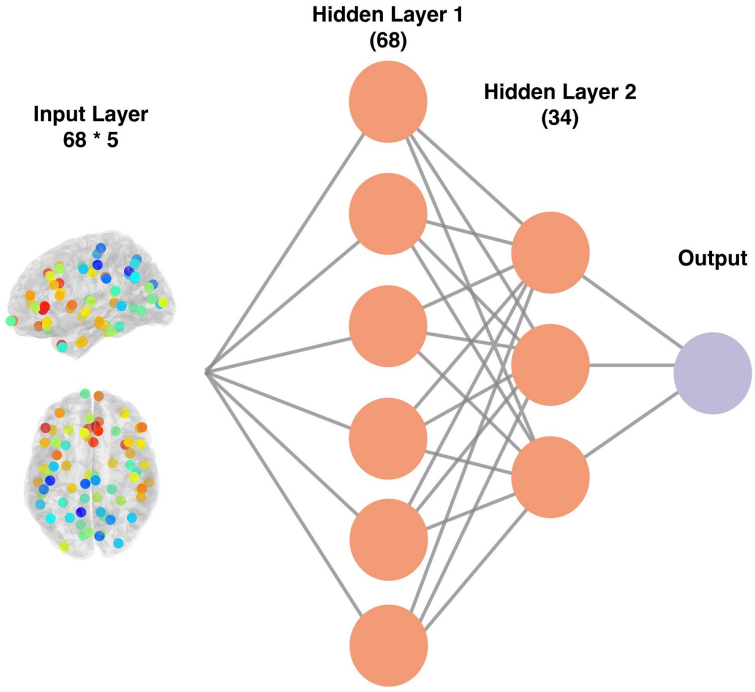

Figure 6.1: Structure of the proposed feedforward neural network. The input is 5 node centrality features from 68 brain regions, and comprises 2 hidden layers consisting of 68 and 34 neurons, respectively, as well as an output layer.

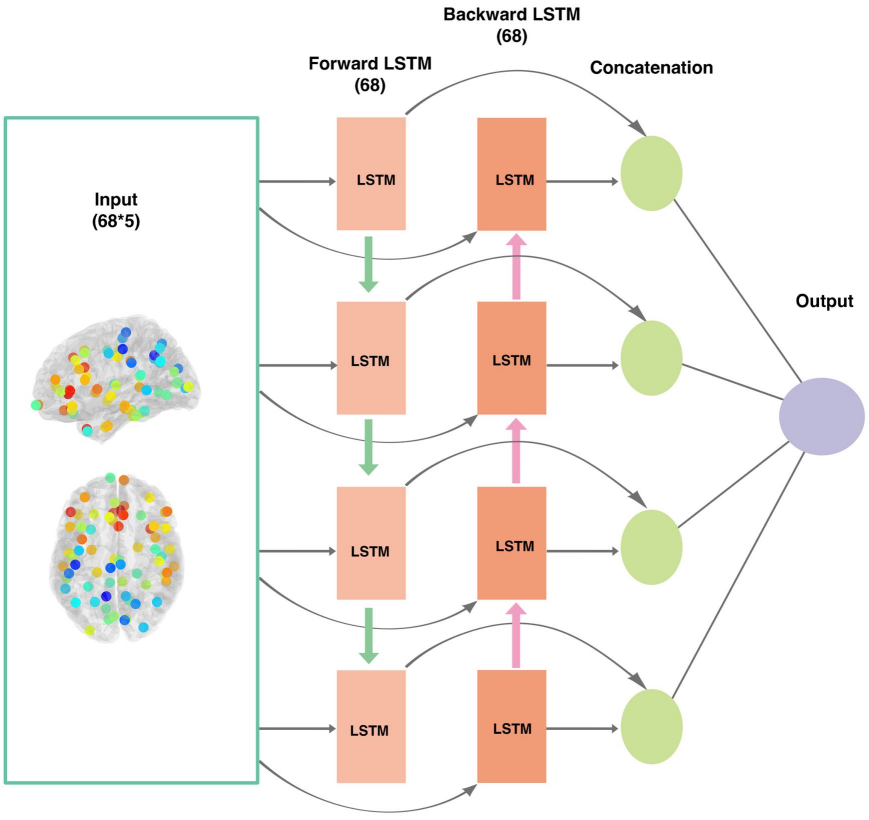

Figure 6.2: Structure of the proposed bidirectional LSTM. The input are FCN node centralities of size 68*5, 2 hidden Bi-LSTM layers consisting of 68 neurons, and an output layer.

COH	IVA		ARV	
	Bi-LSTM	FFNN	Bi-LSTM	FFNN
Theta	0.018	0.013	0.015	0.009
Alpha	0.012	0.012	0.006	0.006
Low Alpha	0.011	0.012	0.007	0.007
High alpha	0.012	0.014	0.005	0.006
Beta	0.011	0.010	0.008	0.005

Table 6.1: Prediction errors (MSE) of the models for rtACS induced vision recovery prediction model using COH data after 3-fold cross-validation.

PLV	IVA		ARV	
	Bi-LSTM	FFNN	Bi-LSTM	FFNN
Theta	0.019	0.015	0.018	0.013
Alpha	0.012	0.014	0.009	0.006
Low Alpha	0.013	0.015	0.010	0.008
High alpha	0.013	0.013	0.009	0.007
Beta	0.012	0.010	0.010	0.007

Table 6.2: Prediction errors (MSE) of the models for rtACS-induced vision recovery prediction model using PLV after 3-fold cross-validation.

measures how close the predicted value is to the target true value, by calculating the average of the squared differences. The optimization algorithm continuously minimizes the error (cost) by constantly updating the weights and biases in the model.

In order to explore the generalization ability of the model, a Leave One Subject Out (LOSO) cross-validation method was employed in this study to ensure that the training model is person-independent. In this approach, observations associated with a specific subject from the entire dataset were dropped out in each iteration and used as the test data for evaluating the model, while data from the remaining subjects were employed to train the model. This process was repeated until every subject has been used for testing, finally generating an average loss. These tasks were performed using the Python language and the Keras library on the Google Colab platform.

6.5 Results

According to different stimulus detection rate, the visual field of patients were subdivided into the intact visual area, the areas of residual vision and the blind areas. Visual evoked potential EEG recordings were then collected during a visual discrimination task in all these visual areas. By evaluating functional brain networks that were used extensively in neuroscience to assess the interrelationships among brain regions, I extracted and assessed node centralities from four different network structures, including PLV, COH, iPLV, and iCOH, as training data for predicting the vision recovery after rtACS treatment.

The MSE of the rtACS-induced vision recovery prediction model after 3-fold cross-validation were summarized in Table 6.1 and 6.2. The results showed that FFNN and bidirectional LSTM models perform slightly differently in various frequency bands, but both showed the ability to predict the outcome of rtACS-induced visual recovery, especially in the ARV. Specifically, the prediction performance using the ARV dataset outperforms the IVA dataset in all frequency bands. In particular, in the low alpha frequency, the prediction error of Bi-LSTM was 36% lower than that of IVA when using the ARV dataset, while that of FFNN from ARV is 42% lower than that of IVA. Also in the high alpha band,

the MSE of Bi-LSTM constructed using ARV data is more than half of the MSE of Bi-LSTM constructed using IVA data (Fig. 6.3 and 6.4).

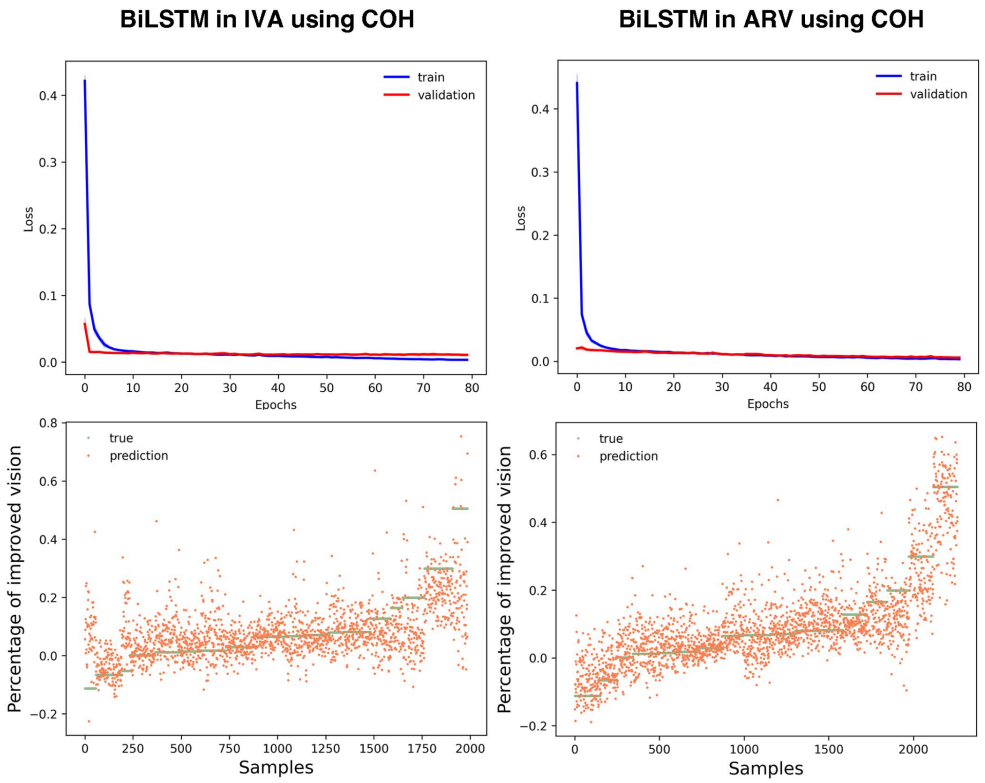

Figure 6.3: Performance of rtACS induced visual recovery prediction models constructed on bidirectional LSTM after 3-fold cross-validation using high alpha-band COH data from ARV and IVA, respectively.

In addition, the predictions with node centralities of COH structure were comparable to those with the PLV structure (Table 6.2). In contrast, no more valid information could be learned for predicting visual field recovery using the iPLV and iCOH training data.

In order to assess the generalization performance of the model independently of individual subjects, the results of the 3-fold cross-validation were compared with those obtained using Leave-One-Subject-Out (LOSO) cross-validation. The MSE results of the FFNN and Bi-LSTM models after LOSO cross-validation were shown in Table 6.3 and 6.4.

The results indicated that both Bi-LSTM and FFNN models showed similar performance in all frequency bands, whether constructed using COH or PLV obtained from IVA or ARV. For example, the MSE of Bi-LSTM and FFNN models constructed using the COH node centralities from ARV after LOSO cross-validation were 0.025 and 0.021, respectively. The MSE in IVA has a small but very slight increase.

However, as illustrated in Fig. 6.5 and 6.6, there were outliers in predicting extreme visual field improvement. ID 6 and ID 5 exhibited high loss values during the training of the model, exceeding the distribution of loss values for most subjects. In fact, ID 6 showed the greatest visual field improvement after receiving rtACS treatment, as evidenced by the high-resolution perimetry test, which showed a wide distribution of gray residual visual fields. On the other hand, the visual field of ID5 not only did not improve after treatment with rtACS, but became worse. By observing the HRP of ID5, it was found that its initial visual field status was extremely poor.

COH	IVA		ARV	
	Bi-LSTM	FFNN	Bi-LSTM	FFNN
Theta	0.034	0.025	0.030	0.026
Alpha	0.026	0.026	0.023	0.022
Low Alpha	0.029	0.024	0.027	0.023
High alpha	0.027	0.027	0.025	0.021
Beta	0.030	0.027	0.024	0.028

Table 6.3: MSE of FFNN and Bi-LSTM models using COH data after LOSO cross-validation.

In general, both proposed Bi-LSTM and FFNN models exhibited the capability of predicting rtACS-induced visual recovery, and this capability was validated in various frequency bands and with distinct network construction methods (Fig. 6.7). Those that demonstrated a higher MSE across multiple frequencies and various networks were concentrated in the two subjects with the greatest visual field recovery, which is ID 6 and ID 14, and the one with the smallest visual field change on ID 5.

Importantly, the consistency of the results obtained by LOSO cross-validation with 3-fold cross-validation highlights the strong generalization ability of our proposed model across different subject populations.

6.6 Discussion

The present study aims to analyze EEG-based brain network node attributes data with deep learning algorithms to predict the treatment outcome of vision restoration using non-invasive brain stimulation, specifically rtACS.

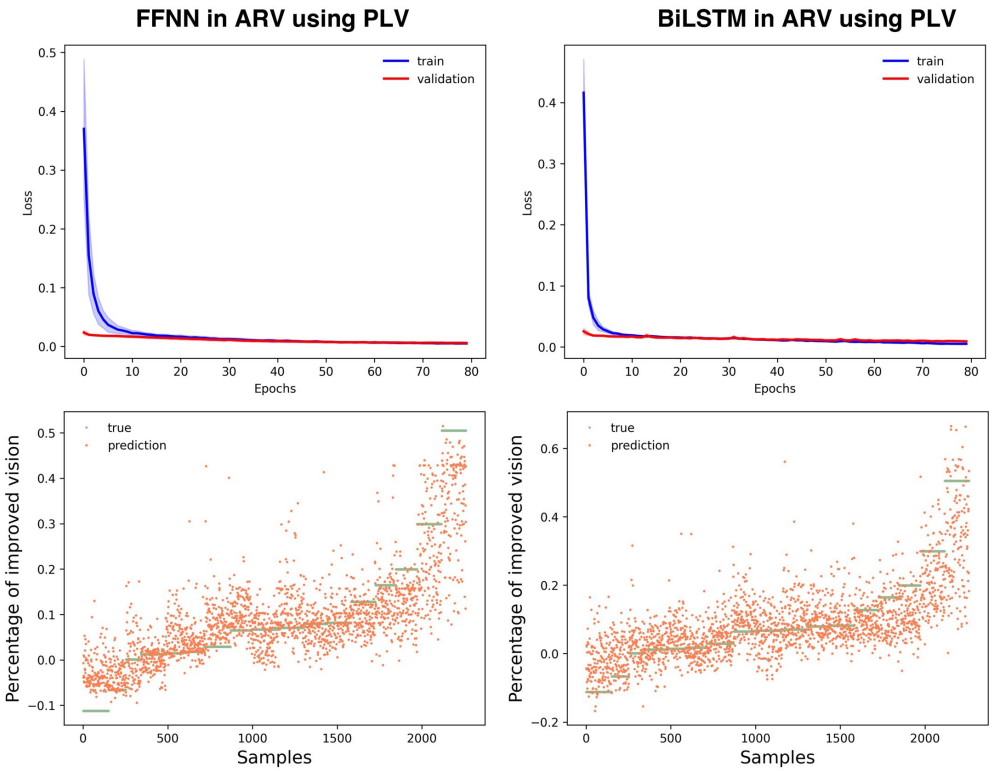

Figure 6.4: The performance of the FFNN and Bi-LSTM models after 3-fold cross-validation using PLV data from ARV in high alpha band.

PLV	IVA		ARV	
	Bi-LSTM	FFNN	Bi-LSTM	FFNN
Theta	0.031	0.025	0.027	0.026
Alpha	0.027	0.025	0.022	0.020
Low Alpha	0.028	0.023	0.028	0.025
High alpha	0.027	0.025	0.023	0.023
Beta	0.028	0.027	0.025	0.028

Table 6.4: MSE of FFNN and Bi-LSTM models using PLV data after LOSO cross-validation.

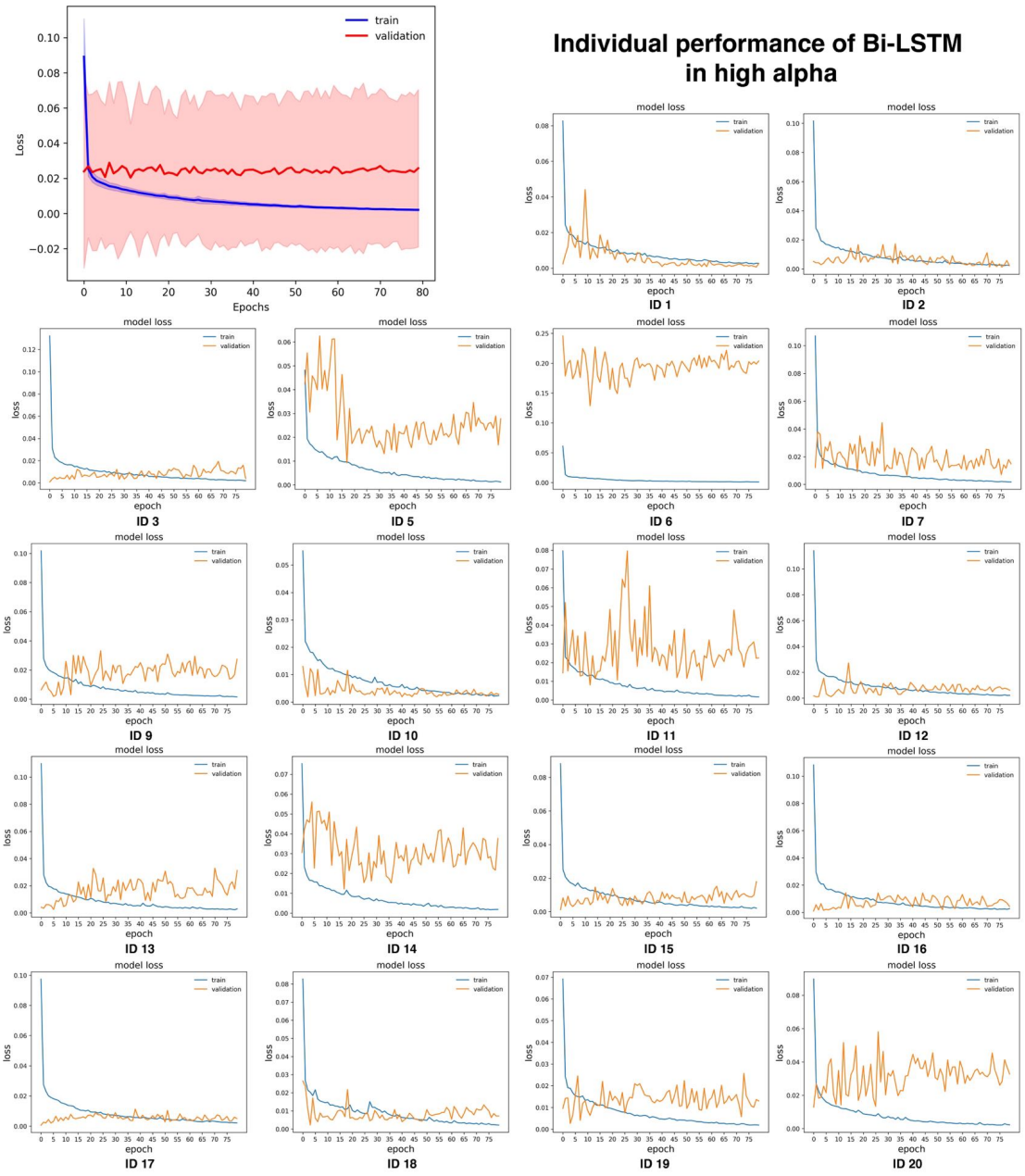

Figure 6.5: Individual performance of Bi-LSTM training on high alpha COH data of ARV using Leave-One-Subject-Out cross-validation.

I emphasize the concept of FCN as an important factor in understanding the neural basis of visual recovery. Loss of vision due to optic nerve damage not only affects the visual field, but also alters the functional brain connections supporting cognitive processes. This highlights the intricate relationship between vision and broader brain cognitive functions.

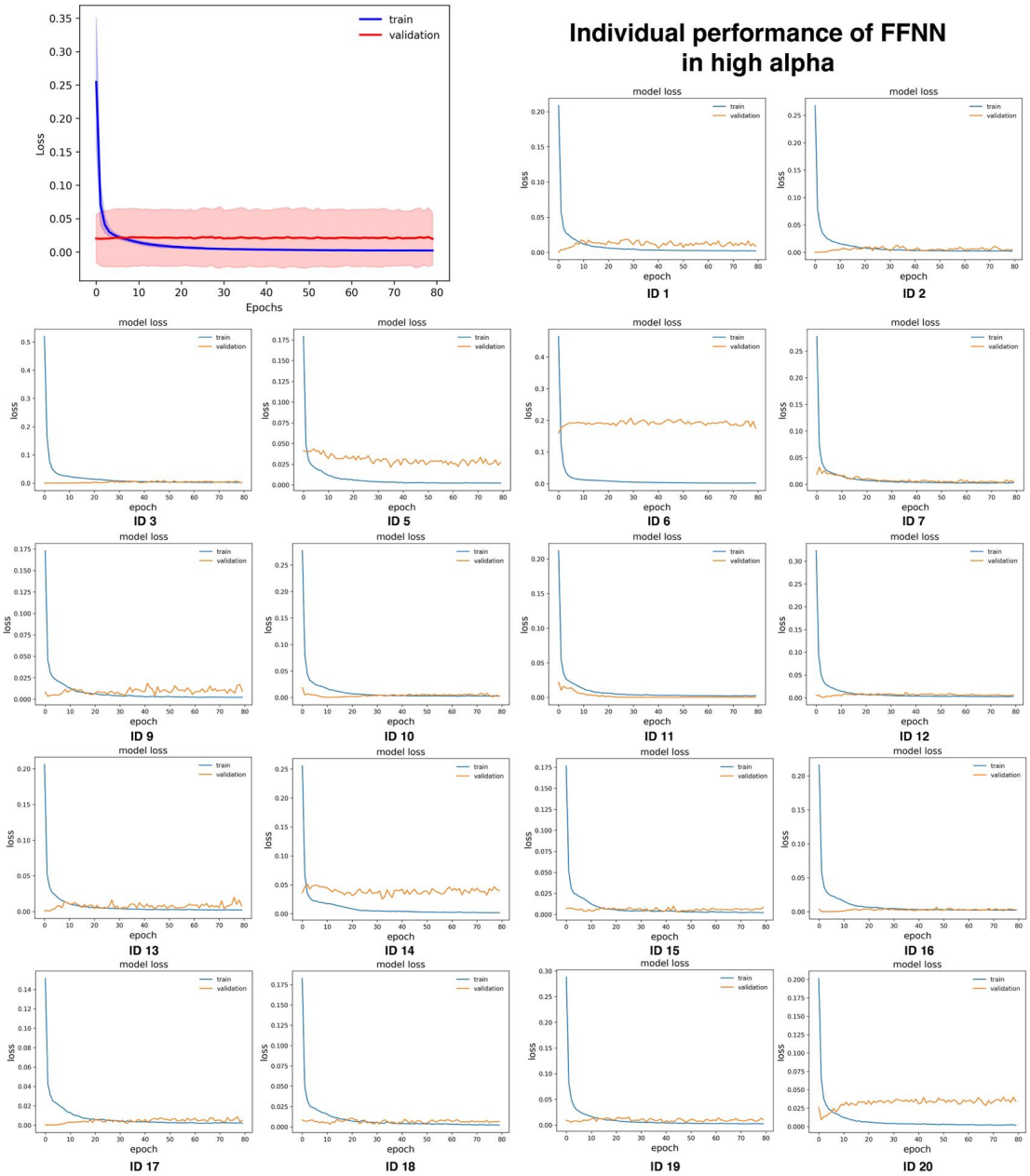

Figure 6.6: Individual performance of FFNN after training on high alpha COH data of ARV using Leave-One-Subject-Out cross-validation.

Visual function has been shown to be enhanced to some extent by noninvasive brain stimulation. However, A challenge to vision restoration therapy is the wide variation in outcomes between patients. This variation highlights the need for a more personalized and precise approach.

The application of deep learning is an important step toward developing more accurate predictive models for vision recovery. This study seeks to develop a valid predictive model of vision recovery treatment outcomes by investigating the potential of noninvasive rtACS in vision recovery, providing a new reference for personalized treatment plans in terms of efficacy prediction.

Through deep learning techniques with FFNN and Bi-LSTM, the models were trained on node centralities of functional brain networks extracted from EEG. The extraction

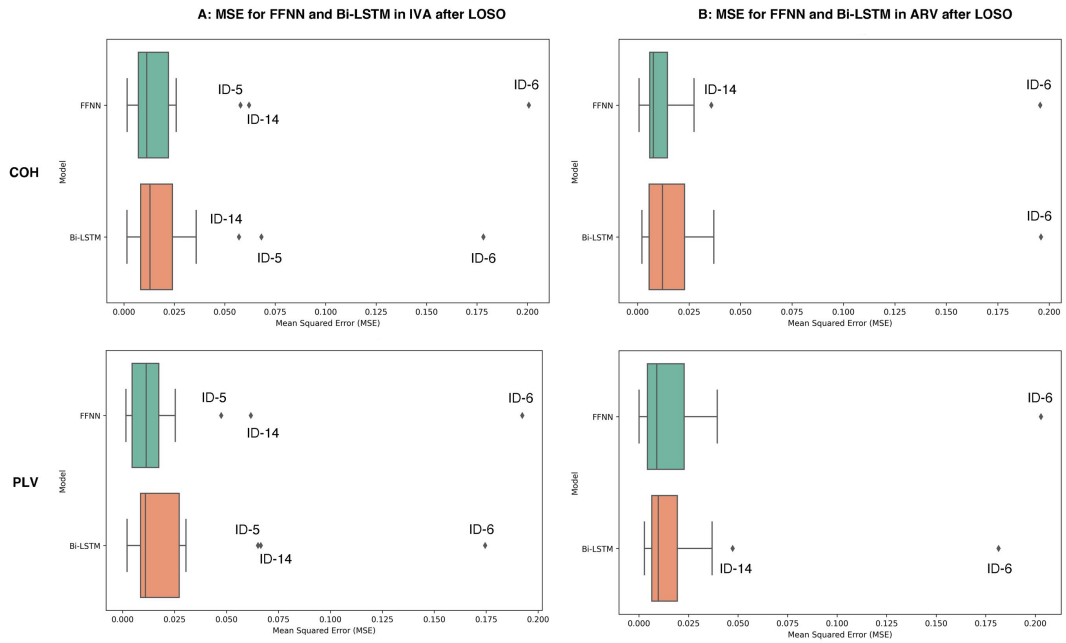

Figure 6.7: Boxplot of MSE for FFNN and Bi-LSTM models using COH data in high alpha after Leave-One-Subject-Out cross-validation.

of node centralities, which represent the influence of specific brain regions on network function, provides crucial features for the deep learning models. The study provided a detailed comparison of the FFNN and Bi-LSTM models after 3-fold and leave-one-subject-out cross-validation, and the results indicated that both the proposed FFNN and Bi-LSTM models provided promising prediction performance in predicting the treatment outcome of rtACS-induced vision restoration.

Furthermore, I employed Leave-One-Subject-Out cross-validation to rigorously assess the generalizability of findings. Remarkably, the outcomes after LOSO demonstrated consistency with the results obtained from the 3-fold cross-validation method. While the model performance showed differences in the 3-fold cross-validation results for various frequency bands and network construction methods, such differences no longer existed after the LOSO cross-validation. Although the performance of the models in some cases of individual extreme vision recovery conditions was out of the prediction distribution, especially in cases where the initial visual field conditions were extremely poor or the gray residual visual field was widely distributed, our models still showed great potential in predicting rtACS-induced vision recovery. In addition, the robustness across different cross-validation strategies reinforces the reliability and stability of our observed patterns, further supporting the validity of our study's findings in vision restoration.

Regarding limitations, if more data could be included in the training and a more powerful machine learning analytics platform could be used, it would be possible to expand the range of parameters optimized for the proposed model and potentially improve the overall performance of the model.

Furthermore, regarding possible limitations of the proposed model, the requirement for the input data was node centralities data of the functional brain network generated based on EEG. It can be seen that the input data must have been subjected to a series of data

processing including EEG preprocessing, source reconstruction as well as the configuration of the functional brain network, and the calculation of node centralities. This may take some time. Therefore, the emphasis of future work could be placed on developing machine learning models that directly use EEG as input data and comparing the results with the models proposed in this article that used feature-extracted input data to expand the application of the models.

6.7 Conclusions

I presented the bidirectional LSTM or FFNN-based deep learning architecture for predicting the outcome of vision restoration therapy using non-invasive brain stimulation. The proposed architectures are simple and efficient. The method absorbed node-centrality relationships hidden in the functional brain networks, predicting vision recovery for post-rtACS effects with a small error. The results showed that the level of vision restoration can be predicted using individual visual field topography and EEG markers at baseline. Future work includes analyzing deeper layers or more architectures for a better understanding of EEG patterns to predict vision recovery.

AI-based deep neural networks may provide useful information for future therapy outcomes to patients before rtACS treatment starts. Since in this study, only a limited dataset of subjects was trained for the models, if larger sample datasets could be used to validate our findings, the proposed models could help clinicians and patients to have more realistic expectations of treatment outcomes.

However, patients and clinicians should view these results as a statistical prediction, not a ground truth. The final outcome of the treatment needs to be judged by a professional physician in conjunction with additional data. In addition, considering the fact that EEG requires high-quality data and complex pre-processing, it would take some time in practical clinical applications. Future work should explore EEG directly and larger datasets to further validate the performance of these prediction models.

In summary, my study is an important step forward in exploring the potential of deep learning to predict the outcome of vision recovery treatments for patients with optic nerve damage. By exploring the relationship between the properties of functional brain network nodes and the effects of rtACS, an understanding of the intricate neural mechanisms behind vision recovery has been deepened. Deep learning techniques may offer new solutions to overcome the variability and unpredictability of treatment outcomes and might provide better patient care and management in ophthalmology and neurorehabilitation.

7 Towards an Early Warning Model for Vision Loss Based on Deep Learning

Traditional assessment of visual field damage relies on ocular imaging and perimetric visual field tests. They work well to diagnose already-existing visual field loss, but they are unable to predict vision loss in slowly developing visual impairments such as glaucoma. In other words, the current state of the visual field test cannot predict future vision loss before it actually happens. However, in recent years, the development of deep learning techniques has made impressive advances in the fields of medical image processing and brain science, providing new opportunities for early warning systems.

With the study described in the present chapter, I explored electroencephalography (EEG)-based functional brain networks with deep learning modeling aimed at automatically detecting early signs of visual field damage. The fundamental idea was to study brain physiological changes as a new biomarker of visual field impairment. Though my aim was not to test normal subjects and wait to see if they later experience vision problem. Rather, I studied to what extent EEG biomarkers based on deep learning can be correlated with the extent of visual field loss and if abnormalities can be found even in sectors of the visual field considered to be "normal".

7.1 Introduction

Visual field impairment is a critical problem that affects the visual health for millions of people, including glaucoma, hemianopsia, macular degeneration, optic neuritis, as well as a variety of retinal and other ocular diseases that can cause visual field impairment. The assessment of visual field impairment is usually accomplished by visual field testing. Visual field test results are typically displayed as visual detection sensitivity producing charts based on the mean deviation from normal sensory (visual) sensitivity. However, as I we have previously demonstrated, even visual fields regions identified to be normal in visual field assessment showed remarkable differences from normal brain network responses during visual processing, especially during dynamic functional network reorganization (Wu and Sabel, 2021). This suggests that it might be possible to predict visual field damage even before deficits become apparent in visual field testing of other means used by clinical ophthalmologists.

This "hidden" visual field impairment is not accompanied by obvious symptoms in the early stages. To prevent vision loss as early as possible, the development of early warning systems based on "intact" visual field testing is needed for the early detection of visual field damage and prompt intervention.

In recent years, significant advances in deep learning techniques in medical image processing and brain science have provided new opportunities to identify key features from functional brain networks and to establish early warning systems. In my present study, EEG-based functional brain networks were investigated by deep learning modeling in order to detect brain physiological abnormalities in "intact" regions of patients that have known visual field damage.

Being a safe and non-invasive technique that can record real-time brain activity, EEG has a very high temporal resolution and can be used to capture subtle information transfer

between different brain regions. By analyzing the EEG associated with neurological dysfunction, some progress has also been made in developing detection models for different disorders such as seizure detection (Nhu et al., 2022; O'Shea et al., 2021), depression (Ay et al., 2019), schizophrenia (Barros et al., 2021), Autism Disorder (Ardakani et al., 2022) and Mild cognitive impairment (Huggins et al., 2021; Kim et al., 2023).

In this chapter, I investigated deep learning-based early warning models that hope to identify potential visual field damage in the "intact" visual field by analyzing EEG data from normal subjects and patients with optic nerve damage. Specifically, I analyzed the architecture and implementation of deep learning models, as well as the methods for evaluating EEG datasets, with the hope of developing a tool for the early detection of visual impairment that would allow for intervention in the very early stages to minimize visual field damage and improve the patient's quality of life.

7.2 Dataset Preparation

I analysed the EEG of 20 patients with optic nerve damage and 15 healthy controls during visual processing in areas diagnosed as intact vision by visual field (perimetry) assessment (Table A.1).

For all of the patients, visual field assessment was initially conducted using high-resolution perimetry (HRP), a computer-based method. During the test, subjects were instructed to press the space bar upon perceiving light stimuli presented on a computer screen or when the color of the fixation point changed. Depending on the subjects' responses, the visual field was categorized into three distinct areas: intact visual area where all stimuli were consistently detected at the same location, the area representing absolute impairment in which all stimuli were missed (described as black), and the area in which only some stimuli were missed (referred to as the "grey area" as shown in Fig. 2.1). The latter are partially impaired areas, denoted as "areas of residual vision".

To collect visual evoked potentials (VEPs), EEG recordings were analysed as a function of distinct visual field positions the respective stimulus was presented in each patient. Per patient eight different positions were selected based on the visual field diagnosis results. One position was located within the intact area, while another was always within the completely impaired area. The remaining six positions were chosen from areas where the HRP detection accuracy ranged from 33% to 66%. VEP stimuli consisted of circles (1° diameter) or squares (1x1°) presented at distinct vision areas based on HRP results for 400ms, with 180 trials per location per subject. Visual evoked potentials (VEPs) were then recorded with EEG amplifiers using 32 sintered Ag/AgCl electrodes placed according to the 10-10 system, referenced to the nose-tip with a ground electrode at Fz and Cz.

Afterwards, the EEG data were pre-processed, and Independent Component Analysis (ICA) was applied to remove the epochs with artifacts and noisy channels. To derive source neuronal activities from EEG recordings, the head forward model was constructed using the boundary element method (BEM) (Hallez et al., 2007). And the reverse model was constructed using the weighted minimum-norm estimation (WMNE) method (Iwaki and Ueno, 1998). The recorded EEG signals were then transformed from the sensor electrodes to the brain cortex. The Desikan–Killiany atlas (Desikan et al., 2006) was utilized to delineate 68 regions of interest (ROIs), 34 for each hemisphere afterwards. For each ROI,

the average of the voxel time series was calculated to represent that specific area of interest. After obtaining source neuronal activities, I transformed the EEG signals recorded by the sensor electrodes into the brain cortex. I utilized the Desikan–Killiany atlas (Desikan et al., 2006) to delineate 68 regions of interest (ROIs), with 34 in each hemisphere. For each ROI, I computed the mean of the voxel time series to represent that particular region of interest.

The Hilbert transform was then applied to estimate the discrete-time analytic signals in five frequency bands, including theta, alpha, low alpha, high alpha, and beta (Le et al., 2001). This study assessed coherence and phase synchronization between two or more brain regions, which were two general mathematical methods for quantifying the frequency and phase correlation of measured brain activity. Specifically, four network construction metrics were assessed as the input dataset for deep learning, namely the phase locking value (PLV), coherence (COH), the imaginary part of the phase locking value (iPLV), and the imaginary part of coherence (iCOH).

7.3 Deep Learning Algorithms and Models

Taking into account the insidious nature of early "normal" visual field impairment and its relevance to the progression of visual impairment, the early warning for visual field impairment becomes an essential issue for visually impaired patients. Considering the spatial relevance of brain regions, this work implemented a convolutional neural network, which can be effective in the spatial dimension. The data used for the analysis were brain functional connectivity network (FCN) data during visual processing. The label assessed was the accuracy with which the algorithm correctly classified functional brain networks into two categories: patients with hidden visual field impairments and healthy subjects.

Convolutional Neural Network (CNN) is a representative feed-forward neural network for deep learning with convolutional computation. CNN usually consists of an input layer, convolutional layer, pooling layer, fully connected layer, and an output layer. The convolution layer of CNN learns characteristics through scanning filters to extract features, following which the dimension is reduced through a pooling layer, and finally using a fully connected layer to accomplish the classification task. In my present analysis, functional network responses in the intact visual field in visual processing were identified as the input data from 4,620 trials of 20 patients with optic nerve damage and 15 controls, size of $68 * 68$, to classify controls and patients.

In my analysis, the algorithm decomposed the brain networks into channelized images that have a size of $68 * 68 * 1$, and applied the resulting matrices to the inputs of the CNN. The input data was considered an image for extracting information about the relationships between neighboring nodes of the brain network. All data were then passed through a series of kernel convolutional filters with a size of $5 * 5$ that scanned across the training dataset, followed by dropout batch normalization and max pooling layers. Based on the experience gained in employing CNN models for EEG signal feature extraction, including tasks such as recognizing human emotions through EEG spectrogram images Khan et al. (2022) and EEG-based person identification Das et al. (2019), an initial kernel count of 34 was selected to build a 3-layer CNN. The quantity of kernels was doubled following each max-pooling layer. Thereafter, a flattening layer was applied to convert the training data into one-dimensional data for the fully connected layer with no trainable parameters.

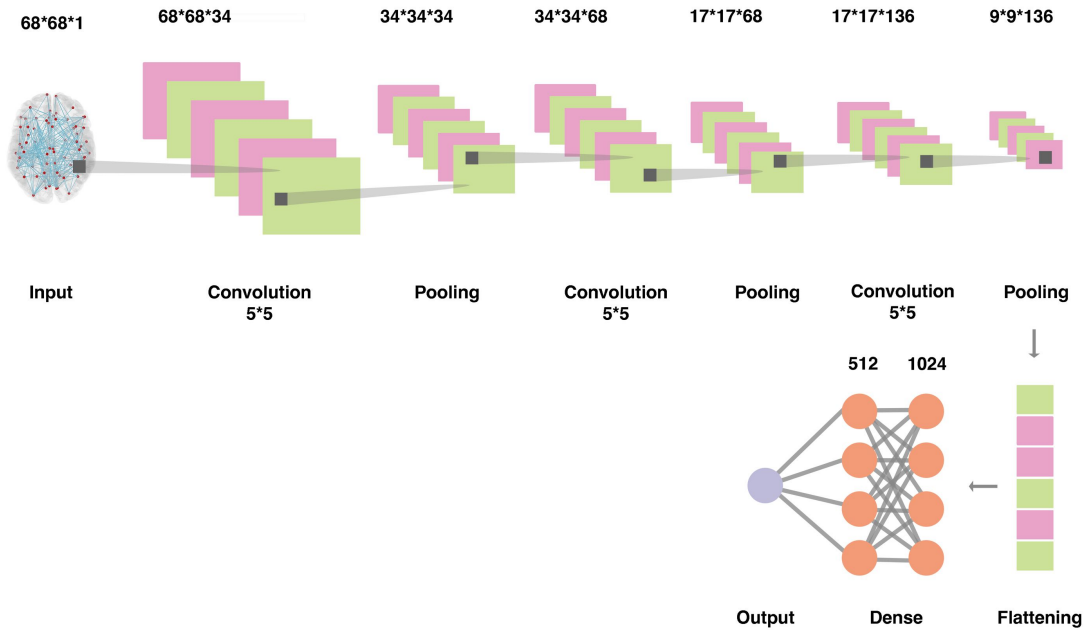

Figure 7.1: Schematic of the structure of the CNN model used in the study. Brain functional network parameters were used as input data.

The subsequent 3 fully connected (FC) layers were added in the end to build the visual field damage early warning model, where the last layer is the prediction layer with 2 output values. Rectified Linear Unit (ReLU) activation function was applied following each convolutional layer, with the exception of the final layers, where sigmoid activation was utilized to scale the output within the range of zero to one. Fig. 7.1 presents the CNN modal structure implemented in my research.

I further evaluate the proposed CNN model by comparing it to a FFNN, in which each neuron is connected with neurons in the preceding layer. The FFNN was composed of an input layer, two hidden layers containing 68 and 34 neurons, and an output layer. The output is the classification of patients with optic nerve damage and controls. Likewise, a ReLU activation function was used after each fully connected layer, but a sigmoid activation function was applied to the last layer to scale the output over a range from 0 to 1. The architecture is illustrated in Fig. 7.2.

By studying the dynamic responses of functional brain networks to visual stimuli during visual cognition in "intact" vision area, I tested two types of neural architectures and developed a discriminative system that can categorize patients with optic nerve damage from healthy controls, thus modeling the early warning of visual field impairment.

7.4 Training and Evaluation Metrics

The selection of parameters also matters during the training of the network architecture. The input data of 4,620 trials was partitioned, with 70% allocated to the training dataset and the remaining 30% reserved for the test dataset, which accounts for the 1386 trials used for testing, utilizing a 3-fold cross-validation strategy.

The model was trained using the Adam optimizer, known for its robustness and ability

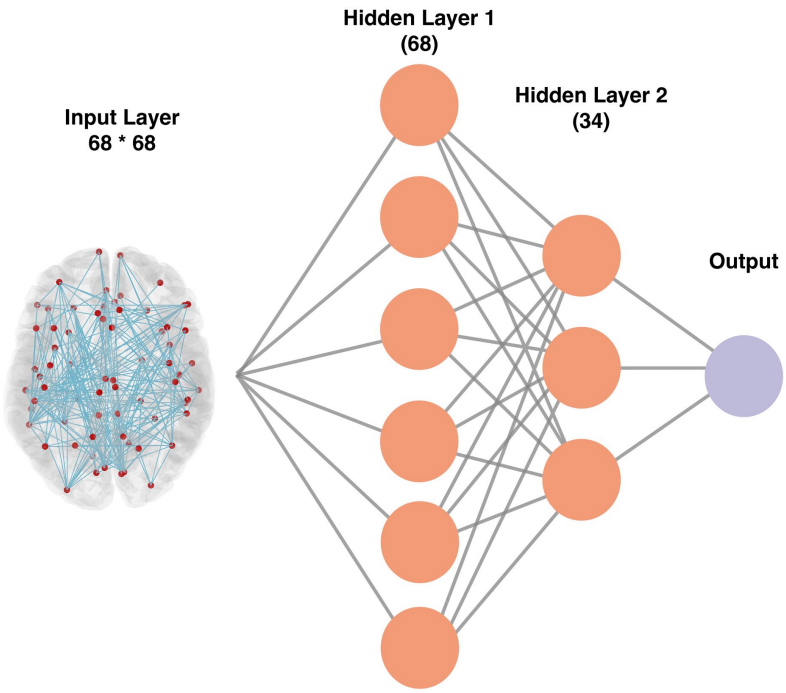

Figure 7.2: Schematic of the structure of the FFNN model using functional brain networks as input data.

to rapidly reduce training costs. It employed a batch size of 50, ran for 100 training epochs, utilized a learning rate of 0.001, and incorporated a momentum term of 0.99. The early stopping was used to stop training when there was no improvement after 10 epochs. Furthermore, to prevent overfitting, a dropout technique with a rate of 0.5 was applied. It randomly excludes neurons and connections during training. Binary cross-entropy was employed as the loss function. Accuracy and loss were used as evaluation metrics in order to assess the performance of proposed classification model.

To further assess the model's generalization capability, this study adopted a Leave-One-Subject-Out (LOSO) cross-validation method to guarantee a person-independent training model. In this strategy, data corresponding to a specific subject was systematically kept aside from the overall dataset during each iteration and utilized as the test set for model evaluation. The remaining subjects' data were used for model training. This iterative process continued until every subject had been tested, culminating in an average accuracy. The python language on the Google Colab platform and the Keras library were employed to execute these tasks.

7.5 Results

The performance of two models, CNN and FFNN, was firstly compared under 3-Fold cross-validation by training the brain network states of the "intact" visual field during visual processing in normal subjects and patients, as shown in Table 7.1. Fig. 7.3 and 7.4 display the performance of CNN and FFNN models in terms of classification accuracy, loss and confusion matrix in beta band using COH and PLV network data, respectively.

The findings demonstrate that among the models constructed from PLV and COH networks, FFNN performs slightly better than CNN in certain frequency bands. Especially

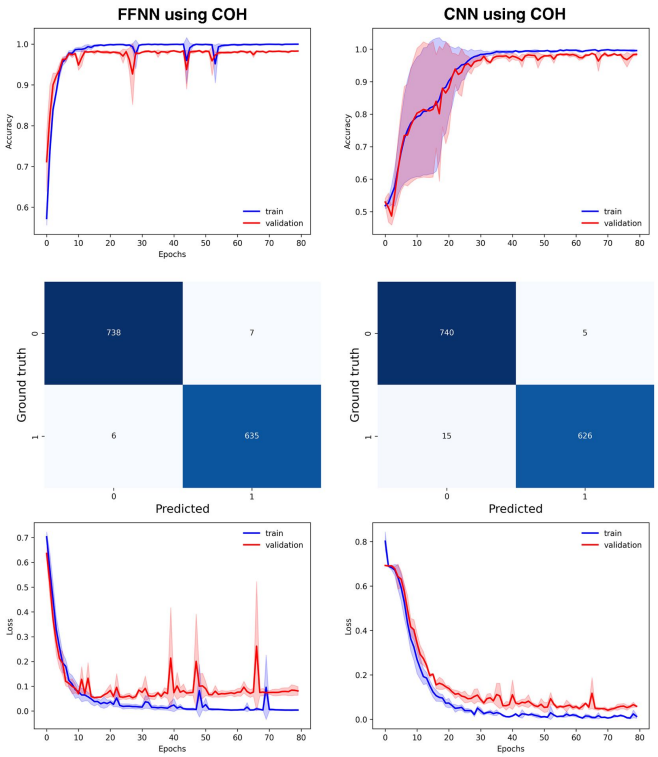

Figure 7.3: Performance of CNN and FFNN models in beta band using COH networks data after 3-Fold cross validation. The prediction results as the confusion matrix revealed the average classification confounding after 3-fold cross-validation. The diagonal line indicates the number of correctly classified samples. The shade of color represents the number of correct or incorrect classifications. The higher the number of correct classifications, the darker the color. In this context, '0' denotes 'patient', while '1' signifies 'control'.

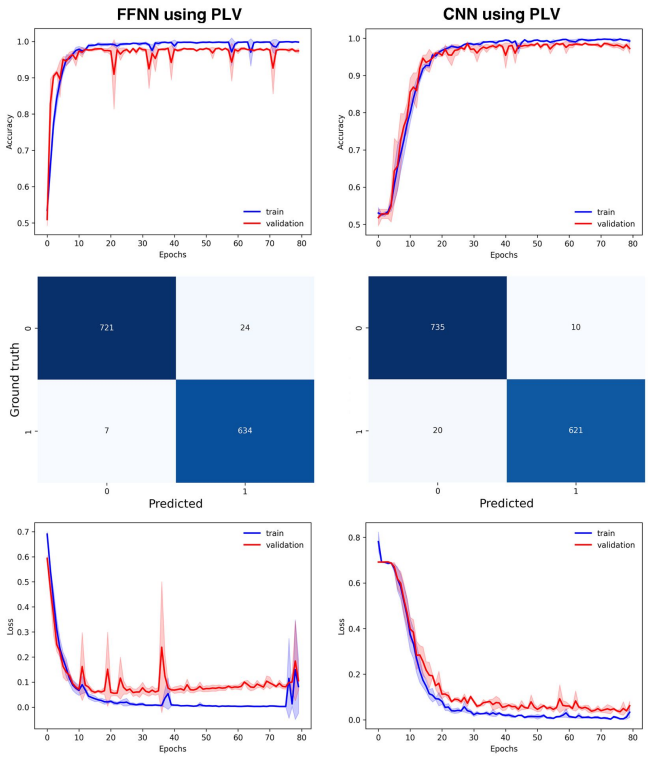

Figure 7.4: The performance comparison of CNN with FFNN model in beta band when using PLV network data to classify control and patient brain responses in intact vision area after 3-fold cross-validation. The confusion matrix-derived prediction results reflected the average classification accuracy following 3-fold cross-validation. Here, '0' denotes 'patient', while '1' signifies 'control'.

Accuracy	FFNN		CNN	
	COH	PLV	COH	PLV
Theta	0.876	0.842	0.682	0.564
Alpha	0.944	0.929	0.940	0.779
Low Alpha	0.803	0.910	0.862	0.691
High alpha	0.941	0.804	0.787	0.669
Beta	0.991	0.978	0.985	0.979

Table 7.1: Comparison of classification accuracy results across frequency bands using CNN and FFNN to build deep learning models after 3-fold cross-validation.

in the high alpha frequency band, the FFNN model built using the data from COH and PLV networks outperforms CNN by 15.4% and 13.5%, respectively.

In addition, in the model constructed using PLV, the FFNN exhibits even higher accuracy in almost each frequency band compared to CNN. Specifically, the FFNN constructed with PLV has a decoding accuracy of 92.9% at alpha frequency. This is closely followed by the low alpha frequency FFNN with 91.0% accuracy, and the theta FFNN with 84.2% decoding accuracy. The CNN models constructed based on PLV showed poor classification performance except for the use of beta data (Table 7.1). However, as shown in Figures 7.3 and 7.4, in the beta band, the accuracy of both CNN and FFNN were higher than 97%, and there was not much differences between the accuracy of these two models. In contrast, there was no more valid information learned for predicting visual field recovery using the iPLV and iCOH training data.

To ascertain the model's independence from individual subjects and assess its generalization performance, I conducted a comparative analysis between the results of 3-

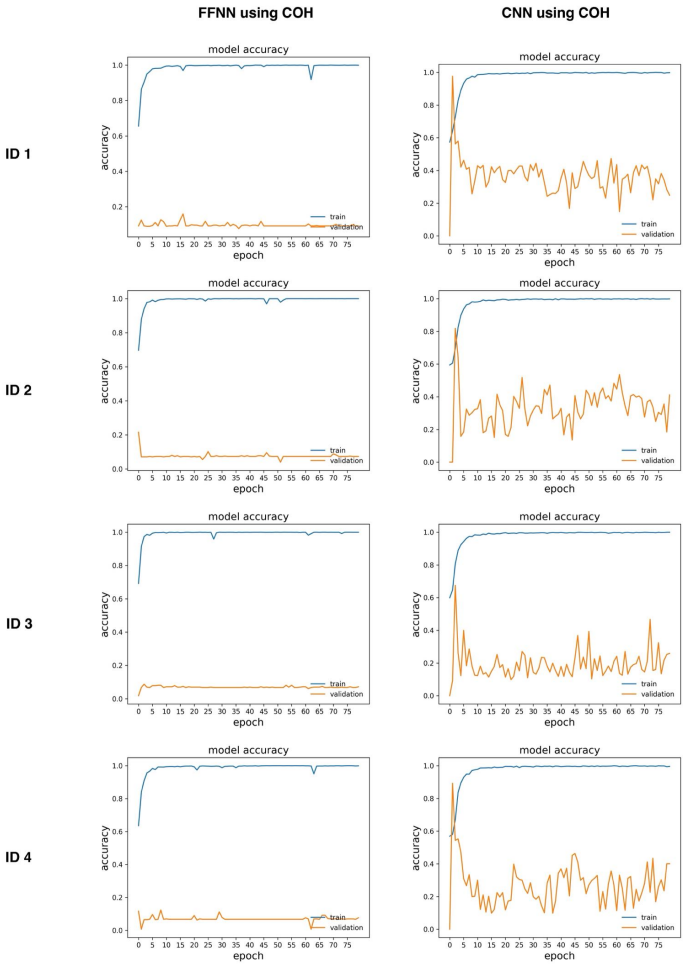

Figure 7.5: Performance comparison of the CNN and FFNN models using Leave-One-Subject-Out cross-validation in the beta frequency band. The prediction accuracies of the models were shown schematically for the four subjects.

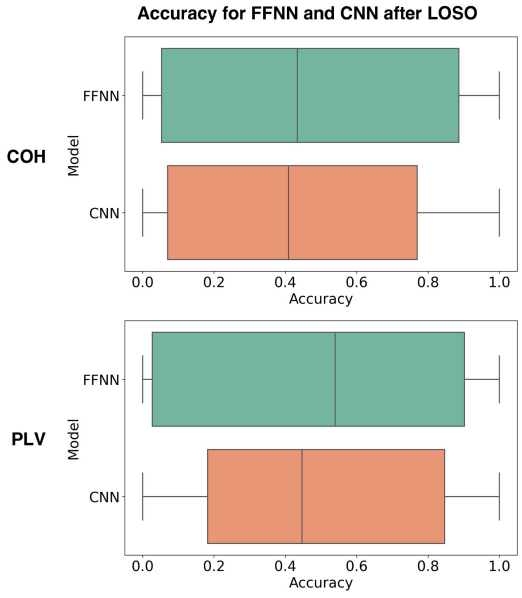

Figure 7.6: Boxplot of accuracy for FFNN and CNN models after LOSO cross-validation in the beta band.

fold cross-validation and Leave-One-Subject-Out (LOSO) cross-validation. Focusing on the beta frequency band, which exhibited superior model performance after 3-fold cross-validation, I validated the CNN and FFNN models using a dataset comprising network response data from both healthy individuals and patients with optic nerve damage during visual processing. The results revealed that despite training on the beta-band network data, which performs optimally in the 3-fold cross-validation results, neither the CNN model nor the FFNN model was effective in LOSO cross-validation. As shown in Fig. 7.5, the accuracy curves learned by the FFNN and CNN models were significantly different from the results obtained from the 3-fold cross-validation, both of which indicated that the models were not generalizable to individual subjects. The accuracy distribution after LOSO indicated the similar result (Fig. 7.6). Neither model exhibited robust generalization to unseen subjects, indicating potential overfitting issues. The constrained ability to generalize suggests that the models may overpredict the training subjects, leading to a lack of adaptability when faced with new and diverse subjects. The observed subject dependencies underscore the risk of overfitting, as the models seem overly specialized and less capable of handling variations beyond the training set.

To further evaluate the generalization capabilities of the models, I employed smaller frameworks designed to extract meaningful and realistic features while reducing the risk of overfitting. The goal was to simplify the models, reducing complexity and ensuring a more focused extraction of relevant features and characteristics without overfitting issues. Various configurations were tested, including a single-layer FFNN with 8, 16, and 32 neurons, a two-layer CNN with neuron counts of 8, 16, and 16, 32 in their respective layers, and a one-layer CNN with neuron counts of 8 and 34. Despite these variations, the average classification accuracy after LOSO cross-validation remained below 50%. Additionally, efforts were made to optimize hyperparameters using Optuna, including tuning the number of layers and neurons per layer for FFNN and CNN models, respectively. However, even with the newly obtained best models of FFNN and CNN, the highest achieved accuracy after LOSO validation was only 52.8%. In addition, other experiments were conducted using node centralities as input data to further test the generalization ability of the proposed models. However, the experimental results were similar to those using networks as input data.

In summary, despite exploring various model configurations and conducting hyperparameter optimization, the models, including both FFNN and CNN, exhibited limited generalization ability, with an average accuracy below 50% after LOSO cross-validation.

7.6 Discussion

In this study, I explored the potential of deep learning models to serve as an early warning system to detect visual field impairment by analyzing EEG-based functional brain networks.

My study compared the performance of CNN and FFNN in classifying functional brain network data derived from EEG recordings during visual processing in intact vision areas. As I showed, FFNN outperformed CNN in most frequency bands after 3-fold cross-validation, particularly for PLV and COH networks. In addition, variations in performance across different frequency bands were observed. Specifically, in the theta and high alpha bands, FFNN models consistently demonstrated superior accuracy compared to CNN.

However, both FFNN and CNN achieved high accuracies over 97.0% in the beta frequency band. These variations in performance highlight the importance of considering the specific frequency characteristics of EEG data when developing early warning models for visual field impairment.

However, a comparative analysis between 3-fold cross-validation and Leave-One-Subject-Out cross-validation, especially for the beta band, revealed different findings in terms of validating the independence of the models from individual subjects and assessing their generalization performances. Using network response data from both healthy individuals and patients with optic nerve damage during visual processing, I conducted model validations for both the CNN and FFNN. The results demonstrated that neither the FFNN nor the CNN models were effective in predicting accuracy during LOSO cross-validation. The prediction accuracies of both CNN and FFNN models were affected by individual differences in subjects. Importantly, in the model validation of individual subjects, both models were shown to deviate significantly from the accuracy obtained through 3-fold cross-validation. This inconsistency shown in different cross-validation techniques suggests that our proposed models may have a strong subject dependency without generalization ability. This may be strongly related to the limited number of trials for individual subjects as well as the severe individual variations in the original visual condition among subjects as well. Despite experimenting with diverse model configurations and optimizing hyperparameters, both FFNN and CNN models demonstrated constrained generalization, reflected in an average accuracy below 50% during LOSO cross-validation.

There are some limitations to this study. Limitations regarding the fact that the training data in this study is relatively small. Further studies with larger and more diverse samples to the training and more powerful machine learning analytics platforms are necessary to expand the range of optimization parameters of the proposed model to validate the overall performance of the model as far as possible. In addition, ways to generalize the findings to a wider population and different clinical settings should be explored. Finally, another limitation was that our visual field test (HRP) was an easier task than the perimetric tests which were conducted in clinical ophthalmology. Therefore, visual field regions that are presumably "intact" cannot be certain, in fact, damage when using a more difficult perimetric test where the stimuli are smaller or less bright, i.e., closer to the perceptual threshold.

In terms of the limitations of the proposed model, neither the FFNN nor the CNN models demonstrated generalization capabilities. Therefore, other machine learning models that would be more suitable for brain network characterization, such as graph neural networks, should also be explored in the future.

Other aspects that could be considered for future work include the following: exploring models with higher generalization capabilities and integrating other datasets to apply the model to different ophthalmic diseases, not just optic nerve damage; and directly extracting EEG data features for modeling. Future studies could also explore the integration of EEG-based early warning models with other diagnostic techniques (e.g., ocular imaging) to improve the accuracy and reliability of visual field impairment diagnosis.

7.7 Conclusion

In conclusion, this study is an important step in the development of a visual field impairment early warning model using deep learning techniques and EEG-based functional brain networks. Although the proposed CNN and FFNN models in both did not show classification performance and accuracy with generalization ability. However, considering the small sample size and the large inter-individual variation in visual impairment, the model after the inclusion of covariates may hold promise for early warning of visual field impairment.

Early detection and intervention are essential to protect visual health and improve patients' quality of life. However, further exploration in the field of visual processing research is also needed to improve the generalization capabilities of these models, to make them be promising tools for further exploration in the field of visual processing research, and to improve their potential applicability to assessing and understanding the neural responses of patients with optic nerve injuries in a clinical setting.

While this study provides promising insights, further research on larger data sets and clinical validation is needed to determine the applicability of these models in the real world of clinical neuro-ophthalmology. The development of accurate and reliable early warning systems for visual field impairment has the potential to have a significant impact on patient care and visual health management.

8 Summary and Outlook

The thesis explored the role of brain network plasticity in vision loss and recovery of vision. It describes changes and adjustments (recovery) of visually evoked brain networks in patients with optic nerve damage and control subjects, relating visual performance to global network reorganization, properties of local central hubs and nodes, and the complex dynamic intra- and inter-module interactions. Specifically, I described the dynamic responses of brain networks to visual stimulation and neuromodulation after non-invasive brain stimulation. Subsequently, I investigated and tested a prediction model for rtACS-induced visual recovery and an early warning model for visual field damage using deep learning tools to characterize the complex dynamic brain network features under different function conditions: normal vision vs. abnormal vision and vision recovery vs. no recovery. In a nutshell, I used the EEG to described, developed and validated brain physiological network features as a new biomarker of low vision.

8.1 Network Science in Understanding Spacetime of the Brain

The exploration of the brain's functional connectivity networks and their rapid dynamics in response to visual stimuli has revealed the complexity of neural processing and cognitive function, especially in the context of optic nerve damage. This study introduces the concept of FCN plasticity at the millisecond scale, providing a framework for understanding how fast and accurate different brain regions interact during conditions of normal and abnormal vision, and their role in vision restoration.

I used high-temporal-resolution EEG recordings to investigate how FCN respond to visual stimuli in IVA and ARV in patients with optic nerve damage in Chapter 3. The findings reveal significant differences in FCN dynamics between healthy controls and patients. Notably, patients exhibit higher clustering coefficients, longer characteristic path lengths, and weaker small-world organization in the theta band, indicating that neural processing during visual performance is less efficient in patients. This confirms early studies by the Sabel group (Bola and Sabel, 2015), but it extends their results in terms of hubs connections and modularity by considering the domain of TIME at the msec-scale. Thus, my studies combined information of brain regions (3D-brain-SPACE) with that of the TIME domain, which we termed "Spacetime of the Brain".

Specifically, regarding areas of partial vision loss ("areas of residual vision"), I delve into how patients with optic nerve damage react to stimuli and how this relates to weighted brain network topology characteristics. The analysis shows that when patients respond correctly to visual stimuli (hits), the FCN exhibits larger global strength, higher clustering and longer path lengths. Furthermore, the study compares FCN reorganization between intact visual field and areas of residual vision in patients. I found that IVA had stronger global strength, greater clustering coefficient, longer characteristic path length, and higher small-worldness compared to ARV.

These findings suggest that network dynamics play a vital role in the cognitive processing of visual information in patients with optic nerve damage, emphasizing the importance of studying FCN in various parts of the visual field. In addition, when compared to normal subjects, patients with optic nerve damage showed stronger global strength, higher

clustering aggregation and used longer path lengths to complete visual processing.

In addition, in control subjects with normal vision, I identified 20 key FCN hubs distributed across different brain networks as described in Chapter 4. These hubs played crucial roles in the processing of visual information and exhibited dynamic interactions during different phases of visual processing. In patients with optic nerve damage, disruptions were observed in both hub and non-hub regions, highlighting the impact of vision impairment on FCN dynamics.

Furthermore, the dynamics of brain network modularity were explored in Chapter 5. I confirmed the presence of a modular organization in visual processing, revealing four distinct functional modules: motor, attention, visual, and other. These modules played a crucial role in the coordination of brain functions during visual processing. I found that optic nerve damage patients displayed differences in module interactions compared to healthy controls, suggesting that the brain adapted to the damage by engaging other modules more extensively.

In summary, my research underscores the significance of FCN in understanding brain function, especially in the context of optic nerve damage and visual impairment. It provides valuable insights into the dynamic nature of neural processing. Clearly, understanding the intricate interaction of FCN in different brain regions holds promise for improving the cognitive and visual functions of patients with optic nerve damage, ultimately enhancing their quality of life.

8.2 Non-invasive Brain Stimulation for Vision Restoration

In the context of neuromodulation using rtACS, the study demonstrates that rtACS can normalize FCN dynamics and enhance the balance between integration and segregation of global rFCN. This confirms and extends earlier studies by Bola et al (Bola et al., 2015). I extended their findings showing that application of rtACS neuromodulation also shows promise in inducing positive changes in patients' local properties of FCN. Specific hubs and non-hub regions exhibited altered connectivity patterns after treatment, suggesting that the more detailed hub-structure is relevant to understand the neurophysiological basis of vision recovery. I also found correlations between FCN attributes and visual performance, indicating that enhanced network synchronization is associated with improved vision. In addition, visual improvements were stable for at least 2-months. This suggests a potential avenue for therapeutic interventions to improve FCN function in patients with optic nerve damage.

Using also a dynamic modular analysis approach, I found that rtACS treatment induced changes in the multilayer community structure, promoting a more optimized and stable modular organization. In patients who received rtACS, global modularity increased and the flexibility of the multilayer network decreased. This is a sign that rtACS leads to a more stable community structure and greater specialization of neurons within modules.

These findings have important implications for understanding the functional reorganization of brain networks in response to local damage and the potential of neuromodulation techniques like rtACS. The modulation of intra- and inter-module interactions plays a crucial role in visual performance and other cognitive functions. My research provides valuable insights into the underlying neural mechanisms and offers promising prospects

for the development of therapeutic interventions in various brain disorders.

8.3 Deep Learning Models for Vision Restoration and Early Warning

I also explored the potential of deep learning to solve problems in practical ophthalmology and neurorehabilitation using data from dynamic brain network responses. I built a model for predicting treatment outcomes for vision recovery in patients with optic nerve damage in Chapter 6, and in Chapter 7, I explored the possibilities of an early warning system for visual field impairment.

To address the unpredictability and varying efficacy of non-invasive brain stimulation therapy, particularly rtACS in patients with optic nerve damage, I built two deep learning models, including FFNN and Bi-LSTM. They proved useful to analyze the node centralities of functional brain networks based on patients' EEG data during visual tasks to predict vision recovery outcomes after rtACS. My analyses demonstrate the potential of deep learning models to predict visual field recovery, with the FFNN exhibiting superior performance over the Bi-LSTM in various frequency bands.

The traditional diagnostic methods for visual field impairment rely on eye imaging and visual field testing. However, they may fail to detect early signs of visual field damage, i.e., long before the visual (functional) loss is apparent. Here, deep learning models based on EEG recordings may be useful. By applying CNNs and FFNNs to EEG-based functional brain networks, I investigated the possibility of using these proposed models to detect indicators of visual field impairment in "intact" visual fields. However, the results indicated that neither the FFNN nor the CNN models exhibited subject-independent generalization capabilities in the classification of brain functional network data from patients and controls, which remains to be further explored considering the potential of early diagnostic models for early, pre-symptomatic diagnosis and intervention in visual health.

8.4 Outlook

My study provides a deep insight into the dynamic changes that occur in the brain's FCN during visual processing, and how these networks adapt to vision loss and vision restoration. The research raises several important points and avenues for future investigation:

Applications Beyond Visual Processing: This study represents a significant step in unraveling the complexity of brain network and its response to local damage and neuromodulation. While my work focused on visual processing and optic nerve damage, the principles of FCN dynamics and neuromodulation could apply to various cognitive functions, neurological and psychiatric conditions. Further research can explore how these findings translate to other brain disorders and functional modalities.

Network Plasticity and Neuromodulation: Future research can further explore the mechanisms of neuromodulation and develop targeted interventions to optimize FCN dynamics in patients with visual impairments. In addition, understanding the plasticity of FCN and their ability to adapt to different cognitive processes and sensory inputs could have broader implications for various brain-related conditions, not just vision impairment. Further studies can delve into the optimization of neuromodulation techniques for vision

restoration and potentially other neurological conditions.

Closed-Loop Adaptive Brain Stimulation: Recent advances in the simultaneous collection of EEG during rtACS open up new possibilities for closed-loop adaptive brain stimulation protocols. This approach allows real-time monitoring of brain oscillations and the modulation of stimulation parameters to target specific brain networks and functions more effectively.

Clinical Implications and Individualized Treatment: As I showed, FCN metrics can serve as potential biomarkers for assessing and monitoring the effects of vision restoration interventions. Future research can delve into the development of clinical applications for such metrics for patients with vision damage and neurological disorders. In addition, understanding the relationship between FCN and cognitive performance suggests the potential for individualized treatment approaches. Tailoring neuromodulation techniques to an individual's specific network architecture could optimize therapeutic outcomes.

Optimization of Deep Learning Models: Further validation with larger and more diverse samples is essential to ensure the generalizability of the models. And the integration of these EEG-based deep learning models with other diagnostic techniques, such as ocular imaging, represents a promising avenue for improving accuracy and reliability in visual field impairment diagnosis and vision recovery prediction. Furthermore, the exploration of more sophisticated machine learning models could yield even more robust results when correlating brain network features with normal human behavior or neuropsychiatric dysfunctions.

In conclusion, the research presented in this study provides a solid foundation for understanding the dynamic nature of FCN on the millisecond scale, its role in cognitive functions, and the potential for neuromodulation to enhance brain plasticity and adaptation. Further investigations using "Spacetime of the Brain" hold promise not only for vision restoration but also for gaining deeper insights into the functioning of the human brain in health and disease. As research in this field continues to evolve, the Concept of Spacetime in the Brain promises to inspire and enrich the development of innovative diagnostics and interventions for a wide range of neuro-ophthalmological and neuropsychiatric conditions.

References

R. Abiri, S. Borhani, E. W. Sellers, Y. Jiang, and X. Zhao. A comprehensive review of eeg-based brain-computer interface paradigms. *Journal of Neural Engineering*, 16(1): 011001, 2019.

M. D. Abràmoff, P. T. Lavin, M. G. Birch, N. Shah, and J. C. Folk. Pivotal trial of an autonomous ai-based diagnostic system for detection of diabetic retinopathy in primary care offices. *Npj Digital Medicine*, 1(1):Article 1, 2018.

N. Accornero, P. Li Voti, M. La Riccia, and B. Gregori. Visual evoked potentials modulation during direct current cortical polarization. *Experimental Brain Research*, 178(2): 261–266, 2007.

U. R. Acharya, S. L. Oh, Y. Hagiwara, J. H. Tan, H. Adeli, and D. Subha. Automated eeg-based screening of depression using deep convolutional neural network. *Computer Methods and Programs in Biomedicine*, 161:103–113, 2018.

S. Agarwal, G. Koch, A. E. Hillis, W. Huynh, N. S. Ward, S. Vucic, and M. C. Kiernan. Interrogating cortical function with transcranial magnetic stimulation: Insights from neurodegenerative disease and stroke. *Journal of Neurology, Neurosurgery & Psychiatry*, 90(1):47–57, 2019.

N. Ahmed, M. S. Abbasi, F. Zuberi, W. Qamar, M. S. B. Halim, A. Maqsood, and M. K. Alam. Artificial intelligence techniques: Analysis, application, and outcome in dentistry—a systematic review. *BioMed Research International*, 2021:9751564, 2021.

S. Ahn, J. M. Mellin, S. Alagapan, M. L. Alexander, J. H. Gilmore, L. F. Jarskog, and F. Fröhlich. Targeting reduced neural oscillations in patients with schizophrenia by transcranial alternating current stimulation. *NeuroImage*, 186:126–136, 2019.

A.-R. Al-Saegh, S. A. Dawwd, and J. M. Abdul-Jabbar. Deep learning for motor imagery eeg-based classification: A review. *Biomedical Signal Processing and Control*, 63:102172, 2021.

A. F. Alexander-Bloch, N. Gogtay, D. Meunier, R. Birn, L. Clasen, F. Lalonde, R. Lenroot, J. Giedd, and E. T. Bullmore. Disrupted modularity and local connectivity of brain functional networks in childhood-onset schizophrenia. *Frontiers in Systems Neuroscience*, 4:147, 2010.

M. M. Ali, K. K. Sellers, and F. Frohlich. Transcranial alternating current stimulation modulates large-scale cortical network activity by network resonance. *Journal of Neuroscience*, 33(27):11262–11275, 2013.

R. Alkawadri, R. C. Burgess, Y. Kakisaka, J. C. Mosher, and A. V. Alexopoulos. Assessment of the utility of ictal magnetoencephalography in the localization of the epileptic seizure onset zone. *JAMA Neurology*, 75(10):1264–1272, 2018.

A. Antal and W. Paulus. Transcranial alternating current stimulation (tacs). *Frontiers in Human Neuroscience*, 7:317, 2013.

A. Antal, K. Boros, C. Poreisz, L. Chaieb, D. Terney, and W. Paulus. Comparatively weak after-effects of transcranial alternating current stimulation (tacs) on cortical excitability in humans. *Brain Stimulation*.

H. A. Ardakani, M. Taghizadeh, and F. Shayegh. Diagnosis of autism disorder based on deep network trained by augmented eeg signals. *International Journal of Neural Systems*, 32(11):2250046, 2022.

T. M. Aslam, H. R. Zaki, S. Mahmood, Z. C. Ali, N. A. Ahmad, M. R. Thorell, and K. Balaskas. Use of a neural net to model the impact of optical coherence tomography abnormalities on vision in age-related macular degeneration. *American Journal of Ophthalmology*, 185:94–100, 2018.

L. Avitan, Z. Pujic, J. Mölter, M. v. d. Poll, B. Sun, H. Teng, R. Amor, E. K. Scott, and G. J. Goodhill. Spontaneous activity in the zebrafish tectum reorganizes over development and is influenced by visual experience. *Current Biology*, 27(16):2407–2419.e4, 2017.

B. Ay, O. Yildirim, M. Talo, U. B. Baloglu, G. Aydin, S. D. Puthankattil, and U. R. Acharya. Automated depression detection using deep representation and sequence learning with eeg signals. *Journal of Medical Systems*, 43(7):205, 2019.

M. Babaee, D. T. Dinh, and G. Rigoll. A deep convolutional neural network for video sequence background subtraction. *Pattern Recognition*, 76:635–649, 2018.

M. Bahr-Hosseini and M. Bikson. Neurovascular-modulation: A review of primary vascular responses to transcranial electrical stimulation as a mechanism of action. *Brain Stimulation*, 14(4):837–847, 2021.

C. Barros, C. A. Silva, and A. P. Pinheiro. Advanced eeg-based learning approaches to predict schizophrenia: Promises and pitfalls. *Artificial Intelligence in Medicine*, 114: 102039, 2021.

D. S. Bassett and E. Bullmore. Small-world brain networks. *Neuroscientist*, 12(6):512–523, 2006.

D. S. Bassett, N. F. Wymbs, M. A. Porter, P. J. Mucha, J. M. Carlson, and S. T. Grafton. Dynamic reconfiguration of human brain networks during learning. *Proceedings of the National Academy of Sciences*, 108(18):7641–7646, 2011.

D. S. Bassett, M. A. Porter, N. F. Wymbs, S. T. Grafton, J. M. Carlson, and P. J. Mucha. Robust detection of dynamic community structure in networks. *Chaos: An Interdisciplinary Journal of Nonlinear Science*, 23(1):013142, 2013.

D. S. Bassett, M. Yang, N. F. Wymbs, and S. T. Grafton. Learning-induced autonomy of sensorimotor systems. *Nature Neuroscience*, 18(5):744–751, 2015. doi: 10.1038/nn.3993.

J. F. Beattie, R. C. Martin, R. K. Kana, H. Deshpande, S. Lee, J. Curé, and L. V. Hoef. Hippocampal dentation: Structural variation and its association with episodic memory in healthy adults. *Neuropsychologia*, 101:65–75, 2017.

R. M. Beatty, A. A. Sadun, L. E. H. Smith, J. P. Vonsattel, and E. P. Richardson. Direct demonstration of transsynaptic degeneration in the human visual system: A comparison of retrograde and anterograde changes. *Journal of Neurology Neurosurgery and Psychiatry*, 45(2):143–146, 1982.

P. Bednarik, D. Goranovic, A. Svatkova, F. Niess, L. Hingerl, B. Strasser, D. K. Deelchand, B. Spurny-Dworak, M. Krssak, S. Trattnig, et al. 1h magnetic resonance spectroscopic imaging of deuterated glucose and of neurotransmitter metabolism at 7t in the human brain. *Nature Biomedical Engineering*, 2023.

M. A. Bertolero, B. T. Thomas Yeo, and M. D'Esposito. The modular and integrative functional architecture of the human brain. *Proceedings of the National Academy of Sciences*, 112(49):E6798–E6807, 2015.

J. Betancur, F. Commandeur, M. Motlagh, T. Sharir, A. J. Einstein, S. Bokhari, M. B. Fish, T. D. Ruddy, P. Kaufmann, A. J. Sinusas, et al. Deep learning for prediction of obstructive disease from fast myocardial perfusion spect. *JACC: Cardiovascular Imaging*, 11(11):1654–1663, 2018.

R. F. Betzel, K. C. Wood, C. Angeloni, M. N. Geffen, and D. S. Bassett. Stability of spontaneous, correlated activity in mouse auditory cortex. *PLOS Computational Biology*, 15(12):e1007360, 2019.

V. D. Blondel, J.-L. Guillaume, R. Lambiotte, and E. Lefebvre. Fast unfolding of communities in large networks. *Journal of Statistical Mechanics: Theory and Experiment*, 2008(10), 2008.

M. Bola and B. A. Sabel. Dynamic reorganization of brain functional networks during cognition. *NeuroImage*, 114:398–413, 2015.

M. Bola, C. Gall, C. Moewes, A. Fedorov, H. Hinrichs, and B. A. Sabel. Brain functional connectivity network breakdown and restoration in blindness. *Neurology*, 83(6):542–551, 2014.

M. Bola, C. Gall, and B. A. Sabel. Disturbed temporal dynamics of brain synchronization in vision loss. *Cortex*, 67:134–146, 2015.

U. Braun, A. Schäfer, D. S. Bassett, F. Rausch, J. I. Schweiger, E. Bilek, S. Erk, N. Romanczuk-Seiferth, O. Grimm, L. S. Geiger, et al. Dynamic brain network reconfiguration as a potential schizophrenia genetic risk mechanism modulated by nmda receptor function. *Proceedings of the National Academy of Sciences*, 113(44):12568–12573, 2016.

D. Brignani, M. Ruzzoli, P. Mauri, and C. Miniussi. Is transcranial alternating current stimulation effective in modulating brain oscillations? *PLoS ONE*, 2013.

J. M. Brown, J. P. Campbell, A. Beers, K. Chang, S. Ostmo, R. V. P. Chan, J. Dy, D. Erdogmus, S. Ioannidis, J. Kalpathy-Cramer, et al. Automated diagnosis of plus disease in retinopathy of prematurity using deep convolutional neural networks. *JAMA Ophthalmology*, 136(7):803–810, 2018.

J. Brunelin, M. Mondino, F. Haesebaert, M. Saoud, M.-F. Suaud-Chagny, and E. Poulet. Efficacy and safety of bifocal tdcs as an interventional treatment for refractory schizophrenia. *Brain Stimulation*, 5(3):431–432, 2012.

A. R. Brunoni, L. Valiengo, A. Baccaro, T. A. Zanão, J. F. de Oliveira, A. Goulart, P. S. Boggio, P. A. Lotufo, I. M. Benseñor, and F. Fregni. The sertraline vs. electrical current therapy for treating depression clinical study: Results from a factorial, randomized, controlled trial. *JAMA Psychiatry*, 70(4):383–391, 2013.

R. L. Buckner, J. R. Andrews-Hanna, and D. L. Schacter. The brain's default network: Anatomy, function, and relevance to disease. *Annals of the New York Academy of Sciences*, 1124(1):1–38, 2008.

S. Budisavljevic, F. Dell'Acqua, and U. Castiello. Cross-talk connections underlying dorsal and ventral stream integration during hand actions. *Cortex*, 103:224–239, 2018.

E. Bullmore and O. Sporns. Complex brain networks: Graph theoretical analysis of structural and functional systems. *Nature Publishing Group*, 10(3):186–198, 2009.

E. Bullmore and O. Sporns. The economy of brain network organization. *Nature Reviews Neuroscience*, 2012.

N. Burgos, S. Bottani, J. Faouzi, E. Thibeau-Sutre, and O. Colliot. Deep learning for brain disorders: From data processing to disease treatment. *Briefings in Bioinformatics*, 22 (2):1560–1576, 2021.

G. Buzsáki, N. Logothetis, and W. Singer. Scaling brain size, keeping timing: Evolutionary preservation of brain rhythms. *Neuron*, 80(3):751–764, 2013.

M. A. Caldieraro and P. Cassano. Transcranial and systemic photobiomodulation for major depressive disorder: A systematic review of efficacy, tolerability and biological mechanisms. *Journal of Affective Disorders*, 243:262–273, 2019.

E. M. Callaway and L. Luo. Monosynaptic circuit tracing with glycoprotein-deleted rabies viruses. *Journal of Neuroscience*, 35(24):8979–8985, 2015.

S. Campana, C. Caltagirone, and P. Marangolo. Combining voxel-based lesion-symptom mapping (vlsm) with a-tdcs language treatment: Predicting outcome of recovery in nonfluent chronic aphasia. *Brain Stimulation*, 8(4):769–776, 2015.

R. T. Canolty and R. T. Knight. The functional role of cross-frequency coupling. *Trends in Cognitive Sciences*, 14(11):506–515, 2010.

D. Cappon, T. den Boer, C. Jordan, W. Yu, E. Metzger, and A. Pascual-Leone. Transcranial magnetic stimulation (tms) for geriatric depression. *Ageing Research Reviews*, 74: 101531, 2022.

M. Catani and D. H. Ffytche. The rises and falls of disconnection syndromes. *Brain*, 128 (10):2224–2239, 2005.

M. Catani, F. Dell'Acqua, A. Bizzi, S. J. Forkel, S. C. Williams, A. Simmons, D. G. Murphy, and M. Thiebaut de Schotten. Beyond cortical localization in clinico-anatomical correlation. *Cortex*, 48(10):1262–1287, 2012.

A. Catarino, A. Andrade, O. Churches, A. P. Wagner, S. Baron-Cohen, and H. Ring. Task-related functional connectivity in autism spectrum conditions: An eeg study using wavelet transform coherence. *Molecular Autism*, 4(1):1, 2013.

L. Chaieb, W. Paulus, and A. Antal. Evaluating aftereffects of short-duration transcranial random noise stimulation on cortical excitability. *Neural Plasticity*, 2011:105927, 2011.

Z. Chen, H. Fu, W.-L. Lo, and Z. Chi. Strabismus recognition using eye-tracking data and convolutional neural networks. *Journal of Healthcare Engineering*, 2018:7692198, 2018.

N. Cheng, D. Chen, B. Lou, J. Fu, and H. Wang. A biosensing method for the direct serological detection of liver diseases by integrating a sers-based sensor and a cnn classifier. *Biosensors & Bioelectronics*, 186:113246, 2021.

H.-M. Cho, J. Lee, S.-J. Kang, W.-H. Kim, S. Choi, J.-M. Ko, H.-J. Min, G. Choi, D.-W. Kang, P. H. Lee, et al. Angiography-based machine learning for predicting fractional flow reserve in intermediate coronary artery lesions. *Journal of the American Heart Association*, 8(4):e011685, 2019.

Y.-S. Choi, S. Bae, J. H. Chang, S.-G. Kang, S.-H. Kim, J. Kim, T. Rim, S. H. Choi, R. Jain, and S.-K. Lee. Fully automated hybrid approach to predict the idh mutation status of gliomas via deep learning and radiomics. *Neuro-Oncology*, 23(2):304–313, 2021.

E. Christiaen, M.-G. Goossens, B. Descamps, L. E. Larsen, P. Boon, R. Raedt, and C. Vanhove. Dynamic functional connectivity and graph theory metrics in a rat model of temporal lobe epilepsy reveal a preference for brain states with lower functional connectivity, segregation and integration. *Neurobiology of Disease*, 139:104808, 2020.

D. Y. Chu, N. Adluru, V. A. Nair, T. Choi, A. Adluru, C. Garcia-Ramos, K. Dabbs, J. Mathis, A. S. Nencka, C. Gundlach, et al. Association of neighborhood deprivation with white matter connectome abnormalities in temporal lobe epilepsy. *Epilepsia*, 2023.

R. M. Cichy, D. Pantazis, and A. Oliva. Similarity-based fusion of meg and fmri reveals spatio-temporal dynamics in human cortex during visual object recognition. *Cerebral Cortex*, 26(8):3563–3579, 2016.

M. S. Clayton, N. Yeung, and R. C. Kadosh. Electrical stimulation of alpha oscillations stabilizes performance on visual attention tasks. *Journal of Experimental Psychology: General*, 148(2):203–220, 2019.

J. R. Cohen and M. D'Esposito. The segregation and integration of distinct brain networks and their relationship to cognition. *Journal of Neuroscience*, 36(48):12083–12094, 2016.

T. E. Cope, T. Rittman, R. J. Borchert, P. S. Jones, D. Vatansever, K. Allinson, L. Passamonti, P. Vazquez Rodriguez, W. R. Bevan-Jones, J. T. O'Brien, and J. B. Rowe. Tau burden and the functional connectome in alzheimer's disease and progressive supranuclear palsy. *Brain*, 141(2):550–567, 2018.

A. S. Coyner, R. Swan, J. M. Brown, J. Kalpathy-Cramer, S. J. Kim, J. P. Campbell, K. E. Jonas, S. Ostmo, R. V. P. Chan, and M. F. Chiang. Deep learning for image quality assessment of fundus images in retinopathy of prematurity. *AMIA Annual Symposium Proceedings*, 2018:1224–1232, 2018.

R. C. Craddock, S. Jbabdi, C.-G. Yan, J. Vogelstein, F. X. Castellanos, A. Di Martino, C. Kelly, K. Heberlein, S. Colcombe, and M. P. Milham. Imaging human connectomes at the macroscale. *Nature Methods*, 10(6):524–539, 2013.

M. Crespo-Garcia, D. Pinal, J. L. Cantero, F. Díaz, M. Zurrón, and M. Atienza. Working memory processes are mediated by local and long-range synchronization of alpha oscillations. *Journal of Cognitive Neuroscience*, 25(8):1343–1357, 2013.

B. B. Das, P. Kumar, D. Kar, S. K. Ram, K. S. Babu, and R. K. Mohapatra. A spatio-temporal model for eeg-based person identification. *Multimedia Tools and Applications*, 78(19):28157–28177, 2019.

F. S. de Aguiar Neto and J. L. G. Rosa. Depression biomarkers using non-invasive eeg: A review. *Neuroscience & Biobehavioral Reviews*, 105:83–93, 2019.

J. de Fauw, J. R. Ledsam, B. Romera-Paredes, S. Nikolov, N. Tomasev, S. Blackwell, H. Askham, X. Glorot, B. O'Donoghue, D. Visentin, G. van den Driessche, B. Lakshminarayanan, C. Meyer, F. Mackinder, S. Bouton, K. Ayoub, R. Chopra, D. King, A. Karthikesalingam, and O. Ronneberger. Clinically applicable deep learning for diagnosis and referral in retinal disease. *Nature Medicine*, 24(9):Article 9, 2018.

F. de la Cruz, A. Schumann, S. Köhler, J. R. Reichenbach, G. Wagner, and K.-J. Bär. The relationship between heart rate and functional connectivity of brain regions involved in autonomic control. *NeuroImage*, 196:318–328, 2019.

R. S. Desikan, F. Ségonne, B. Fischl, B. T. Quinn, B. C. Dickerson, D. Blacker, R. L. Buckner, A. M. Dale, R. P. Maguire, B. T. Hyman, M. S. Albert, and R. J. Killiany. An automated labeling system for subdividing the human cerebral cortex on mri scans into gyral based regions of interest. *NeuroImage*, 31(3):968–980, 2006.

J. Deveau and A. R. Seitz. Applying perceptual learning to achieve practical changes in vision. *Frontiers in Psychology*, 5, 2014.

M. Diana, T. Raij, M. Melis, A. Nummenmaa, L. Leggio, and A. Bonci. Rehabilitating the addicted brain with transcranial magnetic stimulation. *Nature Reviews Neuroscience*, 18(11):685–693, 2017.

E. V. R. DiBella, A. Sharma, L. Richards, V. Prabhakaran, J. J. Majersik, and S. K. HashemizadehKolowri. Beyond diffusion tensor mri methods for improved characterization of the brain after ischemic stroke: A review. *AJNR: American Journal of Neuroradiology*, 43(5):661–669, 2022.

C. A. Dockery, R. Hueckel-Weng, N. Birbaumer, and C. Plewnia. Enhancement of planning ability by transcranial direct current stimulation. *The Journal of Neuroscience: The Official Journal of the Society for Neuroscience*, 29(22):7271–7277, 2009.

Y. Dong, Q. Zhang, Z. Qiao, and J.-J. Yang. Classification of cataract fundus image based on deep learning. In *2017 IEEE International Conference on Imaging Systems and Techniques (IST)*, page 1–5, 2017.

C. M. J. M. Dourado, S. P. P. da Silva, R. V. M. da Nobrega, P. P. Rebouças Filho, K. Muhammad, and V. H. C. de Albuquerque. An open ioht-based deep learning

framework for online medical image recognition. *IEEE Journal on Selected Areas in Communications*, 39(2):541–548, 2021.

C. M. Dunham, B. P. Brocker, B. D. Collier, and D. J. Gemmel. Risks associated with magnetic resonance imaging and cervical collar in comatose, blunt trauma patients with negative comprehensive cervical spine computed tomography and no apparent spinal deficit. *Critical Care*, 12(4):R89, 2008.

T. B. Dyrby, L. V. Sgaard, M. G. Hall, M. Ptito, and D. C. Alexander. Contrast and stability of the axon diameter index from microstructure imaging with diffusion mri. *Magnetic Resonance in Medicine*, 70(3):711–721, 2013.

J. S. Elam, M. F. Glasser, M. P. Harms, S. N. Sotiropoulos, J. L. R. Andersson, G. C. Burgess, S. W. Curtiss, R. Oostenveld, L. J. Larson-Prior, J.-M. Schoffelen, M. R. Hodge, E. A. Cler, D. M. Marcus, D. M. Barch, E. Yacoub, S. M. Smith, K. Ugurbil, and D. C. Van Essen. The human connectome project: A retrospective. *NeuroImage*, 244:118543, 2021.

A. Elias, N. Thomas, and H. A. Sackeim. Electroconvulsive therapy in mania: A review of 80 years of clinical experience. *American Journal of Psychiatry*, 178(3):229–239, 2021.

A. K. Engel, P. Fries, and W. Singer. Dynamic predictions: Oscillations and synchrony in top–down processing. *Nature Reviews Neuroscience*, 2(10):704–716, 2001.

G. Eraslan, Avsec, J. Gagneur, and F. J. Theis. Deep learning: New computational modelling techniques for genomics. *Nature Reviews Genetics*, 20(7):389–403, 2019.

A. Esteva, B. Kuprel, R. A. Novoa, J. Ko, S. M. Swetter, H. M. Blau, and S. Thrun. Dermatologist-level classification of skin cancer with deep neural networks. *Nature*, 542 (7639):Article 7639, 2017.

Q. Fan, A. Nummenmaa, T. Witzel, R. Zanzonico, B. Keil, S. Cauley, J. R. Polimeni, D. Tisdall, K. R. A. Van Dijk, R. L. Buckner, V. J. Wedeen, B. R. Rosen, and L. L. Wald. Investigating the capability to resolve complex white matter structures with high b-value diffusion magnetic resonance imaging on the mgh-usc connectom scanner. *Brain Connectivity*, 4(9):718–726, 2014.

F. V. Farahani, W. Karwowski, and N. R. Lighthall. Application of graph theory for identifying connectivity patterns in human brain networks: A systematic review. *Frontiers in Neuroscience*, 13:585, 2019.

R. Farivar. Dorsal–ventral integration in object recognition. *Brain Research Reviews*, 61 (2):144–153, 2009.

O. Faust, Y. Hagiwara, T. J. Hong, O. S. Lih, and U. R. Acharya. Deep learning for healthcare applications based on physiological signals: A review. *Computer Methods and Programs in Biomedicine*, 161:1–13, 2018.

H. M. Fayek, M. Lech, and L. Cavedon. Evaluating deep learning architectures for speech emotion recognition. *Neural Networks*, 92:60–68, 2017.

L. M. J. Fernandez and A. Lüthi. Sleep spindles: Mechanisms and functions. *Physiological Reviews*, 100(2):805–868, 2020.

R. Ferrucci, F. Cortese, M. Bianchi, D. Pittera, R. Turrone, T. Bocci, B. Borroni, M. Vergari, F. Cogiamanian, G. Ardolino, A. Di Fonzo, A. Padovani, and A. Priori. Cerebellar and motor cortical transcranial stimulation decrease levodopa-induced dyskinesias in parkinson's disease. *Cerebellum (London, England)*, 15(1):43–47, 2016.

R. Ferrucci, F. Cortese, M. Bianchi, D. Pittera, R. Turrone, T. Bocci, B. Borroni, M. Vergari, F. Cogiamanian, G. Ardolino, A. Di Fonzo, A. Padovani, and A. Priori. Examining and modulating neural circuits in psychiatric disorders with transcranial magnetic stimulation and electroencephalography: Present practices and future developments. *The American Journal of Psychiatry*, 178(5):400–413, 2021.

A. Fertonani, C. Pirulli, and C. Miniussi. Random noise stimulation improves neuroplasticity in perceptual learning. *The Journal of Neuroscience: The Official Journal of the Society for Neuroscience*, 31(43):15416–15423, 2011.

M. Feurra, G. Bianco, E. Santarnecchi, M. Del Testa, A. Rossi, and S. Rossi. Frequency-dependent tuning of the human motor system induced by transcranial oscillatory potentials. *Journal of Neuroscience*, 2011.

M. Fiene, B. C. Schwab, J. Misselhorn, C. S. Herrmann, T. R. Schneider, and A. K. Engel. Phase-specific manipulation of rhythmic brain activity by transcranial alternating current stimulation. *Brain Stimulation*, 13(5):1254–1262, 2020.

A. Fiske and K. Holmboe. Neural substrates of early executive function development. *Developmental Review*, 52:42–62, 2019.

A. Fiske, P. Henningsen, and A. Buyx. Your robot therapist will see you now: Ethical implications of embodied artificial intelligence in psychiatry, psychology, and psychotherapy. *Journal of Medical Internet Research*, 21(5):e13216, 2019.

A. Fornito, A. Zalesky, and M. Breakspear. Graph analysis of the human connectome: Promise, progress, and pitfalls. *NeuroImage*, 80:426–444, 2013.

A. Fornito, A. Zalesky, and M. Breakspear. The connectomics of brain disorders. *Nature Reviews Neuroscience*, 16(3):159–172, 2015.

M. D. Fox, A. Z. Snyder, J. L. Vincent, M. Corbetta, D. C. Van Essen, and M. E. Raichle. The human brain is intrinsically organized into dynamic, anticorrelated functional networks. *Proceedings of the National Academy of Sciences*, 102(27):9673–9678, 2005.

S. Fresnoza, M. Christova, T. Feil, E. Gallasch, C. Körner, U. Zimmer, and A. Ischebeck. The effects of transcranial alternating current stimulation (tacs) at individual alpha peak frequency (iapf) on motor cortex excitability in young and elderly adults. *Experimental Brain Research*, 236(10):2573–2588, 2018.

P. Frezzotti, A. Giorgio, I. Motolese, A. De Leucio, M. Iester, E. Motolese, A. Federico, and N. De Stefano. Structural and functional brain changes beyond visual system in patients with advanced glaucoma. *PLoS ONE*, 9(8):e105931, 2014.

A. D. Friederici, N. Chomsky, R. C. Berwick, A. Moro, and J. J. Bolhuis. Language, mind and brain. *Nature Human Behaviour*, 1(10):Article 10, 2017.

B. Fritsch, J. Reis, K. Martinowich, H. M. Schambra, Y. Ji, L. G. Cohen, and B. Lu. Direct current stimulation promotes bdnf-dependent synaptic plasticity: Potential implications for motor learning. *Neuron*, 66(2):198–204, 2010.

F. Fröhlich, K. K. Sellers, and A. L. Cordle. Targeting the neurophysiology of cognitive systems with transcranial alternating current stimulation (tacs). *Expert Review of Neurotherapeutics*, 15(2):145–167, 2015.

C. Gall, S. Sgorzaly, S. Schmidt, S. Brandt, A. Fedorov, and B. A. Sabel. Noninvasive transorbital alternating current stimulation improves subjective visual functioning and vision-related quality of life in optic neuropathy. *Brain Stimulation*, 4(4):175–188, 2011.

C. Gall, S. Schmidt, M. P. Schittkowski, A. Antal, G. G. Ambrus, W. Paulus, M. Dannhauer, R. Michalik, A. Mante, M. Bola, A. Lux, S. Kropf, S. A. Brandt, and B. A. Sabel. Alternating current stimulation for vision restoration after optic nerve damage: A randomized clinical trial. *PLoS ONE*, 11(6), 2016.

C. L. Gallen and M. D'Esposito. Brain modularity: A biomarker of intervention-related plasticity. *Trends in Cognitive Sciences*, 23(4):293–304, 2019.

C. D. Gilbert and W. Li. Top-down influences on visual processing. *Nature Reviews Neuroscience*, 14(5):350–363, 2013.

C. D. Gilbert and T. N. Wiesel. Receptive field dynamics in adult primary visual cortex. *Nature*, 356(6365):150–152, 1992.

M. F. Glasser, T. S. Coalson, E. C. Robinson, C. D. Hacker, J. Harwell, E. Yacoub, K. Ugurbil, J. Andersson, C. F. Beckmann, M. Jenkinson, S. M. Smith, and D. C. Van Essen. A multi-modal parcellation of human cerebral cortex. *Nature*, 536(7615): 171–178, 2016.

A.-L. Goddings, D. Roalf, C. Lebel, and C. K. Tamnes. Development of white matter microstructure and executive functions during childhood and adolescence: A review of diffusion mri studies. *Developmental Cognitive Neuroscience*, 51:101008, 2021.

C. M. Gorick, V. R. Breza, K. M. Nowak, V. W. T. Cheng, D. G. Fisher, A. C. Debski, M. R. Hoch, Z. E. F. Demir, N. M. Tran, M. R. Schwartz, N. D. Sheybani, and R. J. Price. Applications of focused ultrasound-mediated blood-brain barrier opening. *Advanced Drug Delivery Reviews*, 191:114583, 2022.

A. Gramfort, T. Papadopoulo, E. Olivi, and M. Clerc. Openmeeg: Opensource software for quasistatic bioelectromagnetics. *BioMedical Engineering Online*, 9, 2010.

F. Grassmann, J. Mengelkamp, C. Brandl, S. Harsch, M. E. Zimmermann, B. Linkohr, A. Peters, I. M. Heid, C. Palm, and B. H. F. Weber. A deep learning algorithm for prediction of age-related eye disease study severity scale for age-related macular degeneration from color fundus photography. *Ophthalmology*, 125(9):1410–1420, 2018.

M. D. Greicius, G. Srivastava, A. L. Reiss, and V. Menon. Default-mode network activity distinguishes alzheimer's disease from healthy aging: Evidence from functional mri. *Proceedings of the National Academy of Sciences of the United States of America*, 101 (13):4637–4642, 2004.

A. Griffa, P. S. Baumann, J.-P. Thiran, and P. Hagmann. Structural connectomics in brain diseases. *NeuroImage*, 80:515–526, 2013.

A. Grzybowski, P. Brona, G. Lim, P. Ruamviboonsuk, G. S. W. Tan, M. Abramoff, and D. S. W. Ting. Artificial intelligence for diabetic retinopathy screening: A review. *Eye*, 34(3):451–460, 2020.

M. Guidetti, S. Marceglia, A. Loh, I. E. Harmsen, S. Meoni, G. Foffani, A. M. Lozano, E. Moro, J. Volkmann, and A. Priori. Clinical perspectives of adaptive deep brain stimulation. *Brain Stimulation*, 14(5):1238–1247, 2021.

V. Gulshan, L. Peng, M. Coram, M. C. Stumpe, D. Wu, A. Narayanaswamy, S. Venugopalan, K. Widner, T. Madams, J. Cuadros, R. Kim, R. Raman, P. C. Nelson, J. L. Mega, and D. R. Webster. Development and validation of a deep learning algorithm for detection of diabetic retinopathy in retinal fundus photographs. *JAMA*, 316(22): 2402–2410, 2016.

J. G. V. Habets, M. Heijmans, M. L. Kuijf, M. L. F. Janssen, Y. Temel, and P. L. Kubben. An update on adaptive deep brain stimulation in parkinson's disease. *Movement Disorders: Official Journal of the Movement Disorder Society*, 33(12):1834–1843, 2018.

S. Haegens, B. F. Händel, and O. Jensen. Top-down controlled alpha band activity in somatosensory areas determines behavioral performance in a discrimination task. *Journal of Neuroscience*, 31(14):5197–5204, 2011.

M. Hallett. Transcranial magnetic stimulation: A primer. *Neuron*, 55(2):187–199, 2007.

H. Hallez, B. Vanrumste, R. Grech, J. Muscat, W. De Clercq, A. Vergult, Y. D'Asseler, K. P. Camilleri, S. G. Fabri, S. Van Huffel, and I. Lemahieu. Review on solving the forward problem in eeg source analysis. *Journal of NeuroEngineering and Rehabilitation*, 4, 2007.

J. E. D. Han, X. Liu, C. Bunce, A. Douiri, L. Vale, A. Blandford, J. Lawrenson, R. Hussain, G. Grimaldi, A. E. Learoyd, A. Kernohan, C. Dinah, E. Minos, D. Sim, T. Aslam, P. J. Patel, A. K. Denniston, P. A. Keane, and K. Balaskas. Teleophthalmology-enabled and artificial intelligence-ready referral pathway for community optometry referrals of retinal disease (hermes): A cluster randomised superiority trial with a linked diagnostic accuracy study—hermes study report 1—study protocol. *BMJ Open*, 12(2):e055845, 2022.

Y. Hao, H. M. Khoo, N. von Ellenrieder, N. Zazubovits, and J. Gotman. Deepied: An epileptic discharge detector for eeg-fmri based on deep learning. *NeuroImage: Clinical*, 17:962–975, 2017.

J. R. Harrison, S. Bhatia, Z. X. Tan, A. Mirza-Davies, H. Benkert, C. M. W. Tax, and D. K. Jones. Imaging alzheimer's genetic risk using diffusion mri: A systematic review. *NeuroImage: Clinical*, 27:102359, 2020.

D. Haslacher, K. Nasr, S. E. Robinson, C. Braun, and S. R. Soekadar. Stimulation artifact source separation (sass) for assessing electric brain oscillations during transcranial alternating current stimulation (tacs). *NeuroImage*, 228:117571, 2021.

D. Haslacher, A. Narang, A. Cavallo, K. Nasr, E. Santarnecchi, and S. R. Soekadar. In-vivo phase-dependent enhancement and suppression of brain oscillations by transcranial alternating current stimulation (tacs). *Neuroscience*, 2022.

M. N. Hebart, B. B. Bankson, A. Harel, C. I. Baker, and R. M. Cichy. The representational dynamics of task and object processing in humans. *eLife*, 7, 2018.

R. F. Helfrich, T. R. Schneider, S. Rach, S. A. Trautmann-Lengsfeld, A. K. Engel, and C. S. Herrmann. Entrainment of brain oscillations by transcranial alternating current stimulation. *Current Biology*, 2014.

G. Herbet and H. Duffau. Revisiting the functional anatomy of the human brain: Toward a meta-networking theory of cerebral functions. *Physiological Reviews*, 100(3):1181–1228, 2020.

C. S. Herrmann, D. Strüber, R. F. Helfrich, and A. K. Engel. Transcranial alternating current stimulation: A review of the underlying mechanisms and modulation of cognitive processes. *Frontiers in Human Neuroscience*, 7, 2013.

C. S. Herrmann, D. Strüber, R. F. Helfrich, and A. K. Engel. Eeg oscillations: From correlation to causality. *International Journal of Psychophysiology: Official Journal of the International Organization of Psychophysiology*, 103:12–21, 2016.

D. G. C. Hildebrand, M. Cicconet, R. M. Torres, W. Choi, T. M. Quan, J. Moon, A. W. Wetzel, A. Scott Champion, B. J. Graham, O. Randlett, G. S. Plummer, R. Portugues, I. H. Bianco, S. Saalfeld, A. D. Baden, K. Lillaney, R. Burns, J. T. Vogelstein, A. F. Schier, and F. Engert. Whole-brain serial-section electron microscopy in larval zebrafish. *Nature*, 545(7654):Article 7654, 2017.

A. T. Hill, P. B. Fitzgerald, and K. E. Hoy. Effects of anodal transcranial direct current stimulation on working memory: A systematic review and meta-analysis of findings from healthy and neuropsychiatric populations. *Brain Stimulation*, 9(2):197–208, 2016.

S. Hochreiter and J. Schmidhuber. Long short-term memory. *Neural Computation*, 9(8): 1735–1780, 1997.

D. C. Hood, S. La Bruna, E. Tsamis, K. A. Thakoor, A. Rai, A. Leshno, C. G. V. de Moraes, G. A. Cioffi, and J. M. Liebmann. Detecting glaucoma with only oct: Implications for the clinic, research, screening, and ai development. *Progress in Retinal and Eye Research*, 90:101052, 2022.

J. B. Hopfinger, J. Parsons, and F. Fröhlich. Differential effects of 10-hz and 40-hz transcranial alternating current stimulation (tacs) on endogenous versus exogenous attention. *Cognitive Neuroscience*, 8(2):102–111, 2017.

M. S. Hossain and G. Muhammad. Emotion recognition using deep learning approach from audio–visual emotional big data. *Information Fusion*, 49:69–78, 2019.

S. Y. Huang, Q. Fan, N. Machado, A. Eloyan, J. D. Bireley, A. W. Russo, S. M. Tobyne, K. R. Patel, K. Brewer, S. F. Rapaport, A. Nummenmaa, T. Witzel, J. C. Sherman, L. L. Wald, and E. C. Klawiter. Corpus callosum axon diameter relates to cognitive impairment in multiple sclerosis. *Annals of Clinical and Translational Neurology*, 6(5): 882–892, 2019.

C. J. Huggins, J. Escudero, M. A. Parra, B. Scally, R. Anghinah, A. Vitória Lacerda De Araújo, L. F. Basile, and D. Abasolo. Deep learning of resting-state electroencephalogram signals for three-class classification of alzheimer's disease, mild cognitive impairment and healthy ageing. *Journal of Neural Engineering*, 18(4), 2021.

T. T. Høye, J. Ärje, K. Bjerge, O. L. P. Hansen, A. Iosifidis, F. Leese, H. M. R. Mann, K. Meissner, C. Melvad, and J. Raitoharju. Deep learning and computer vision will transform entomology. *Proceedings of the National Academy of Sciences of the United States of America*, 118(2):e2002545117, 2021.

S. Itthipuripat, T. C. Sprague, and J. T. Serences. Functional mri and eeg index complementary attentional modulations. *The Journal of Neuroscience: The Official Journal of the Society for Neuroscience*, 39(31):6162–6179, 2019.

S. Iwaki and S. Ueno. Weighted minimum-norm source estimation of magnetoencephalography utilizing the temporal information of the measured data. *Journal of Applied Physics*, 83(11):6441–6443, 1998.

W. Jamal, S. Das, K. Maharatna, I. Pan, and D. Kuyucu. Brain connectivity analysis from eeg signals using stable phase-synchronized states during face perception tasks. *Physica A: Statistical Mechanics and Its Applications*, 434:273–295, 2015.

N. Jaušovec, K. Jaušovec, and A. Pahor. The influence of theta transcranial alternating current stimulation (tacs) on working memory storage and processing functions. *Acta Psychologica*, 146:1–6, 2014.

B. Jeurissen, M. Descoteaux, S. Mori, and A. Leemans. Diffusion mri fiber tractography of the brain. *NMR in Biomedicine*, 32(4):e3785, 2019.

L. Jiang, X. Sun, F. Mercaldo, and A. Santone. Decab-lstm: Deep contextualized attentional bidirectional lstm for cancer hallmark classification. *Knowledge-Based Systems*, 210:106486, 2020.

M. E. Johansson, I. G. M. Cameron, N. M. Van der Kolk, N. M. de Vries, E. Klimars, I. Toni, B. R. Bloem, and R. C. Helmich. Aerobic exercise alters brain function and structure in parkinson's disease: A randomized controlled trial. *Annals of Neurology*, 91(2):203–216, 2022.

K. W. Johnson, S. J. Torres, B. S. Glicksberg, K. Shameer, R. Miotto, M. Ali, E. Ashley, and J. T. Dudley. Artificial intelligence in cardiology. *Journal of the American College of Cardiology*, 71(23):2668–2679, 2018.

D. K. Jones, D. C. Alexander, R. Bowtell, M. Cercignani, F. Dell'Acqua, D. J. McHugh, K. L. Miller, M. Palombo, G. J. M. Parker, U. S. Rudrapatna, and C. M. W. Tax. Microstructural imaging of the human brain with a 'super-scanner': 10 key advantages of ultra-strong gradients for diffusion mri. *NeuroImage*, 182:8–38, 2018.

A. Kammen, M. Law, B. S. Tjan, A. W. Toga, and Y. Shi. Automated retinofugal visual pathway reconstruction with multi-shell hardi and fod-based analysis. *NeuroImage*, 125: 767–779, 2016.

N. Kang, J. J. Summers, and J. H. Cauraugh. Transcranial direct current stimulation facilitates motor learning post-stroke: A systematic review and meta-analysis. *Journal of Neurology, Neurosurgery, and Psychiatry*, 87(4):345–355, 2016.

N. Karamzadeh, A. Medvedev, A. Azari, A. Gandjbakhche, and L. Najafizadeh. Capturing dynamic patterns of task-based functional connectivity with eeg. *NeuroImage*, 66: 311–317, 2013.

E. Kasten, S. Wüst, W. Behrens-Baumann, and B. A. Sabel. Computer-based training for the treatment of partial blindness. *Nature Medicine*, 4(9):1083–1087, 1998.

F. H. Kasten, J. Dowsett, and C. S. Herrmann. Sustained aftereffect of α-tacs lasts up to 70 min after stimulation. *Frontiers in Human Neuroscience*, 10:245, 2016.

A. S. Khakhalin. Graph analysis of looming-selective networks in the tectum, and its replication in a simple computational model. *Neuroscience*, 2019.

M. S. Khan, N. Salsabil, M. G. R. Alam, M. A. A. Dewan, and M. Z. Uddin. Cnn-xgboost fusion-based affective state recognition using eeg spectrogram image analysis. *Scientific Reports*, 12(1):14122, 2022.

M.-J. Kim, Y. C. Youn, and J. Paik. Deep learning-based eeg analysis to classify normal, mild cognitive impairment, and dementia: Algorithms and dataset. *NeuroImage*, 272: 120054, 2023.

M. G. Kitzbichler, R. N. A. Henson, M. L. Smith, P. J. Nathan, and E. T. Bullmore. Cognitive effort drives workspace configuration of human brain functional networks. *Journal of Neuroscience*, 31(22):8259–8270, 2011.

A. Klimovich-Gray, L. K. Tyler, B. Randall, E. Kocagoncu, B. Devereux, and W. D. Marslen-Wilson. Balancing prediction and sensory input in speech comprehension: The spatiotemporal dynamics of word recognition in context. *Journal of Neuroscience*, 39 (3):519–527, 2019.

V. Krishna, F. Sammartino, and A. Rezai. A review of the current therapies, challenges, and future directions of transcranial focused ultrasound technology: Advances in diagnosis and treatment. *JAMA Neurology*, 75(2):246–254, 2018.

A. Krizhevsky, I. Sutskever, and G. E. Hinton. Imagenet classification with deep convolutional neural networks. In *Advances in Neural Information Processing Systems*, volume 25, 2012.

K. Kusunose, T. Abe, A. Haga, D. Fukuda, H. Yamada, M. Harada, and M. Sata. A deep learning approach for assessment of regional wall motion abnormality from echocardiographic images. *Cardiovascular Imaging*, 13(2_Part_1):374–381, 2020.

J. P. Lachaux, E. Rodriguez, J. Martinerie, and F. J. Varela. Measuring phase synchrony in brain signals. *Human Brain Mapping*, 8(4):194–208, 1999.

B. Laczó, A. Antal, R. Niebergall, S. Treue, and W. Paulus. Transcranial alternating stimulation in a high gamma frequency range applied over v1 improves contrast perception but does not modulate spatial attention. *Brain Stimulation*, 5(4):484–491, 2012.

B. Lampinen, J. Lätt, J. Wasselius, D. van Westen, and M. Nilsson. Time dependence in diffusion mri predicts tissue outcome in ischemic stroke patients. *Magnetic Resonance in Medicine*, 86(2):754–764, 2021.

A. Lancichinetti and S. Fortunato. Community detection algorithms: A comparative analysis. *Physical Review E - Statistical, Nonlinear, and Soft Matter Physics*, 80(5), 2009.

K. Lankinen, J. Saari, Y. Hlushchuk, P. Tikka, L. Parkkonen, R. Hari, and M. Koskinen. Consistency and similarity of meg- and fmri-signal time courses during movie viewing. *NeuroImage*, 173:361–369, 2018.

S. Laurence and D. G. Stein. Recovery after brain damage and the concept of localization of function. In *Recovery from Brain Damage*, pages 369–407. Springer US, 1978.

A. Lavric and P. Valentin. Keratodetect: Keratoconus detection algorithm using convolutional neural networks. *Computational Intelligence and Neuroscience*, 2019, 2019.

M. Le, V. Quyen, J. Foucher, J.-P. Lachaux, E. Rodriguez, A. Lutz, J. Martinerie, and F. J. Varela. Comparison of hilbert transform and wavelet methods for the analysis of neuronal synchrony. *Journal of Neuroscience Methods*, 111:83–98, 2001.

Y. LeCun, Y. Bengio, and G. Hinton. Deep learning. *Nature*, 521(7553):436–444, 2015.

H. Lee, G. V. Simpson, N. K. Logothetis, and G. Rainer. Phase locking of single neuron activity to theta oscillations during working memory in monkey extrastriate visual cortex. *Neuron*, 45(1):147–156, 2005.

W.-C. A. Lee, V. Bonin, M. Reed, B. J. Graham, G. Hood, K. Glattfelder, and R. C. Reid. Anatomy and function of an excitatory network in the visual cortex. *Nature*, 532 (7599), 2016.

J. León, J. J. Escobar, A. Ortiz, J. Ortega, J. González, P. Martín-Smith, J. Q. Gan, and M. Damas. Deep learning for eeg-based motor imagery classification: Accuracy-cost trade-off. *PLOS ONE*, 15(6):e0234178, 2020.

F. Li, Y. Su, F. Lin, Z. Li, Y. Song, S. Nie, J. Xu, L. Chen, S. Chen, H. Li, K. Xue, H. Che, Z. Chen, B. Yang, H. Zhang, M. Ge, W. Zhong, C. Yang, L. Chen, and X. Zhang. A deep-learning system predicts glaucoma incidence and progression using retinal photographs. *Journal of Clinical Investigation*, 132(11):e157968, 2022.

J.-P. O. Li, H. Liu, D. S. J. Ting, S. Jeon, R. V. P. Chan, J. E. Kim, D. A. Sim, P. B. M. Thomas, H. Lin, Y. Chen, T. Sakomoto, A. Loewenstein, D. S. C. Lam, L. R. Pasquale, T. Y. Wong, L. A. Lam, and D. S. W. Ting. Digital technology, tele-medicine and artificial intelligence in ophthalmology: A global perspective. *Progress in Retinal and Eye Research*, 82:100900, 2021.

W. Li, B. D. Ward, X. Liu, G. Chen, J. L. Jones, P. G. Antuono, S. J. Li, and J. S. Goveas. Disrupted small world topology and modular organisation of functional networks in late-life depression with and without amnestic mild cognitive impairment. *Journal of Neurology, Neurosurgery and Psychiatry*, 86(10):1097–1105, 2015.

W. Li, X. Lin, and X. Chen. Detecting alzheimer's disease based on 4d fmri: An exploration under deep learning framework. *Neurocomputing*, 388:280–287, 2020.

E. Lin, C.-H. Lin, and H.-Y. Lane. Deep learning with neuroimaging and genomics in alzheimer's disease. *International Journal of Molecular Sciences*, 22(15):7911, 2021.

A. Lipka, E. Niess, A. Dal-Bianco, G. J. Hangel, P. S. Rommer, B. Strasser, S. Motyka, L. Hingerl, T. Berger, P. Hnilicová, E. Kantorová, F. Leutmezer, E. Kurča, S. Gruber, S. Trattnig, and W. Bogner. Lesion-specific metabolic alterations in relapsing-remitting multiple sclerosis via 7 t magnetic resonance spectroscopic imaging. *Investigative Radiology*, 58(2):156–165, 2023.

H. Liu, L. Li, I. M. Wormstone, C. Qiao, C. Zhang, P. Liu, S. Li, H. Wang, D. Mou, R. Pang, D. Yang, L. M. Zangwill, S. Moghimi, H. Hou, C. Bowd, L. Jiang, Y. Chen, M. Hu, Y. Xu, and N. Wang. Development and validation of a deep learning system to detect glaucomatous optic neuropathy using fundus photographs. *JAMA Ophthalmology*, 137(12):1353–1360, 2019.

M. Liu, F. Li, H. Yan, K. Wang, Y. Ma, A. D. N. Initiative, L. Shen, and M. Xu. A multi-model deep convolutional neural network for automatic hippocampus segmentation and classification in alzheimer's disease. *NeuroImage*, 208:116459, 2020.

M. Lobier, J. M. Palva, and S. Palva. High-alpha band synchronization across frontal, parietal and visual cortex mediates behavioral and neuronal effects of visuospatial attention. *NeuroImage*, 165:222–237, 2018.

F. Lopez-Jimenez, Z. Attia, A. M. Arruda-Olson, R. Carter, P. Chareonthaitawee, H. Jouni, S. Kapa, A. Lerman, C. Luong, J. R. Medina-Inojosa, P. A. Noseworthy, P. A. Pellikka, M. M. Redfield, V. L. Roger, G. S. Sandhu, C. Senecal, and P. A. Friedman. Artificial intelligence in cardiology: Present and future. *Mayo Clinic Proceedings*, 95(5):1015–1039, 2020.

M. Y. Lu, T. Y. Chen, D. F. K. Williamson, M. Zhao, M. Shady, J. Lipkova, and F. Mahmood. Ai-based pathology predicts origins for cancers of unknown primary. *Nature*, 594 (7861):7861, 2021.

K. Luedtke, A. Rushton, C. Wright, T. Jürgens, A. Polzer, G. Mueller, and A. May. Effectiveness of transcranial direct current stimulation preceding cognitive behavioural management for chronic low back pain: Sham controlled double blinded randomised controlled trial. *BMJ (Clinical Research Ed.)*, 350:h1640, 2015.

S. Luo, Q. Rabbani, and N. E. Crone. Brain-computer interface: Applications to speech decoding and synthesis to augment communication. *Neurotherapeutics: The Journal of the American Society for Experimental NeuroTherapeutics*, 19(1):263–273, 2022.

M.-E. Lynall, D. S. Bassett, R. Kerwin, P. J. McKenna, M. Kitzbichler, U. Muller, and E. Bullmore. Functional connectivity and brain networks in schizophrenia. *Journal of Neuroscience*, 30(28):9477–9487, 2010.

D. Mantini, M. G. Perrucci, C. Del Gratta, G. L. Romani, and M. Corbetta. Electrophysiological signatures of resting state networks in the human brain. *Proceedings of the*

National Academy of Sciences of the United States of America, 104(32):13170–13175, 2007.

P. Marangolo, V. Fiori, S. Campana, M. A. Calpagnano, C. Razzano, C. Caltagirone, and A. Marini. Something to talk about: enhancement of linguistic cohesion through tdcs in chronic non fluent aphasia. *Neuropsychologia*, 53:246–256, 2014.

E. Maris and R. Oostenveld. Nonparametric statistical testing of eeg- and meg-data. *Journal of Neuroscience Methods*, 164(1):177–190, 2007.

E. H. Martínez-Lapiscina, S. Ortiz-Pérez, E. Fraga-Pumar, E. Martínez-Heras, I. Gabilondo, S. Llufriu, S. Bullich, M. Figueras, A. Saiz, B. Sánchez-Dalmau, and P. Villoslada. Colour vision impairment is associated with disease severity in multiple sclerosis. *Multiple Sclerosis Journal*, 20(9):1207–1216, 2014.

D. Maurer, T. L. Lewis, and C. J. Mondloch. Missing sights: consequences for visual cognitive development. *Trends in cognitive sciences*, 9(3):144–151, 2005.

K. McKenna, D. M. Cooke, J. Fleming, A. Jefferson, and S. Ogden. The incidence of visual perceptual impairment in patients with severe traumatic brain injury. *Brain Injury*, 20 (5):507–518, 2006.

J. A. McNab, B. L. Edlow, T. Witzel, S. Y. Huang, H. Bhat, K. Heberlein, T. Feiweier, K. Liu, B. Keil, J. Cohen-Adad, M. D. Tisdall, R. D. Folkerth, H. C. Kinney, and L. L. Wald. The human connectome project and beyond: Initial applications of 300mt/m gradients. *NeuroImage*, 80:234–245, 2013.

F. A. Medeiros, L. M. Zangwill, C. Bowd, R. M. Vessani, R. Susanna, and R. N. Weinreb. Evaluation of retinal nerve fiber layer, optic nerve head, and macular thickness measurements for glaucoma detection using optical coherence tomography. *American Journal of Ophthalmology*, 139(1):44–55, 2005.

O. Meiron and M. Lavidor. Prefrontal oscillatory stimulation modulates access to cognitive control references in retrospective metacognitive commentary. *Clinical Neurophysiology: Official Journal of the International Federation of Clinical Neurophysiology*, 125(1):77–82, 2014.

Y. Mekki, V. Guillemot, H. Lemaître, A. Carrión-Castillo, S. Forkel, V. Frouin, and C. Philippe. The genetic architecture of language functional connectivity. *NeuroImage*, 249:118795, 2022.

M. J. Mentis, V. Dhawan, T. Nakamura, M. F. Ghilardi, A. Feigin, C. Edwards, C. Ghez, and D. Eidelberg. Enhancement of brain activation during trial-and-error sequence learning in early pd. *Neurology*, 60(4):612–619, 2003.

T. Merk, V. Peterson, R. Köhler, S. Haufe, R. M. Richardson, and W.-J. Neumann. Machine learning based brain signal decoding for intelligent adaptive deep brain stimulation. *Experimental Neurology*, 351:113993, 2022.

R. Messina, M. Rocca, S. B. Marzoli, M. Petrolini, I. Milesi, F. Darvizeh, F. Bandello, G. Comi, A. Falini, and M. Filippi. Regional patterns of brain gray and white matter abnormalities in patients with hereditary optic neuropathies: Dominant optic atrophy vs leber hereditary optic neuropathy (s48. 006), 2016.

C. K. Milton, V. Dhanaraj, I. M. Young, H. M. Taylor, P. J. Nicholas, R. G. Briggs, M. Y. Bai, R. D. Fonseka, J. Hormovas, Y.-H. Lin, O. Tanglay, A. K. Conner, C. A. Glenn, C. Teo, S. Doyen, and M. E. Sughrue. Parcellation-based anatomic model of the semantic network. *Brain and Behavior*, 11(4):e02065, 2021.

M. Mishkin and L. G. Ungerleider. Contribution of striate inputs to the visuospatial functions of parieto-preoccipital cortex in monkeys. *Behavioural Brain Research*, 6(1): 57–77, 1982.

F. Moeller, M. Maneshi, F. Pittau, T. Gholipour, P. Bellec, F. Dubeau, C. Grova, and J. Gotman. Functional connectivity in patients with idiopathic generalized epilepsy. *Epilepsia*, 52(3):515–522, 2011.

J. Moll, R. Zahn, R. de Oliveira-Souza, F. Krueger, and J. Grafman. The neural basis of human moral cognition. *Nature Reviews Neuroscience*, 6(10):799–809, 2005.

C. Monakow. *Die lokalisation im grosshirn und der abbau der funktion durch kortikale herde*. 1914.

S. Monteith, T. Glenn, J. Geddes, P. C. Whybrow, E. Achtyes, and M. Bauer. Expectations for artificial intelligence (ai) in psychiatry. *Current Psychiatry Reports*, 24(11):709–721, 2022.

E. A. Mosilhy, E. E. Alshial, M. M. Eltaras, M. M. A. Rahman, H. I. Helmy, A. H. Elazoul, O. Hamdy, and H. S. Mohammed. Non-invasive transcranial brain modulation for neurological disorders treatment: A narrative review. *Life Sciences*, 307:120869, 2022.

P. J. Mucha, T. Richardson, K. Macon, M. A. Porter, and J. P. Onnela. Community structure in time-dependent, multiscale, and multiplex networks. *Science*, 328(5980): 876–878, 2010.

T. Mussigmann, B. Bardel, and J.-P. Lefaucheur. Resting-state electroencephalography (eeg) biomarkers of chronic neuropathic pain. a systematic review. *NeuroImage*, 258: 119351, 2022.

N. Nasrullah, J. Sang, M. S. Alam, M. Mateen, B. Cai, and H. Hu. Automated lung nodule detection and classification using deep learning combined with multiple strategies. *Sensors (Basel, Switzerland)*, 19(17):3722, 2019.

T. Neuling, S. Rach, and C. S. Herrmann. Orchestrating neuronal networks: Sustained after-effects of transcranial alternating current stimulation depend upon brain states. *Frontiers in Human Neuroscience*, 7:161, 2013.

M. E. J. Newman. The structure and function of complex networks. *SIAM Review*, 45(2): 167–256, 2003.

M. E. J. Newman. Communities, modules and large-scale structure in networks. *Nature Physics*, 8(1):25–31, 2012.

M. E. J. Newman and M. Girvan. Finding and evaluating community structure in networks. *Physical Review E*, 69(2):026113, 2004.

D. Nhu, M. Janmohamed, A. Antonic-Baker, P. Perucca, T. J. O'Brien, A. K. Gilligan, P. Kwan, C. W. Tan, and L. Kuhlmann. Deep learning for automated epileptiform discharge detection from scalp eeg: A systematic review. *Journal of Neural Engineering*, 19(5), 2022.

F. Niess, L. Hingerl, B. Strasser, P. Bednarik, D. Goranovic, E. Niess, G. Hangel, M. Kršňák, B. Spurny-Dworak, T. Scherer, R. Lanzenberger, and W. Bogner. Non-invasive 3-dimensional 1 h-magnetic resonance spectroscopic imaging of human brain glucose and neurotransmitter metabolism using deuterium labeling at 3t: Feasibility and interscanner reproducibility. *Investigative Radiology*, 58(6):431–437, 2023.

M. A. Nitsche and W. Paulus. Excitability changes induced in the human motor cortex by weak transcranial direct current stimulation. *The Journal of Physiology*, 527(Pt 3): 633–639, 2000.

M. B. T. Noor, N. Z. Zenia, M. S. Kaiser, S. A. Mamun, and M. Mahmud. Application of deep learning in detecting neurological disorders from magnetic resonance images: A survey on the detection of alzheimer's disease, parkinson's disease and schizophrenia. *Brain Informatics*, 7(1):11, 2020.

R. Nuzzi, L. Dallorto, and T. Rolle. Changes of visual pathway and brain connectivity in glaucoma: A systematic review. *Frontiers in Neuroscience*, 12:363, 2018.

K. T. E. Olde Dubbelink, A. Hillebrand, D. Stoffers, J. B. Deijen, J. W. R. Twisk, C. J. Stam, and H. W. Berendse. Disrupted brain network topology in parkinson's disease: A longitudinal magnetoencephalography study. *Brain*, 137(1):197–207, 2014.

M. C. Oldham, G. Konopka, K. Iwamoto, P. Langfelder, T. Kato, S. Horvath, and D. H. Geschwind. Functional organization of the transcriptome in human brain. 2008.

A. O'Shea, R. Ahmed, G. Lightbody, E. Pavlidis, R. Lloyd, F. Pisani, W. Marnane, S. Mathieson, G. Boylan, and A. Temko. Deep learning for eeg seizure detection in preterm infants. *International Journal of Neural Systems*, 31(08):2150008, 2021.

V. Paban, J. Modolo, A. Mheich, and M. Hassan. Psychological resilience correlates with eeg source-space brain network flexibility. *Network Neuroscience*, 3(2):539–550, 2019.

E. Paraskevopoulos, C. Dobel, A. Wollbrink, V. Salvari, P. D. Bamidis, and C. Pantev. Maladaptive alterations of resting state cortical network in tinnitus: A directed functional connectivity analysis of a larger meg data set. *Scientific Reports*, 9:15452, 2019.

A. Pascual-Leone, A. Amedi, F. Fregni, and L. B. Merabet. The plastic human brain cortex. *Annu. Rev. Neurosci.*, 28:377–401, 2005.

P. Perconti and A. Plebe. Deep learning and cognitive science. *Cognition*, 203:104365, 2020.

J. B. Pereira, C. Junqué, D. Bartrés-Faz, M. J. Martí, R. Sala-Llonch, Y. Compta, C. Falcón, P. Vendrell, A. Pascual-Leone, J. Valls-Solé, and E. Tolosa. Modulation of verbal fluency networks by transcranial direct current stimulation (tdcs) in parkinson's disease. *Brain Stimulation*, 6(1):16–24, 2013.

C. R. Pernet, M. Latinus, T. E. Nichols, and G. A. Rousselet. Cluster-based computational methods for mass univariate analyses of event-related brain potentials/fields: A simulation study. *Journal of Neuroscience Methods*, 250:85–93, 2015.

A. A. Phillips, F. H. Chan, M. M. Z. Zheng, A. V. Krassioukov, and P. N. Ainslie. Neurovascular coupling in humans: Physiology, methodological advances and clinical implications. *Journal of Cerebral Blood Flow and Metabolism*, 36(4):647–664, 2015.

O. S. Pianykh, G. Langs, M. Dewey, D. R. Enzmann, C. J. Herold, S. O. Schoenberg, and J. A. Brink. Continuous learning ai in radiology: Implementation principles and early applications. *Radiology*, 297(1):6–14, 2020.

P. J. Pickhardt, B. D. Pooler, T. Lauder, A. M. del Rio, R. J. Bruce, and N. Binkley. Opportunistic screening for osteoporosis using abdominal computed tomography scans obtained for other indications. *Annals of Internal Medicine*, 158(8):588–595, 2013.

M. Pievani, W. de Haan, T. Wu, W. W. Seeley, and G. B. Frisoni. Functional network disruption in the degenerative dementias. *The Lancet Neurology*, 10(9):829–843, 2011.

D. A. Poggel, E. Kasten, and B. A. Sabel. Attentional cueing improves vision restoration therapy in patients with visual field defects. *Neurology*, 63(11):2069–2076, 2004.

D. A. Poggel, E. Kasten, E. M. Müller-Oehring, U. Bunzenthal, and B. A. Sabel. Improving residual vision by attentional cueing in patients with brain lesions. *Brain Research*, 1097 (1):142–148, 2006.

D. A. Poggel, E. M. Müller-Oehring, J. Gothe, S. Kenkel, E. Kasten, and B. A. Sabel. Visual hallucinations during spontaneous and training-induced visual field recovery. *Neuropsychologia*, 45(11):2598–2607, 2007.

J. D. Power, A. L. Cohen, S. M. Nelson, G. S. Wig, K. A. Barnes, J. A. Church, A. C. Vogel, T. O. Laumann, F. M. Miezin, B. L. Schlaggar, and S. E. Petersen. Functional network organization of the human brain. *Neuron*, 72(4):665–678, 2011.

L. M. Prevedello, B. S. Erdal, J. L. Ryu, K. J. Little, M. Demirer, S. Qian, and R. D. White. Automated critical test findings identification and online notification system using artificial intelligence in imaging. *Radiology*, 285(3):923–931, 2017.

M. G. Puxeddu, J. Faskowitz, R. F. Betzel, M. Petti, L. Astolfi, and O. Sporns. The modular organization of brain cortical connectivity across the human lifespan. *NeuroImage*, 218:116974, 2020.

H. Quintero, Y. Shiga, N. Belforte, L. Alarcon-Martinez, S. El Hajji, D. Villafranca-Baughman, F. Dotigny, and A. Di Polo. Restoration of mitochondria axonal transport by adaptor disc1 supplementation prevents neurodegeneration and rescues visual function. *Cell Reports*, 40(11):111324, 2022.

T. Radman, R. L. Ramos, J. C. Brumberg, and M. Bikson. Role of cortical cell type and morphology in subthreshold and suprathreshold uniform electric field stimulation in vitro. *Brain Stimulation*, 2(4):215–228.e3, 2009.

M. E. Raichle. The brain's default mode network. *Annual Review of Neuroscience*, 38(1): 433–447, 2015.

A. Raj and Y. H. Chen. The wiring economy principle: Connectivity determines anatomy in the human brain. *PLoS ONE*, 6(9):e14832, 2011.

A. Rajkomar, J. Dean, and I. Kohane. Machine learning in medicine. *New England Journal of Medicine*, 380(14):1347–1358, 2019.

T. G. Rhee, S. R. Shim, B. P. Forester, A. A. Nierenberg, R. S. McIntyre, G. I. Papakostas, J. H. Krystal, G. Sanacora, and S. T. Wilkinson. Efficacy and safety of ketamine vs electroconvulsive therapy among patients with major depressive episode. *JAMA Psychiatry*, 79(12):1162–1172, 2022.

A. W. Rives and T. Galitski. Modular organization of cellular networks. *Proceedings of the National Academy of Sciences of the United States of America*, 100(3):1128–1133, 2003.

M. A. Rocca, S. Bianchi-Marzoli, R. Messina, M. L. Cascavilla, M. Zeviani, C. Lamperti, J. Milesi, A. Carta, G. Cammarata, L. Leocani, E. Lamantea, F. Bandello, G. Comi, A. Falini, and M. Filippi. Distributed abnormalities of brain white matter architecture in patients with dominant optic atrophy and opa1 mutations. *Journal of Neurology*, 262 (5):1216–1227, 2015.

A. Rodán, E. Candela Marroquín, and L. C. Jara García. An updated review about perceptual learning as a treatment for amblyopia. *Journal of Optometry*, 15(1):3–34, 2022.

M. Rohm, V. Tresp, M. Müller, C. Kern, I. Manakov, M. Weiss, D. A. Sim, S. Priglinger, P. A. Keane, and K. Kortuem. Predicting visual acuity by using machine learning in patients treated for neovascular age-related macular degeneration. *Ophthalmology*, 125 (7):1028–1036, 2018.

E. T. Rolls, G. Deco, C.-C. Huang, and J. Feng. The human language effective connectome. *NeuroImage*, 258:119352, 2022.

G. Rompianesi, F. Pegoraro, C. D. Ceresa, R. Montalti, and R. I. Troisi. Artificial intelligence in the diagnosis and management of colorectal cancer liver metastases. *World Journal of Gastroenterology*, 28(1):108–122, 2022.

P. M. Rossini, R. Di Iorio, M. Bentivoglio, G. Bertini, F. Ferreri, C. Gerloff, R. J. Ilmoniemi, F. Miraglia, M. A. Nitsche, F. Pestilli, M. Rosanova, Y. Shirota, C. Tesoriero, Y. Ugawa, F. Vecchio, U. Ziemann, and M. Hallett. Methods for analysis of brain connectivity: An ifcn-sponsored review. *Clinical Neurophysiology*, 130(10):1833–1858, 2019.

J. Royer, B. C. Bernhardt, S. Larivière, E. Gleichgerrcht, B. J. Vorderwülbecke, S. Vulliémoz, and L. Bonilha. Epilepsy and brain network hubs. *Epilepsia*, 63(3): 537–550, 2022.

P. Ruamviboonsuk, J. Krause, P. Chotcomwongse, R. Sayres, R. Raman, K. Widner, B. J. L. Campana, S. Phene, K. Hemarat, M. Tadarati, S. Silpa-Archa, J. Limwattanayingyong, C. Rao, O. Kuruvilla, J. Jung, J. Tan, S. Orprayoon, C. Kangwanwongpaisan,

R. Sukumalpaiboon, and D. R. Webster. Deep learning versus human graders for classifying diabetic retinopathy severity in a nationwide screening program. *Npj Digital Medicine*, 2(1):Article 1, 2019.

M. Rubinov and O. Sporns. Complex network measures of brain connectivity: Uses and interpretations. 2009.

J. D. Rudie, J. A. Brown, D. Beck-Pancer, L. M. Hernandez, E. L. Dennis, P. M. Thompson, S. Y. Bookheimer, and M. Dapretto. Altered functional and structural brain network organization in autism. *NeuroImage: Clinical*, 2(1):79–94, 2013.

B. A. Sabel and J. Gudlin. Vision restoration training for glaucoma. a randomized clinical trial. *JAMA Ophthalmology*, 132:381–389, 2014.

B. A. Sabel, A. B. Fedorov, N. Naue, A. Borrmann, C. Herrmann, and C. Gall. Non-invasive alternating current stimulation improves vision in optic neuropathy. *Restorative Neurology and Neuroscience*, 29(6):493–505, 2011a.

B. A. Sabel, P. Henrich-Noack, A. Fedorov, and C. Gall. Vision restoration after brain and retina damage: The "residual vision activation theory". *Progress in Brain Research*, 192:199–262, 2011b.

B. A. Sabel, J. Flammer, and L. B. Merabet. Residual vision activation and the brain-eye-vascular triad: Dysregulation, plasticity and restoration in low vision and blindness-a review. *Restorative Neurology and Neuroscience*, 36(6):767–791, 2018.

B. A. Sabel, A. I. A. Hamid, C. Borrmann, O. Speck, and A. Antal. Transorbital alternating current stimulation modifies bold activity in healthy subjects and in a stroke patient with hemianopia: A 7 tesla fmri feasibility study. *International Journal of Psychophysiology*, 2019.

B. A. Sabel, G. Thut, J. Haueisen, P. Henrich-Noack, C. S. Herrmann, A. Hunold, T. Kammer, B. Matteo, E. G. Sergeeva, W. Waleszczyk, and A. Antal. Vision modulation, plasticity and restoration using non-invasive brain stimulation – an ifcn-sponsored review. *Clinical Neurophysiology*, 131(4):887–911, 2020a.

B. A. Sabel, J. Wang, S. Fähse, L. Cárdenas-Morales, and A. Antal. Personality and stress influence vision restoration and recovery in glaucoma and optic neuropathy following alternating current stimulation: Implications for personalized neuromodulation and rehabilitation. *EPMA Journal*, 11(2):177–196, 2020b.

W. Saelens, R. Cannoodt, and Y. Saeys. A comprehensive evaluation of module detection methods for gene expression data. *Nature Communications*, 9(1):1–12, 2018.

F. Salehpour, J. Mahmoudi, F. Kamari, S. Sadigh-Eteghad, S. H. Rasta, and M. R. Hamblin. Brain photobiomodulation therapy: A narrative review. *Molecular Neurobiology*, 55(8):6601–6636, 2018.

C. Sarica, J.-F. Nankoo, A. Fomenko, T. C. Grippe, K. Yamamoto, N. Samuel, V. Milano, A. Vetkas, G. Darmani, M. N. Cizmeci, A. M. Lozano, and R. Chen. Human studies of transcranial ultrasound neuromodulation: A systematic review of effectiveness and safety. *Brain Stimulation*, 15(3):737–746, 2022.

H. Schmidt, A. Gour, J. Straehle, K. M. Boergens, M. Brecht, and M. Helmstaedter. Axonal synapse sorting in medial entorhinal cortex. *Nature*, 549(7673):Article 7673, 2017.

S. Schmidt, A. Mante, M. Rönnefarth, R. Fleischmann, C. Gall, and S. A. Brandt. Progressive enhancement of alpha activity and visual function in patients with optic neuropathy: A two-week repeated session alternating current stimulation study. *Brain Stimulation*, 6(1):87–93, 2013.

L. A. Schwarz, K. Miyamichi, X. J. Gao, K. T. Beier, B. Weissbourd, K. E. DeLoach, J. Ren, S. Ibanes, R. C. Malenka, E. J. Kremer, and L. Luo. Viral-genetic tracing of the input–output organization of a central noradrenaline circuit. *Nature*, 524(7563):Article 7563, 2015.

F. Sepehrband, D. C. Alexander, N. D. Kurniawan, D. C. Reutens, and Z. Yang. Towards higher sensitivity and stability of axon diameter estimation with diffusion-weighted mri. *NMR in Biomedicine*, 29(3):293–308, 2016.

D. J. Shin, W. H. Jung, Y. He, J. Wang, G. Shim, M. S. Byun, J. H. Jang, S. N. Kim, T. Y. Lee, H. Y. Park, and J. S. Kwon. The effects of pharmacological treatment on functional brain connectome in obsessive-compulsive disorder. *Biological Psychiatry*, 75 (8):606–614, 2014.

N. Shu, Y. Liu, J. Li, Y. Li, C. Yu, and T. Jiang. Altered anatomical network in early blindness revealed by diffusion tensor tractography. *PLoS ONE*, 4(9), 2009.

H. A. Shurtleff, A. Poliakov, D. Barry, J. N. Wright, M. H. Warner, E. J. Novotny, A. Marashly, R. Buckley, H. E. Goldstein, J. S. Hauptman, J. G. Ojemann, and D. W. W. Shaw. A clinically applicable functional mri memory paradigm for use with pediatric patients. *Epilepsy & Behavior: E&B*, 126:108461, 2022.

C. Simon, D. A. E. Bolton, N. C. Kennedy, S. R. Soekadar, and K. L. Ruddy. Challenges and opportunities for the future of brain-computer interface in neurorehabilitation. *Frontiers in Neuroscience*, 15, 2021.

W. Singer. Consciousness and the binding problem. *Annals of the New York Academy of Sciences*, 929(1):123–146, 2006.

Z. Sjoerds, S. M. Stufflebeam, D. J. Veltman, W. Van den Brink, B. W. J. H. Penninx, and L. Douw. Loss of brain graph network efficiency in alcohol dependence. *Addiction Biology*, 22(2):523–534, 2017.

J. Slater, R. Joober, B. L. Koborsy, S. Mitchell, E. Sahlas, and C. Palmer. Can electroencephalography (eeg) identify adhd subtypes? a systematic review. *Neuroscience and Biobehavioral Reviews*, 139:104752, 2022.

A. Snowball, I. Tachtsidis, T. Popescu, J. Thompson, M. Delazer, L. Zamarian, T. Zhu, and R. Cohen Kadosh. Long-term enhancement of brain function and cognition using cognitive training and brain stimulation. *Current Biology*, 23(11):987–992, 2013.

O. Sporns. Graph theory methods: Applications in brain networks. *Dialogues in Clinical Neuroscience*, 20(2):111–121.

O. Sporns. The human connectome: A complex network. *Annals of the New York Academy of Sciences*, 1224(1):109–125, 2011.

O. Sporns and R. F. Betzel. Modular brain networks. *Annual Review of Psychology*, 67 (1):613–640, 2016.

O. Sporns, G. Tononi, and R. Kötter. The human connectome: A structural description of the human brain. *PLOS Computational Biology*, 1(4):e42, 2005.

O. Sporns, C. J. Honey, and R. Kötter. Identification and classification of hubs in brain networks. *PLoS ONE*, 2(10):e1049, 2007.

V. S. Sreeraj, S. Suhas, R. Parlikar, S. Selvaraj, D. Dinakaran, V. Shivakumar, J. C. Narayanaswamy, and G. Venkatasubramanian. Effect of add-on transcranial alternating current stimulation (tacs) on persistent delusions in schizophrenia. *Psychiatry Research*, 290:113106, 2020.

C. Stam, B. Jones, G. Nolte, M. Breakspear, and P. Scheltens. Small-world networks and functional connectivity in alzheimer's disease. *Cerebral Cortex*, 17(1):92–99, 2006.

C. J. Stam, W. de Haan, A. Daffertshofer, B. F. Jones, I. Manshanden, A. M. van Cappellen van Walsum, T. Montez, J. P. A. Verbunt, J. C. de Munck, B. W. van Dijk, H. W. Berendse, and P. Scheltens. Graph theoretical analysis of magnetoencephalographic functional connectivity in alzheimer's disease. *Brain*, 132(1):213–224, 2009.

D. Standage, C. N. Areshenkoff, J. Y. Nashed, R. Matthew Hutchison, M. Hutchison, D. Heinke, R. S. Menon, S. Everling, and J. P. Gallivan. Dynamic reconfiguration, fragmentation, and integration of whole-brain modular structure across depths of unconsciousness. *Cerebral Cortex*, 30(10):5229–5241, 2020.

I. G. Stiell, G. A. Wells, K. Vandemheen, C. Clement, H. Lesiuk, A. Laupacis, R. D. McKnight, R. Verbeek, R. Brison, D. Cass, M. A. Eisenhauer, G. H. Greenberg, and J. Worthington. The canadian ct head rule for patients with minor head injury. *The Lancet*, 357(9266):1391–1396, 2001.

J. J. Summers, N. Kang, and J. H. Cauraugh. Does transcranial direct current stimulation enhance cognitive and motor functions in the ageing brain? a systematic review and meta-analysis. *Ageing Research Reviews*, 25:42–54, 2016.

W. Sun, Y. Tang, Y. Qiao, X. Ge, M. Mather, J. M. Ringman, Y. Shi, and for Alzheimer's Disease Neuroimaging Initiative. A probabilistic atlas of locus coeruleus pathways to transentorhinal cortex for connectome imaging in alzheimer's disease. *NeuroImage*, 223: 117301, 2020.

L. W. Swanson and J. W. Lichtman. From cajal to connectome and beyond. *Annual Review of Neuroscience*, 39(1):197–216, 2016.

S. Takemura, A. Bharioke, Z. Lu, A. Nern, S. Vitaladevuni, P. K. Rivlin, W. T. Katz, D. J. Olbris, S. M. Plaza, P. Winston, T. Zhao, J. A. Horne, R. D. Fetter, S. Takemura, K. Blazek, L.-A. Chang, O. Ogundeyi, M. A. Saunders, V. Shapiro, and D. B. Chklovskii. A visual motion detection circuit suggested by drosophila connectomics. *Nature*, 500 (7461):7461, 2013.

O. Tanglay, N. B. Dadario, E. H. N. Chong, S. J. Tang, I. M. Young, and M. E. Sughrue. Graph theory measures and their application to neurosurgical eloquence. *Cancers*, 15 (2):556, 2023.

D. B. Terhune, S. Tai, A. Cowey, T. Popescu, and R. Cohen Kadosh. Enhanced cortical excitability in grapheme-color synesthesia and its modulation. *Current Biology*, 21(23): 2006–2009, 2011.

D. Terney, L. Chaieb, V. Moliadze, A. Antal, and W. Paulus. Increasing human brain excitability by transcranial high-frequency random noise stimulation. *Journal of Neuroscience*, 28(52):14147–14155, 2008.

D. S. W. Ting, H. Lin, P. Ruamviboonsuk, T. Y. Wong, and D. A. Sim. Artificial intelligence, the internet of things, and virtual clinics: Ophthalmology at the digital translation forefront. *The Lancet Digital Health*, 2(1):e8–e9, 2020.

G. H. Tison, J. M. Sanchez, B. Ballinger, A. Singh, J. E. Olgin, M. J. Pletcher, E. Vittinghoff, E. S. Lee, S. M. Fan, R. A. Gladstone, C. Mikell, N. Sohoni, J. Hsieh, and G. M. Marcus. Passive detection of atrial fibrillation using a commercially available smartwatch. *JAMA Cardiology*, 3(5):409–416, 2018.

S. Tortora, S. Ghidoni, C. Chisari, S. Micera, and F. Artoni. Deep learning-based bci for gait decoding from eeg with lstm recurrent neural network. *Journal of Neural Engineering*, 17(4):046011, 2020.

P. Tschandl, C. Rosendahl, and H. Kittler. The ham10000 dataset, a large collection of multi-source dermatoscopic images of common pigmented skin lesions. *Scientific Data*, 5(1):Article 1, 2018.

P. Tschandl, N. Codella, B. N. Akay, G. Argenziano, R. P. Braun, H. Cabo, D. Gutman, A. Halpern, B. Helba, R. Hofmann-Wellenhof, A. Lallas, J. Lapins, C. Longo, J. Malvehy, M. A. Marchetti, A. Marghoob, S. Menzies, A. Oakley, J. Paoli, and H. Kittler. Comparison of the accuracy of human readers versus machine-learning algorithms for pigmented skin lesion classification: An open, web-based, international, diagnostic study. *The Lancet Oncology*, 20(7):938–947, 2019.

L. Q. Uddin. Salience processing and insular cortical function and dysfunction. *Nature Reviews Neuroscience*, 16(1):55–61, 2015.

M. P. van den Heuvel and O. Sporns. Network hubs in the human brain. *Trends in Cognitive Sciences*, 17(12):683–696, 2013.

M. P. van den Heuvel, C. J. Stam, M. Boersma, and H. E. Hulshoff Pol. Small-world and scale-free organization of voxel-based resting-state functional connectivity in the human brain. *NeuroImage*, 43(3):528–539, 2008.

R. van Dinteren, M. Arns, M. L. A. Jongsma, and R. P. C. Kessels. P300 development across the lifespan: A systematic review and meta-analysis. *PLoS ONE*, 9(2):e87347, 2014.

E. A. Variano, J. H. McCoy, and H. Lipson. Networks, dynamics, and modularity. *Physical Review Letters*, 92(18):188701, 2004.

L. R. Varshney, B. L. Chen, E. Paniagua, D. H. Hall, and D. B. Chklovskii. Structural properties of the caenorhabditis elegans neuronal network. *PLoS Computational Biology*, 7(2):e1001066, 2011.

D. Vatansever, D. K. Menon, A. E. Manktelow, B. J. Sahakian, and E. A. Stamatakis. Default mode network connectivity during task execution. *NeuroImage*, 122:96–104, 2015.

F. Vecchio, F. Miraglia, and P. Maria Rossini. Connectome: Graph theory application in functional brain network architecture. *Clinical Neurophysiology Practice*, 2:206–213, 2017.

F. Vecchio, F. Miraglia, and P. M. Rossini. Tracking neuronal connectivity from electric brain signals to predict performance. *The Neuroscientist: A Review Journal Bringing Neurobiology, Neurology and Psychiatry*, 25(1):86–93, 2019.

F. Vecchio, F. Miraglia, E. Judica, M. Cotelli, F. Alù, and P. M. Rossini. Human brain networks: A graph theoretical analysis of cortical connectivity normative database from eeg data in healthy elderly subjects. *GeroScience*, 42(2):575, 2020.

F. G. Venhuizen, B. van Ginneken, F. van Asten, M. J. J. P. van Grinsven, S. Fauser, C. B. Hoyng, T. Theelen, and C. I. Sánchez. Automated staging of age-related macular degeneration using optical coherence tomography. *Investigative Ophthalmology & Visual Science*, 58(4):2318–2328, 2017.

L. Ver Hoef, H. Deshpande, J. Cure, G. Selladurai, J. Beattie, R. E. Kennedy, R. C. Knowlton, and J. P. Szaflarski. Clear and consistent imaging of hippocampal internal architecture with high resolution multiple image co-registration and averaging (hr-micra). *Frontiers in Neuroscience*, 15, 2021.

C. Veraart, M.-C. Wanet-Defalque, B. Gerard, A. Vanlierde, and J. Delbeke. Pattern recognition with the optic nerve visual prosthesis. *Artificial Organs*, 27(11):996–1004, 2003.

L. Vermunt, E. Dicks, G. Wang, A. Dincer, S. Flores, S. J. Keefe, S. B. Berman, D. M. Cash, J. P. Chhatwal, C. Cruchaga, N. C. Fox, B. Ghetti, N. R. Graff-Radford, J. Hassenstab, C. M. Karch, C. Laske, J. Levin, C. L. Masters, E. McDade, and D. I. A. N. (DIAN). Single-subject grey matter network trajectories over the disease course of autosomal dominant alzheimer's disease. *Brain Communications*, 2(2):fcaa102, 2020.

A. Vossen, J. Gross, and G. Thut. Alpha power increase after transcranial alternating current stimulation at alpha frequency (α-tacs) reflects plastic changes rather than entrainment. *Brain Stimulation*, 8(3):499–508, 2015.

J. Wang, T. Li, B. A. Sabel, Z. Chen, H. Wen, J. Li, X. Xie, D. Yang, W. Chen, N. Wang, J. Xian, and H. He. Structural brain alterations in primary open angle glaucoma: A 3t mri study. *Scientific Reports*, 6:18969, 2016.

Y. Wang, A. Metoki, K. H. Alm, and I. R. Olson. White matter pathways and social cognition. *Neuroscience & Biobehavioral Reviews*, 90:350–370, 2018.

D. J. Watts and S. H. Strogatz. Collective dynamics of 'small-world' networks. *Nature*, 393(6684):440–442, 1998.

A. L. Williams, J. Lackey, S. S. Wizov, T. M. T. Chia, S. Gatla, M. L. Moster, R. Sergott, G. L. Spaeth, and S. Lai. Evidence for widespread structural brain changes in glaucoma: A preliminary voxel-based mri study. *Investigative Ophthalmology & Visual Science*, 54 (8):5880, 2013.

T. Womelsdorf, J.-M. Schoffelen, R. Oostenveld, W. Singer, R. Desimone, A. K. Engel, and P. Fries. Modulation of neuronal interactions through neuronal synchronization. *Science*, 316(5831):1609–1612, 2007.

X. Wu, Y. Huang, Z. Liu, W. Lai, E. Long, K. Zhang, J. Jiang, D. Lin, K. Chen, T. Yu, D. Wu, C. Li, Y. Chen, M. Zou, C. Chen, Y. Zhu, C. Guo, X. Zhang, R. Wang, and H. Lin. Universal artificial intelligence platform for collaborative management of cataracts. *The British Journal of Ophthalmology*, 103(11):1553–1560, 2019.

Z. Wu and B. A. Sabel. Spacetime in the brain: Rapid brain network reorganization in visual processing and recovery. *Scientific Reports*, 11(1):1–12, 2021.

Z. Wu, A. Nurnberger, and B. A. Sabel. Dynamic functional network response to visual stimulus in areas of residual vision. In *2020 IEEE International Conference on Human-Machine Systems (ICHMS)*, pages 1–4, 2020.

Z. Wu, J. Xu, A. Nürnberger, and B. A. Sabel. Global brain network modularity dynamics after local optic nerve damage following noninvasive brain stimulation: An eeg-tracking study. *Cerebral Cortex*, page bhac375, 2022.

H. Y. Xiong, B. Alipanahi, L. J. Lee, H. Bretschneider, D. Merico, R. K. C. Yuen, Y. Hua, S. Gueroussov, H. S. Najafabadi, T. R. Hughes, Q. Morris, Y. Barash, A. R. Krainer, N. Jojic, S. W. Scherer, B. J. Blencowe, and B. J. Frey. The human splicing code reveals new insights into the genetic determinants of disease. *Science*, 347(6218):1254806, 2015.

Y. Xu, A. Hosny, R. Zeleznik, C. Parmar, T. Coroller, I. Franco, R. H. Mak, and H. J. W. L. Aerts. Deep learning predicts lung cancer treatment response from serial medical imaging. *Clinical Cancer Research: An Official Journal of the American Association for Cancer Research*, 25(11):3266–3275, 2019.

S. Yan, C. Zheng, B. Cui, Z. Qi, Z. Zhao, Y. An, L. Qiao, Y. Han, Y. Zhou, and J. Lu. Multiparametric imaging hippocampal neurodegeneration and functional connectivity with simultaneous pet/mri in alzheimer's disease. *European Journal of Nuclear Medicine and Molecular Imaging*, 47(10):2440–2452, 2020.

O. Yildirim, U. B. Baloglu, R.-S. Tan, E. J. Ciaccio, and U. R. Acharya. A new approach for arrhythmia classification using deep coded features and lstm networks. *Computer Methods and Programs in Biomedicine*, 176:121–133, 2019.

W. Yin, L. Li, and F.-X. Wu. Deep learning for brain disorder diagnosis based on fmri images. *Neurocomputing*, 469:332–345, 2022.

Y. You, V. K. Gupta, S. L. Graham, and A. Klistorner. Anterograde degeneration along the visual pathway after optic nerve injury. *PLoS ONE*, 7(12), 2012.

Q. Yu, E. B. Erhardt, J. Sui, Y. Du, H. He, D. Hjelm, M. S. Cetin, S. Rachakonda, R. L. Miller, G. Pearlson, and V. D. Calhoun. Assessing dynamic brain graphs of time-varying connectivity in fmri data: Application to healthy controls and patients with schizophrenia. *NeuroImage*, 107:345–355, 2015.

E. L. Yuh, S. Jain, X. Sun, D. Pisica, M. H. Harris, S. R. Taylor, A. J. Markowitz, P. Mukherjee, J. Verheyden, J. T. Giacino, H. S. Levin, M. McCrea, M. B. Stein, N. R. Temkin, R. Diaz-Arrastia, C. S. Robertson, H. F. Lingsma, D. O. Okonkwo, A. I. R. Maas, and R. Zafonte. Pathological computed tomography features associated with adverse outcomes after mild traumatic brain injury: A track-tbi study with external validation in center-tbi. *JAMA Neurology*, 78(9):1137–1148, 2021.

J.-Y. Yun and Y.-K. Kim. Graph theory approach for the structural-functional brain connectome of depression. *Progress in Neuro-Psychopharmacology and Biological Psychiatry*, 111:110401, 2021.

T. Zaehle, S. Rach, and C. S. Herrmann. Transcranial alternating current stimulation enhances individual alpha activity in human eeg. *PLoS ONE*, 5(11):e13766, 2010.

H. Zeng. Mesoscale connectomics. *Current Opinion in Neurobiology*, 50:154–162, 2018.

J. Zhang, S. Gajjala, P. Agrawal, G. H. Tison, L. A. Hallock, L. Beussink-Nelson, M. H. Lassen, E. Fan, M. A. Aras, C. Jordan, K. E. Fleischmann, M. Melisko, A. Qasim, S. J. Shah, R. Bajcsy, and R. C. Deo. Fully automated echocardiogram interpretation in clinical practice: Feasibility and diagnostic accuracy. *Circulation*, 138(16):1623–1635, 2018.

A Appendix

Subject ID	Group	Gender	Age	Treatment Group	Percentage of improved vision after real rtACS
1	Patient	M	53	Placebo	0.029
2	Patient	M	55	Placebo	0.071
3	Patient	M	60	Placebo	0.082
4	Patient	F	74	Placebo	/
5	Patient	M	20	Placebo	-0.112
6	Patient	M	58	Placebo	0.505
7	Patient	F	24	Placebo	-0.066
8	Patient	F	47	Placebo	/
9	Patient	M	66	Placebo	0.018
10	Patient	M	47	rtACS	0.012
11	Patient	M	33	rtACS	-0.052
12	Patient	M	61	rtACS	0.128
13	Patient	F	65	rtACS	0.065
14	Patient	F	49	rtACS	0.299
15	Patient	M	67	rtACS	0.165
16	Patient	M	68	rtACS	0.08
17	Patient	F	44	rtACS	0.067
18	Patient	F	62	rtACS	0.001
19	Patient	F	41	rtACS	0.014
20	Patient	M	62	Placebo	0.199
21	Control	F	25	/	/
22	Control	F	19	/	/
23	Control	F	42	/	/
24	Control	M	20	/	/
25	Control	M	47	/	/
26	Control	F	74	/	/
27	Control	M	25	/	/
28	Control	M	51	/	/
29	Control	M	66	/	/
30	Control	M	58	/	/
31	Control	F	28	/	/
32	Control	F	55	/	/
33	Control	M	38	/	/
34	Control	M	50	/	/
35	Control	F	44	/	/

Table A.1: Basic information of 20 patients with optic nerve damage and 15 controls.

B Ehrenerklärung

Ich versichere hiermit, dass ich die vorliegende Arbeit ohne unzulässige Hilfe Dritter und ohne Benutzung anderer als der angegebenen Hilfsmittel angefertigt habe; verwendete fremde und eigene Quellen sind als solche kenntlich gemacht. Insbesondere habe ich nicht die Hilfe eines kommerziellen Promotionsberaters in Anspruch genommen. Dritte haben von mir weder unmittelbar noch mittelbar geldwerte Leistungen für Arbeiten erhalten, die im Zusammenhang mit dem Inhalt der vorgelegten Dissertation stehen. Ich habe insbesondere nicht wissentlich:

- Ergebnisse erfunden oder widersprüchliche Ergebnisse verschwiegen.
- Statistische Verfahren absichtlich missbraucht, um Daten in ungerechtfertigter Weise zu interpretieren.
- Fremde Ergebnisse oder Veröffentlichungen plagiiert.
- Fremde Forschungsergebnisse verzerrt wiedergegeben.

Mir ist bekannt, dass Verstöße gegen das Urheberrecht Unterlassungs- und Schadensersatzansprüche des Urhebers sowie eine strafrechtliche Ahndung durch die Strafverfolgungsbehörden begründen kann. Die Arbeit wurde bisher weder im Inland noch im Ausland in gleicher oder ähnlicher Form als Dissertation eingereicht und ist als ganzs auch noch nicht verofftilivht.

Magdeburg, den 11.12.2023